STUDIES OF VOPcPhO AND PTCDA THIN FILMS AND THEIR APPLICATION IN ORGANIC SOLAR CELLS

LIM LIH WEI

DISSERTATION SUBMITTED IN FULLFILLMENT OF THE REQUIREMENT FOR THE DEGREE OF MASTER OF SCIENCE

DEPARTMENT OF PHYSICS
FACULTY OF SCIENCE
UNIVERSITY OF MALAYA
KUALA LUMPUR

2012

UNIVERSITI MALAYA

ORIGINAL LITERARY WORK DECLARATION

Name of Candidate: **Lim Lih Wei** (I.C/Passport No: **840507-06-5201**)

Registration/Matric No: **SGR080112**

Name of Degree: **Master of Science (Dissertation)**

Title of Dissertation ("this Work"):
STUDIES OF VOPcPhO AND PTCDA THIN FILMS AND THEIR APPLICATION IN ORGANIC SOLAR CELLS

Field of Study: Organic Electronics

I do solemnly and sincerely declare that:

(1) I am the sole author/writer of this Work;
(2) This Work is original;
(3) Any use of any work in which copyright exists was done by way of fair dealing and for permitted purposes and any excerpt or extract from, or reference to or reproduction of any copyright work has been disclosed expressly and sufficiently and the title of the Work and its authorship have been acknowledged in this Work;
(4) I do not have any actual knowledge nor do I ought reasonably to know that the making of this work constitutes an infringement of any copyright work;
(5) I hereby assign all and every rights in the copyright to this Work to the University of Malaya ("UM"), who henceforth shall be owner of the copyright in this Work and that any reproduction or use in any form or by any means whatsoever is prohibited without the written consent of UM having been first had and obtained;
(6) I am fully aware that if in the course of making this Work I have infringed any copyright whether intentionally or otherwise, I may be subject to legal action or any other action as may be determined by UM.

Date: **07 December 2012**

Candidate's Signature

Subscribed and solemnly declared before,

Date: **07 December 2012**

Witness's Signature

Name: **Dr. Khaulah Sulaiman**
Designation: **Senior Lecturer**

Abstract

This work is focused on the study of the p-type organic semiconductor, vanadyl 2, 9, 16, 23-tetraphenoxy-29H, 31H-phthalocyanine (VOPcPhO) and n-type organic semiconductor of 3, 4, 9, 10-perylenetetracarboxylic dianhydride (PTCDA) as the possible candidates for organic photovoltaic cells (OPVC) fabrication. The initial phase of this work involved preparation and characterisation of organic semiconductor thin films. The VOPcPhO thin films were prepared by spin-coating method while the PTCDA thin films were deposited by thermal evaporation technique using a homebuilt thermal evaporator in Low Dimensional Materials Research Centre (LDMRC). The optical and structural properties of the deposited thin films were characterised by ultraviolet-visible (UV-VIS) spectroscopy, x-ray diffraction (XRD) spectroscopy, Fourier transform infrared (FTIR) spectroscopy, atomic force microscopy (AFM) and field emission scanning electron microscopy (FESEM). The UV-VIS absorption spectra revealed that the absorption bands of VOPcPhO and PTCDA thin films are in complimentary to each other. PTCDA absorbs most light in the visible range between 450nm to 600nm, whereas VOPcPhO absorbs light in the UV range between 300nm to 400nm as well in the near infrared region of 600nm to 800nm. Therefore, by combining these two organic semiconductors of PTCDA and VOPcPhO to form a bilayer heterojunction, hence a good coverage of the solar spectrum can be explored. The estimated optical band gap, E_g determined for the single layer VOPcPhO and PTCDA thin films as well as bilayer VOPcPhO/PTCDA thin film are 1.6eV, 2.13eV and 1.62eV, respectively. Low optical band gap is favourable in OPVC because relatively low photon energy is required to excite the electron in the material to form exciton (bound electron-hole pair).

The second phase of this work involves the fabrication of OPVC using VOPcPhO and PTCDA thin films. Single layer and bilayer heterojunction structure OPVC were constructed and the performance of these devices were determined and compared by J-V curve. It was found that the single layer devices did not exhibit photovoltaic effect but the bilayer heterojunction devices clearly shown interesting photovoltaic effect when light beam shined upon them. This finding has indicated that the exciton dissociations can only take place at the VOPcPhO/PTCDA interface. However, the power conversion efficiency (PCE) of the primitive OPVC was very low (0.16×10^{-3}%).

The final phase of this work involved the improvements and optimisations of the OPVC. Insertion of hole transport layer, oxygen plasma treatment, thickness optimization, post thermal annealing and vapour treatments were performed in attempts to raise the PCE of the OPVC. Insertion of poly(3,4-ethylenedioxythiophene: poly(styrenesulfonic acid) (PEDOT: PSS) and oxygen plasma treatment are promising methods to improve the OPVC. However, post thermal annealing and vapour treatments were unsuccessful to improve the OPVC. The highest PCE determined for the bilayer heterojunction OPVC after went through the treatments is 3.71×10^{-3}%. Attempts of multilayer heterojunctions OPVC was made in order to further prove the exciton dissociations can only take place at the VOPcPhO/PTCDA interfaces. The multilayer heterojunctions OPVC has a PCE of 5.40×10^{-3}%.

Abstrak

Kerja penyelidikan ini tertumpu kepada penyelidikan organik semikonduktor jenis-p, vanadyl 2, 9, 16, 23-tetraphenoxy-29H, 31H-phthalocyanine (VOPcPhO) dan organik semikonduktor jenis-n, 3, 4, 9, 10-perylenetetracarboxylic dianhydride (PTCDA) sebagai calon yang sesuai untuk fabrikasi sel suria organik. Fasa awal kerja penyelidikan ini melibatkan proses penyediaan dan pencirian filem nipis organik semikonduktor. Filem nipis VOPcPhO disediakan dengan menggunakan kaedah salutan putaran manakala filem nipis PTCDA disediakan melalui kaedah penyejatan terma dengan menggunakan sistem sejatan terma buatan sendiri di Pusat Pemyelidikan Bahan Berdimensi Rendah (LDMRC). Ciri-ciri optikal dan struktural filem nipis yang disediakan telah diukur dengan menggunakan spektroskopi penyerapan ultra-lembayung-nampak (UV-VIS), belauan sinar-x (XRD), spectroskopi transformasi inframerah Fourier (FTIR), mikroskopi daya atomik (AFM), mikroskopi medan pemancar imbasan elektron (FESEM). Pengukuran UV-VIS menunjukkan jalur penyerapan kedua-dua filem nipis VOPcPhO and PTCDA adalah saling melengkapi. PTCDA menyerap cahaya pada panjang gelombang 450nm hingga 600nm manakala VOPcPhO menyerap cahaya pada panjang gelombang 300nm hingga 400nm dan juga menyerap cahaya pada panjang gelombang 600nm hingga 800nm. Ini menunjukkan bahawa kedua-dua filem nipis ini boleh digandingkan sebagai dwilapisan aneka simpang di mana ia dapat menyediakan liputan spektrum suria yang bagus. Jurang jalur optikal, E_g yang dihitung berdasarkan hubungan Tauc bagi lapisan tunggal filem nipis VOPcPhO, PTCDA dan dwilapisan VOPcPhO/PTCDA adalah masing-masing 1.6eV, 2.13eV dan 1.62eV. Jurang jalur optikal yang rendah adalah digalakkan di dalam applikasi sel suria organik kerana secara relatifnya hanya memerlukan tenaga foton yang rendah untuk menguja elektron di dalam bahan untuk membentuk exciton.

Fasa kedua kerja penyelidikan ini melibatkan fabrikasi sel suria organik dengan menggunakan filem nipis VOPcPhO dan PTCDA. Struktur lapisan tunggal dan dwilapisan aneka simpang sel suria organik telah telah dibina dan prestasi peranti ini diukur dan dibandingkan dengan menggunakan lengkungan J-V. Didapati bahawa peranti lapisan tunggal tidak menunjukkan kesan fotovoltaik tetapi peranti dwilapisan aneka simpang menunjukkan kesan fotovoltaik yang menarik ketika alur cahaya dipancarkan atas peranti tersebut. Penemuan ini menunjukkan bahawa exciton hanya dapat diceraikan di antaramuka VOPcPhO/PTCDA. Walaubagaimanapun,kecekapan penukaran kuasa (PCE) sel suria organik ini adalah sangat rendah (0.16×10^{-3}%).

Fasa terakhir kerja ini melibatkan peningkatan dan pengoptimuman sel suria organik. Kemasukan lapisan pengakutan lohong, rawatan plasma oksigen, pengoptimuman ketebalan, pengepuhlindapan terma dan rawatan wap telah dijalankan sebagai cubaan untuk menaikkan kecekapan penukaran kuasa sel suria organik. Kemasukkan poly(3,4-ethylenedioxythiophene: poly(styrenesulfonic acid) (PEDOT: PSS) dan rawatan oksigen adalah kaedah yang berpotensi untuk meningkatkan prestasi sel suria organik. Walaubagaimanapun, pengepuhlindapan terma dan rawatan wap tidak berjaya meningkatkan prestasi sel suria organik. Nilai kecekapan penukaran kuasa tertinggi yang dicapai oleh dwilapisan aneka simpang sel suria organik setelah melalui rawatan tersebut adalah 3.71×10^{-3}%. Cubaan untuk membina sel suria organik yang mempunyai lapisan berbilang aneka simpang adalah bertujuan untuk mengesahkan bahawa penceraian exciton hanya boleh berlaku di antaramuka VOPcPhO/PTCDA. Nilai kecekapan penukaran kuasa sel suria organik yang mempunyai lapisan berbilang aneka simpang adalah 5.40×10^{-3}%.

Acknowledgement

First and foremost, I would like to express my deepest gratitude to my supervisor, Dr. Khaulah Sulaiman for her invaluable guidance, encouragements, advices and assistances given to me throughout the entire progress of this work. Moreover, I am gratefully appreciate her patient and tolerant on me for my mistakes and inefficiency throughout the entire work.

Besides that, I would like to express millions thanks to all the members of Low Dimensional Materials Research Centre especially Professor Datin Dr. Saadah Abdul Rahman, Professor Dr. Wan Haliza Abd. Majid, Dr. Huang Nay Ming, the laboratory assistances, Mdm. Norlela Mohamed Shahardin and Mr. Muhammad Aruf for their kind supports, guidance and advices. Not forgetting to express my gratitude to my seniors especially Dr. Goh Boon Tong and Mr. Gan Wee Chen, my fellow group members especially Dr. Fahmi Fariq Muahammad Shareef, Mr. Ali Imran bin Abdul Hapip, Ms. Toong Way Yun and Mr. Muhamad Saipul Fakir and my fellow colleagues especially Mr. Mohd. Arif Mohd. Sarjidan, Ms. Nor Khairiah Za'aba, Mr. Ng Boon Ki, Mr. Chong Su Kong, Mr. Chan Kee Wah and Mdm. Fatimeh Shariatmadartehrani for their assistances, moral supports and understanding which making my working environment constructive and interesting. The same expression goes to my dear friends, Mr. Lee Yen Sian, Mr. Lee Seng Huat, Mr. Lim Lian Kuang for their companionship, support and suggestions.

I would like to acknowledge University of Malaya and Physics Department for offering the tutorship scheme to me to pursue my master degree. I would also like to acknowledge the financial supports given which included Postgraduate Research Fund (PPP) Cycle 3/2009 (PS302/2009C) and Cycle 2/2010 (PS341/2010B) and University Malaya Research Grant (RG053/09AFR) provided by University of Malaya and the Fundamental Research Grant Scheme (FRGS) under project FP007-2011A provided by the Ministry of Higher Education (MOHE).

Last but not least, I wish to show my sincere appreciation to my family as well as my girlfriend for their concerns, understanding, moral supports and encouragements that have enabled me to persist in my work until the end. This work would have been impossible without their loves.

Table of Contents

Chapter 1

Introduction

Chapter 2

Literature Review

Chapter 3

Experimental Techniques

Chapter 4

Characterisations of Organic Semiconductors VOPcPhO and PTCDA Thin Films

Chapter 5

Electrical Properties and Improvements

Chapter 6

Conclusions and Future Works

References

List of Figures

List of Tables

Chapter 1

Introduction

1.0 Overview

Organic photovoltaic (OPV) is a third generation solar technology that is rapidly developing after silicon based first and second generation solar technologies. Unlike silicon based photovoltaic cell which in other term as inorganic photovoltaic cell, an organic photovoltaic cell (OPVC) is a photovoltaic cell that uses conductive organic polymers or small organic molecule compounds such as dyes or pigments as active layer for light absorption and charge transport.

1.1 Brief History of Organic Photovoltaic Cell

The invention of photovoltaic cell can be attributed to the discovery of the photovoltaic effect (PV). The PV effect is commonly ascribes to a French experimental physicist named Alexandre Edmond Becquerel. In 1839, Alexandre Edmond Becquerel discovered a photocurrent when platinum (Pt) electrodes coated with silver bromide (AgBr) or silver chloride (AgCl) was illuminated in aqueous solution (Martin A, 2002). However, the importance of the PV effect was not being exploited not until forty years later, after the phenomenon of photoconductivity was first observed by an English electrical engineer Willoughby Smith in 1873 and also by William Grylls Adams who was a professor of Natural Philosophy in King’s College, London with his student Richard Evan Day in 1876. They both were working on the selenium (Se) (Adams & Day, 1877; Smith, 1873). Since then, the photovoltaic cell started to emerge.

In general, the history of organic based photovoltaic cells can be dated back to as early as early 20th century. Anthracene was the first organic compound in which its photoconductivity property was observed by Alfedro Pochettino in 1906 and Max Volmer in 1913 respectively. These observations marked the start of this field. In 1950s, the first photovoltaic devices which mainly composed of organic dye, chlorophyll and related compounds were studied. In 1958, Kearns and Calvin worked with magnesium phthalocyanine (MgPc) were able to measure a photovoltage of 200mV. In 1980s, first polymer based solar cells appeared but these simple PV devices typically yield limited power conversion efficiency well below 0.1%. A major breakthrough was made by Ching W. Tang in 1986 when he discovered donor-acceptor based cells which dramatically increased the efficiency to about 1% (Tang, 1986). In 1991, first dye/dye based solar cells were fabricated by Hiramoto. First polymer/C60 based solar cells (or called fullerene based solar cells) were successfully fabricated by Niyazi Serdar Sariciftci in 1993. In fact, this fullerene based organic solar cells is still the most efficient organic solar cells among other type of organic solar cells until this day. In 1995, first polymer/polymer based solar cells were invented by Yu and Hall (Frederik C, 2009; Spanggaard & Krebs, 2004). Nowadays, the development of organic photovoltaic cells has been tremendously improved. Intensive researches have been poured into this field all around the world. Recently, organic solar cells with power conversion efficiency more than 6% have been fabricated (Chen et al., 2009; S. H. Park et al., 2009).

Table 1.0 The development timeline of OPVC.

Year	Achievement	Reference
1839	Alexandre Edmond Becquerel discovered photovoltaic effect.	(Martin A, 2002)
1873	Willoughby Smith observed photoconductivity in selenium.	(Smith, 1873)
1906	Alfedro Pochettino observed photoconductivity in anthracene.	(Spanggaard & Krebs, 2004)
1950s	Organic dye, chlorophyll and related compounds photovoltaic devices.	(Spanggaard & Krebs, 2004)
1958	Kearns and Calvin et al. measured 200mV in their MgPc device.	(Kearns & Calvin, 1958)
1986	Ching W. Tang et al. invented bilayer heterojunction OPVC.	(Tang, 1986)
1991	Hiramoto et al. fabricated first dye/dye based OPVC.	(Spanggaard & Krebs, 2004)
1992	Niyazi Serdar Sariciftci et al. invented first fullerence based OPVC.	(Spanggaard & Krebs, 2004)
1995	First polymer/polymer based solar cells were invented by Yu and Hall.	(Spanggaard & Krebs, 2004)
2005	Kuwat Triyana et al. reported 1.38% efficiency tandem OPVC.	(Triyana, Yasuda, Fujita, & Tsutsui, 2005)

2009	Kwanghee Lee and Alan J. Heeger et al. fullerence based OPVC achieved 6.1% PCE and near 100% internal quantum efficiency.	(S. H. Park, et al., 2009)

1.2 Advantages and Disadvantages

The searching of reliable, cheap, efficient and environmentally friendly source of energy is one of the mankind's biggest tasks for the long term future of civilization. The importance of renewable energy source will increase due to shrinking oil resource with at the same time rising energy demand. In addition, the combustion of organic substances produces carbon dioxide which is known to be responsible for the greenhouse effect or global warming. OPVCs which harvest solar energy from the sun are one of the alternatives that can reduce these problems. OPVCs have been investigated intensively by researchers all around the world in these past few decades due to their many advantages. It is well known that high price of inorganic solar cells is due to the expensive production and purification of silicon wafers. Production and purification of organic materials to be used in fabricating OPV devices are relatively cheap compared to inorganic silicon. Besides that, the devices can be fabricated easily using various simple techniques such as spin coating, ink-jet printing, doctor blading (wet-processing) or evaporation/sublimation (dry-processing) which can make the production potentially inexpensive. Furthermore, the material consumption for OPV devices is very small which is in nanometers scale of thickness, compared to the micron meters scale of the silicon based solar panels. Large scale production of OPV devices is possible which then further significantly shorten the energy payback time which is defined as the operating life of a power-generating device needed to produce the amount of energy invested during manufacturing, installation and maintenance (Kippelen & Bredas, 2009).

The unique properties of lightweight and flexibility of organic materials making them very useful on curved surfaces and ubiquitous applications. In addition, organic materials can be tuned chemically in order to adjust electrical or optical band gap, valance and conduction energies, charge transport as well as solubility and several other structural properties. Vast variety of possible chemical structures and functionalities of organic materials increase the flexibility for different purpose. Nowadays green technologies become a rising trend in both industrial and research field. OPV devices can be considered as a green technology because it has lower impact on the environment compared to inorganic based photovoltaic cells due to easy to dispose and degradation of organic materials in ambient environment.

However, OPVCs have several serious drawbacks. Low power conversion efficiency in the cells is still the major challenge to overcome before these OPVCs can be commercialized. Furthermore, the overall production cost is still very high due to the expensive price for the semiconducting polymers.

1.3 Objectives

Organic photovoltaic cell is a relatively new research field in Malaysia. In this research, the main focus is to prepare a thin film of low molecular weight organic semiconductors. Two types of materials used in this study; donor material (p-type) of vanadyl 2, 9, 16, 23-tetraphenoxy-29H, 31H-phthalocyanine (VOPcPhO) and acceptor material (n-type) of 3, 4, 9, 10-perylenetetracarboxylic dianhydride (PTCDA) VOPcPhO thin films are prepared using the spin-coating method from the material solution. On the other hand, thermal evaporation technique is used to deposit the insoluble PTCDA thin film onto the glass substrate. Therefore, objectives of this research can be listed as follow:

a) To prepare and characterise the single layer films composed of vanadyl 2, 9, 16, 23-tetraphenoxy-29H, 31H-phthalocyanine (VOPcPhO) and 3, 4, 9, 10-perylenetetracarboxylic dianhydride (PTCDA) and bilayer thin films of VOPcPhO/PTCDA organic semiconductors,

b) To fabricate and characterise the single layer and bilayer organic photovoltaic cells consist of the single layer VOPcPhO and bilayer thin films of VOPcPhO/PTCDA,

c) To study the effect of PEDOT: PSS treatment on the performance of VOPhPhO/PTCDA organic photovoltaic cells.

1.4 Thesis Organization

Chapter 1 initially provides a brief historical development of the organic solar cells, followed by the important of the searching of renewable energy source by exploiting solar energy. Advantages and disadvantages of the organic solar cells are presented and the objectives of this reserach were being listed out. Chapter 2 covers the literature reviews of OPVCs. This chapter is devoted to provide information of materials used in organic solar cells fabrication. Reviews of the variation of device architectures and the basic working principle of organic solar cell along with the information about the performance analysis are provided in this chapter. Chapter 3 describes the experimental method used throughout this research work. The processes involved in OPVC fabrication such as substrate preparation (cutting and etching), substrate cleaning, solution preparation, thin films deposition and electrodes deposition as well as the experiment setups are presented in detail. Afterwards, the characterisation methodology and the device assessment are described thoroughly. Chapter 4 mainly focus on the characterisation results of the single and double layers organic thin films deposited using the n-type and p-type organic semiconductors. Optical and structural properties of the thin films are presented and discussed in detail in this chapter.

Electrical properties of the fabricated single layer and bilayer OPVC are presented in chapter 5. The works of improvement and optimisation for the OPVC reported and the results are discussed in detail. Several methods such as addition of hole transport layers, treatments on the substrates and thin films in order to improve the OPVC in aspect of power conversion efficiency (PCE) are being discussed in this chapter. At the end of chapter 5, the results of multilayers OPVC are presented. Finally, chapter 6 presents the conclusions of the research work and provides a summary of the results. At the end, future works or suggestions to improve the OPVC are suggested.

Chapter 2

Literature Review

2.0 Conjugated π-electron System of Conductive Polymers

Conductive polymers are a novel class of materials with extensive potential application in various optoelectronic devices such as organic photovoltaic (OPV) devices, organic light emitting diodes (OLEDs), organic field effect transistors (OFET) and organic sensors. Conductive polymers differ from the usual concept of organic polymers that they are electrical insulators. This special class of polymers can conduct electrical charges under certain circumstances. A few of them exhibit metallic conductivity but most of the conductive polymers have semiconductivity property. Therefore, conductive polymers also can be referred as organic semiconductors.

By definition, a conjugated π-electron system is a system that has connected and overlapping *p*-orbitals with delocalized *pi* electrons in compound with alternating single and double bonds. Ethene as shown in Figure 2.0(a) and benzene ring as shown in Figure 2.0(b) are the basic representative elements of the conjugated systems. The ability of organic semiconductors to transport electric current and absorb light in the ultraviolet (UV) – visible part of the solar spectrum is due to the sp^2-hybridisation of carbon atoms. In conducting polymers, the electrons in the p_z-orbitals of each sp^2-hybridised carbon atom will form π-bonds with neighbouring electrons of p_z-orbitals in a linear chain of sp^2-hybridised carbon atoms. The schematically illustration of this sp^2-hybridisation is illustrated in Figure 2.1. This leads to a dimerization – an alternating single and double bond structure as shown in Figure 2.2. This alternation is termed as conjugation. Due to isometric effect, these π-electrons are of delocalised nature. The π-electrons are much more mobile than the σ-electrons. They can jump from site to site between carbon atoms with low potential energy barriers as compared to the ionization potential.

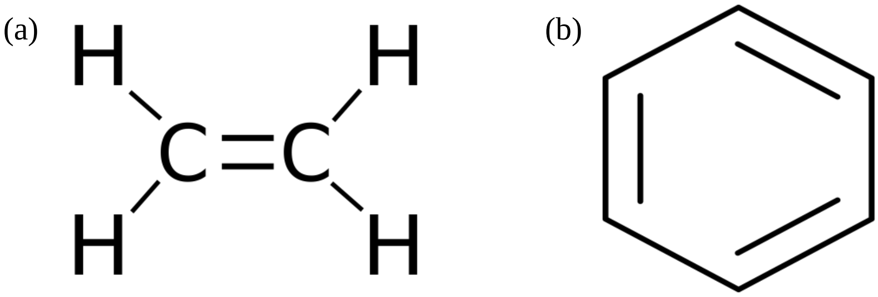

Figure 2.0 Chemical structure of (a) ethene (Image source: Wikimedia Commons), (b) benzene (Images source: Wikimedia Commons).

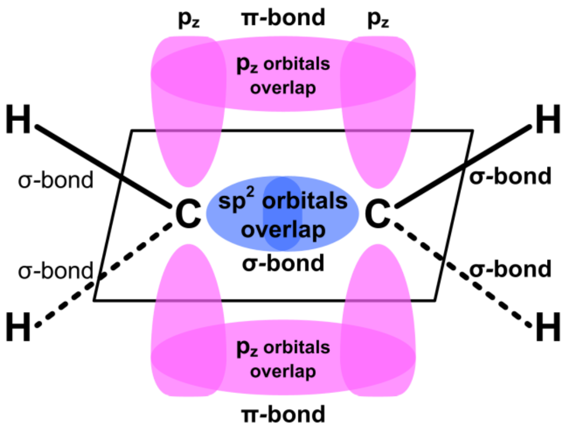

Figure 2.1 Overlap of p_z-orbitals forming π-bonds.

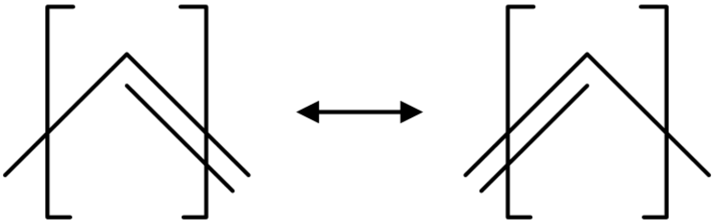

Figure 2.2 A conjugated bond.

An organic semiconductor is an organic compound (normally carbon based compound) that possesses semiconductor properties. There are two general classes of organic semiconductors – small molecules and polymers. Small molecule organic semiconductor does not has the repeated unit, thus the molecular weight is smaller compared to polymer. Figure 2.3 shows the chemical structures of some small molecule organic semiconductors commonly used in organic photovoltaic, namely anthracene, rubrene, aluminum tris(quinoline-8-olate) and phthalocyanine.

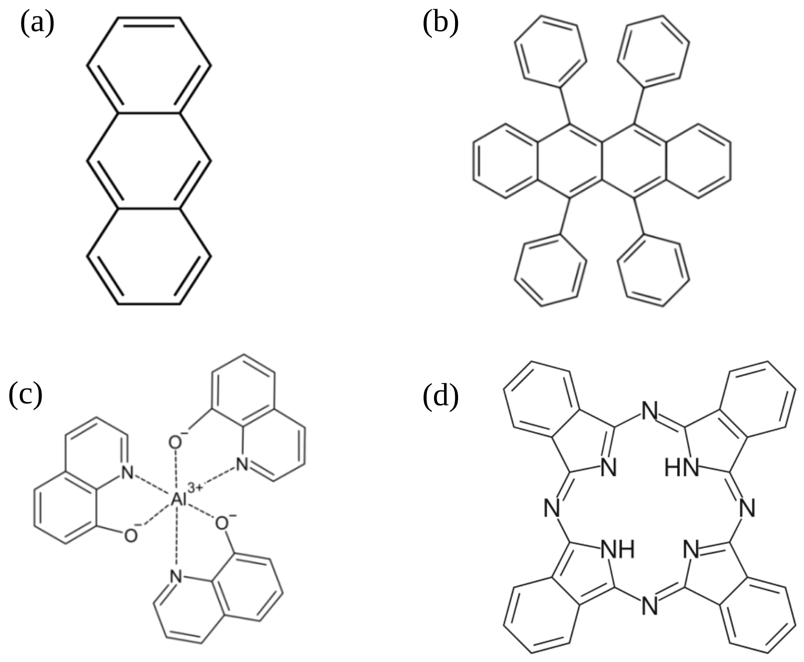

Figure 2.3 Chemical structures of molecular semiconductors used in OPV. (a) anthracene, (b) rubrene, (c) aluminum tris(quinoline-8-olate) (Alq3) and (d) phthalocyanine (Pc).

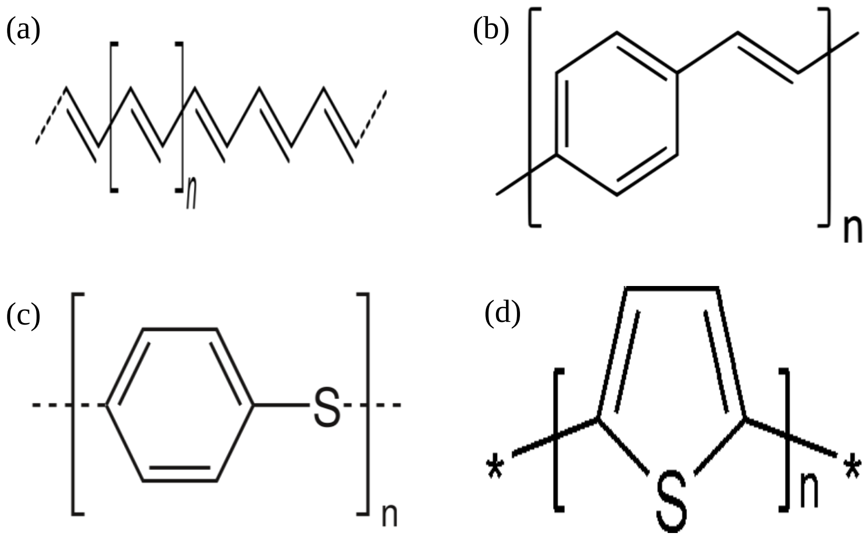

Figure 2.4 Chemical structures of polymer semiconductors used in OPV. (a) polyacetylene, (b) polyphenylene, (c) polyphenylene sulfide, (d) polythiophene.

A polymer semiconductor is a large molecule (macromolecule) composed of periodically repeated structural units/molecule chains, which has the ability of transporting electrical charges. Figure 2.4 shows the repeat units of various polymer semiconductors used in active layer of organic solar cells. All organic semiconductors have a common yet essentially important feature in the chemical structure – conjugated π-electron systems. The semiconductivity of the organic semiconductors is mainly contributed by this conjugated π-electron systems in the compound.

2.1 Materials

2.1.1 3, 4, 9, 10-perylenetetracarboxylic dianhydride (PTCDA)

3, 4, 9, 10-perylenetetracarboxylic dianhydride was used as n-type semiconductor (electron acceptor) in this research, which also characterised as a small molecule organic semiconductor. Figure 2.5 shows the chemical structure of a PTCDA molecule. It is a red pigment that commonly use in colorant industry as a high quality industrial paint especially in automotive field. It is an aromatic, stable, planar and highly symmetric with excellent electrical properties. It has an energy band gap of approximately 2.1eV-2.2eV (Brovelli et al., 2007; Maruyama et al., 2000; Pérez-Merchancano, Marques, & Bolivar-Marinez, 2008). The thin film of PTCDA absorbs radiation in the wavelength ranged from 300nm to 600nm. This absorption range covers almost all the visible spectrum except red region (~620nm-750nm). Studies have suggested that PTCDA is a strong electron acceptor (n-type organic semiconductor). They found out relatively high energy (~200kcal/mol) is needed to just remove one electron from the molecule. Removal of a pair of electrons is thought to be prohibited (~480kcal/mol) (Pérez-Merchancano, et al., 2008).

PTCDA forms highly ordered superstructures on several types of metal substrates. In 2001, Gabriel deposited the monolayer of PTCDA in a base pressure of 2 x 10^{-10}mbar by molecular beam epitaxy (MBE). This research group studied the submonolayer to monolayer coverage of PTCDA on Cu (110) by scanning tunnelling microscopy (STM). They found that no long-range ordering was found after PTCDA deposition on Cu (110) at room temperature but the PTCDA tends to rearrange themselves to form islands with a dense packing after thermal annealing at 450K

(Gabriel et al., 2002). In 1998, another research group, Glöckler et al. found that PTCDA monolayers forms large long range ordered islands on Ag (111) surface at room temperature for the thermal sublimated thin films of PTCDA (Glöckler et al., 1998). A variety of substrates were utilised in a study reported by Wagner et al. in 2004 for the growth of PTCDA on Cu (110), Cu (111) and Au (111). By means of STM measurements, they found that PTCDA crystalline structures grew on these substrates (Wagner et al., 2004).

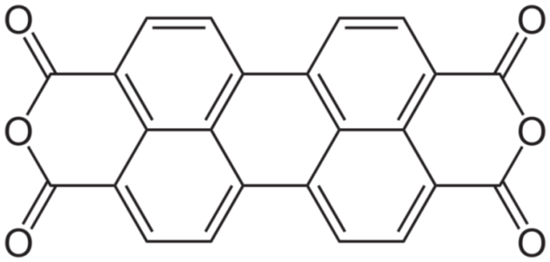

Figure 2.5 Molecular structure of PTCDA.

There are several researchers working on PTCDA as n-type organic semiconductor layer in their OPVC. Liu et al. in 2006 have successfully fabricated two-layer organic photovoltaic cells using 3, 4, 9, 10-perylenetertracarboxylic dianhydride (PTCDA) coupled with 5-vinyl-2, 2’ :5’ ,2” : 5” ,2’”-quaterthiophene (V4T), and 5-vinyl-2, 2’ : 5’ ,2” :5” ,2’” :5” ,2””-quinquethiophene (V5T). Their devices with the cell structure of ITO/V*n*T/PTCDA/Al (n=4, 5) exhibit high open circuit voltage, V_{oc} in the range of 1.87V-2.07V with the power conversion efficiency of 2.32% and 2.67% respectively. Such findings were hypothesised to the intermolecular hydrogen bonding between V*n*T (*n*=4, 5) and PTCDA affects the open circuit voltages of the devices by promoting forward interfacial electron transfer and eliminating the subconducting band trap sites. Besides, they suggested that this bonding increase the molecular order of V*n*T and PTCDA (P. Liu, Li, Huang, Pan, & Deng, 2006).

In 2007, Brovelli et al. successfully fabricated the bilayer heterojunction OPVC using 1, 4-diaminoanthraquinone (1, 4-DAAQ) and PTCDA as the electron acceptors in conjunction with zinc phthalocyanine (ZnPc) as the electron donor. In the research, the HOMO and LUMO energy level were determined for the 1, 4-DAAQ by the cyclic voltammetry (CV) technique. The obtained electrochemical energy gap was then compared to that of the optical energy band gap. In this case, both values are relatively similar therefore they suggested that the electrochemical band gap can be easily estimated from the optical band gap of the material. The same group has fabricated OPVC with the cell structure of ITO (100nm)/PEDOT: PSS (10nm)/ZnPc (45nm)/1, 4-DAAQ (15nm) or PTCDA (30nm)/Al (150nm) and reported to produce the power conversion efficiency in order of ≈ 10^{-2}% and 2.5×10^{-2}% with open circuit voltage of 0.9-1.0V and 0.5-0.6V respectively. Then a better performance of PTCDA over 1, 4-DAAQ was attributed to the larger band offset at the organic heterointerface of donor and acceptor of this bilayer OPVC. The larger band offset caused better exciton dissociation at the heterojunction interface and consequently produced higher short circuit current density. The measured open circuit voltages of the devices follow qualitatively with the theoretically calculated values and found to be dependent on the parallel resistance and interface state (Brovelli, et al., 2007).

By utilising the same materials as Brovelli's group found, another research group of Derouiche and Djara fabricated the bulk heterojunction OPVC in 2007 by thermal co-evaporation process in a high vacuum of 10^{-3} Pa at a rate of 0.2-0.7Å/s. The device with ITO/PEDOT: PSS/ZnPc: 1, 4-DAAQ/Al structure was reported to generate an open circuit voltage of 0.45V, a short circuit current density of 0.79mA/cm^2 and a fill factor of 0.31 and a power conversion efficiency of 0.11%. As for their ITO/PEDOT: PSS/ZnPc: PTCDA/Al device, they acquired an open circuit voltage of 0.49V, a short circuit current density of 0.87mA/cm^2 and a fill factor of 0.41 giving the power conversion efficiency of 0.17%. Similar to the Brovelli's group, Derouiche and Djara group found that the PTCDA device performed better than the 1, 4-DAAQ device. They also concluded that the better performance of PTCDA device over the 1.4-DAAQ device is due to the larger discontinuity of energy gap between the ZnPc and PTCDA resulting in higher dissociation or separation of self-bounded excitons (Derouiche & Djara, 2007).

In 2006, Heggie et al. fabricated OPVC using copper phthalocyanine (CuPc) and PTCDA. The effect of mobile charged impurities on the short circuit current density in the organic heterojunction photovoltaic devices was reported. They found out that the short circuit current density is time dependent under short wavelength illumination (blue region) but not under longer wavelength illumination (green and red regions). Higher energy photons caused the decays of short circuit current density with a time scale on the order of minutes. Thus high energy photons in PTCDA has been suggested to produce a spontaneous exciton dissociation and free hole. These researchers further reported that the charged impurities in PTCDA which developed by the trapping of these free holes drift inside the device forming a Helmholtz double layer at the ITO electrodes. Such holes trapping has caused a redistribution of internal electric fields and a corresponding shift in short circuit current density (Heggie, MacDonald, & Hill, 2006).

In 2007, Mori and Kato have investigated the effect of PTCDA as an exciton diffusion blocking layer (EDBL) in their bilayer OPVC based on CuPc as an electron donor and fullerene (C_{60}) as an electron acceptor. Besides PTCDA, they also introduced bathocuproine (BCP) and aluminium tris-(8-hydroxyquinoline) (Alq3) as EDBLs for comparison. They found that PTCDA performed the best among three materials in the viewpoint of stability of film structure and tractability. Furthermore the short circuit current density and open circuit voltage were found to be independence of PTCDA thickness up to 40nm due to the high carrier transportation in PTCDA. The device with the structure of ITO/CuPc (10nm)/C_{60} (20nm)/PTCDA (20nm)/Al had the short circuit current density of 2.5mA/cm^2, open circuit voltage of 0.42V, power conversion efficiency of 0.57% and fill factor of 0.57 (Mori & Kato, 2007).

Nomura et al. is another group that introduced PTCDA as an EDBL in their pentacene/C_{60} bulk heterojunction solar cells. This EDBL prevents holes from moving from the active layer to the anode. In addition, the interface of pentacene/PTCDA increases the probability of exciton dissociation in the device. An increased in short circuit current from 0.013mA/cm^2 to 0.14mA/cm^2 was reported by suppressing the charge recombination when PTCDA was utilised as a blocking layer. The device of ITO/PEDOT: PSS/pentacene: C_{60}/PTCDA/Al provided the power conversion efficiency of 0.021%, fill factor of 0.26, short circuit current density of 0.14mA/cm^2 and open circuit voltage of 0.57V (Nomura, Oku, Suzuki, Kikuchi, & Kinoshita, 2010).

2.1.2 Vanadyl 2, 9, 16, 23-tetraphenoxy-29H, 31H-phthalocyanine (VOPcPhO)

Metallophthalocyanines (M-Pcs) is a group of small molecules, macrocyclic conjugated compound that contain consist of a ligand and a central metal atom (indicate with an M) that bind together to form a coordinated complex, as shown in the Figure 2.6(b). Traditionally, metallophthalocyanines have been utilised as dyes and pigments, but these organic semiconductors have attracted great interest due to their possibility of being exploited as new functional materials and incorporated into the active layers in organic electronic devices. They are used in a number of wide ranging applications such as gas sensors (Ho & Tsou, 2001; C. J. Liu, Peng, Ju, & Hsieh, 1998), data storage (Lian, Li, Wang, Zhang, & Gamota, 2010; Majumdar, Bandyopadhyay, & Pal, 2003), organic light emitting devices (OLEDs) (Hohnholz, Steinbrecher, & Hanack, 2000; Ichikawa, Kobayashi, Koyama, & Taniguchi, 2007), organic thin film transistors (OTFTs) (Ben Chaabane et al., 2003; Li et al., 2008; Nénon, Kanehira, Yoshimoto, Fages, & Videlot-Ackermann, 2010) and OPVC (Bamsey et al., 2011; Klofta, Linkous, & Armstrong, 1985; Lane et al., 2000; Liang et al., 2010).

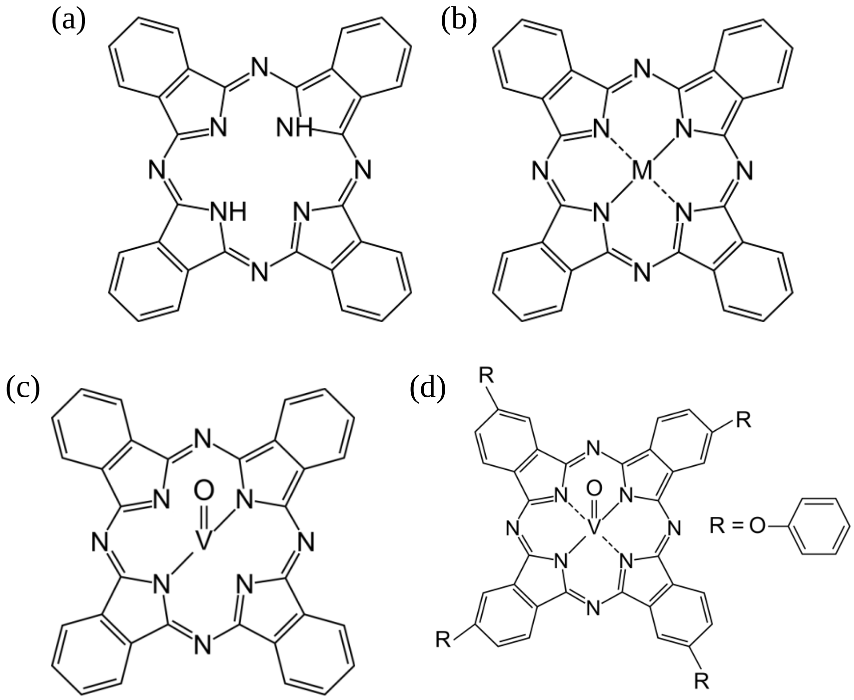

Figure 2.6 Chemical structure of: (a) Pc. (b) M-Pc. (c) VOPc. (d) VOPcPhO.

M-Pcs are the derivatives of phthalocyanice (Pc) as shown in Figure 2.6(a). Two hydrogen atoms in the center of the phthalocyanice can be substituted by different metal ions to form M-. In other words, phthalocyanine can act as a host for the metal ions in its center cavity (Li, et al., 2008). By replacing the hydrogen atoms at the center of the phthalocyanine by one vanadyl ion, VO2+, the material are known as vanadyl phthalocyanine, VOPc and the molecular structure of VOPc is shown in Figure 2.6(c).

Vanadyl phthalocyanine has been reported to show high thermal and chemical stability (Qiu et al., 2005; Wang et al., 2007), good hole conductance (Kolotovska, Friedrich, Zahn, & Salvan, 2006), ultrafast optical response (Y.-l. Pan et al., 1998a). Furthermore, VOPc is a non-toxic material as well as inexpensive in the process of synthesis. The VOPc thin film was reported to generate an absorption spectrum range from 300nm to 1000nm with two distinct absorption bands. A sharp and higher absorption band with a peak centered at around 350nm is called Soret band or B-band.

A broader absorption band with maxima at around 660nm and 730nm is called Q-band (Teodosio Del Caño, Antonio de Saja, & Aroca, 2003; T. Del Caño, Parra, Rodríguez-Méndez, Aroca, & De Saja, 2005; Law, 1985, 1988; Nakano et al., 2001; Yamashita, Maruno, & Hayashi, 1993). Due to the weak absorption property at the green wavelength region (~490nm-560nm), VOPc thin film has a nice and sharp green appearance. Since VOPc has a complementary absorption range to PTCDA, it is believed that the coupling of VOPc and PTCDA should cover all the visible spectrum of solar radiation.

According to the literature, VOPc poccesses a LUMO at 4.2-4.7eV and a HOMO at 5.6eV-5.8eV making its band gap around 0.9eV-1.6eV (Bamsey, et al., 2011; Teodosio Del Caño, et al., 2003). This small band gap enables relatively high probability excitation of the electrons in the HOMO energy level to the LUMO energy level to take place.

VOPc thin film with high crystallization demonstrated by a sharp diffraction peak at 2θ around 7.3° to 7.5°, it indicates that the VOPc molecules are oriented parallel to the substrate corresponding to phase II pattern with interstack spacing of 1.17nm-1.20nm (Kolotovska, et al., 2006; Y.-l. Pan, et al., 1998a; Wang, et al., 2007). High mobility up to 1.5cm^2/Vs was measured reported by Wang et al. on the VOPc deposited on an ordered layer of para-sexiphenyl (*p*-6P). They suggested that the nonplanar VOPc compounds can produce higher mobility than that of the planar VOPc. However, no explanation has been given on high performance of VOPc from its crystal packing structure (Li, et al., 2008; Wang, et al., 2007).

The aforementioned optical, electrical and structural properties of the VOPc make the VOPc a suitable candidature to couple with PTCDA to fabricate organic solar cell. Despite their excellent properties, very few works have been conducted to investigate organic solar cell based on these two materials. Pan et al. fabricated single layer VOPc (in phase II) organic solar cell sandwiched between aluminium and ITO electrodes to study the photovoltaic and electroreflective spectra (Y.-l. Pan, et al., 1998a). Nanai et al. investigated the structures of VOPc in the bilayer films of VOPc and PTCDA. They discovered that the VOPc structures can be affected by the sequence of the deposition (Nanai, Yudasaka, Ohki, & Yoshimura, 1995). Two decades ago, bilayer and multilayer structures using VOPc and PTCDA was utilised to study their absorbance spectra and electrochemical/photoelectrochemical properties. They suggested that the VOPc/PTCDA interface may act like a fixed site impurity where provide a large local electric field to assist in exciton dissociation. They found that the photocurrent yield was directly proportional to the number of VOPc/PTCDA interfaces present confirmed the suggestion proposed by them (Danziger, Dodelet, Lee, Nebesny, & Armstrong, 1991).

However, VOPc, like the parent phthalocyanine and many of its metal derivatives, has low solubility in most organic solvents. This constrain is the reason for the complexity of the thin film deposition and the high cost of the device fabrication for the thermal deposition application. For this reason, it is important to carry out research into more soluble VOPc derivatives, in order to allow a solution based deposition method of such thin films. In this study, a soluble VOPc derivative, called vanadyl 2, 9, 16, 23-tetraphenoxy-29H, 31H-phthalocyanine (VOPcPhO) was selected due to its excellent solubility in organic solvents, especially in chloroform. It is a peripherally substituted VOPc which four phenoxide ions attached at the β-peripheral positions of the VOPc molecule. The molecular structure of the soluble VOPcPhO is shown in Figure 2.6(d). The introduction of the peripheral substituents is believed to dramatically increase the solubility in the organic solvent (Nemykin & Lukyanets, 2010). Owing to the excellent solubility in the chloroform, a simple spin coating technique can be applied in order to deposit the VOPcPhO thin films onto the substrates. It is widely recognised that the solution-based spin coating technique does not require a low vacuum condition and is relatively easier to perform, compared to the thermal evaporation method. Furthermore, a small amount of material can serve to produce large amounts of samples or devices when exploiting this simple solution-based method. Therefore, this method can significantly lower the production cost of organic electronic devices. Hence, the present study aimed to investigate the structure and surface morphology of this soluble VOPcPhO organic semiconductor even the effects of VOPcPhO couples with PTCDA to form bilayer heterojunction OPVC using spin coating method.

2.2 Architecture Structure of Organic Photovoltaic Cell

2.2.1 Single layer organic photovoltaic cell (organic Schottky solar cell)

Single layer organic photovoltaic cell is the simplest form of device among various organic solar cells. It is the first generation of organic photovoltaic cell that has been invented and investigated. This type of device consists only one type of organic semiconductor layer (organic active layer) sandwiched between two metallic conductors, typically a thin layer of semi-transparent higher work function conductor such as indium-tin-oxide (ITO) and a thin layer of metal that has a lower work function such as aluminium (Al), silver (Ag), gold (Au) and etc. A semi-transparent layer of metallic conductor is essential in order to allow the photons to be absorbed by the organic active layer. Therefore, ITO is the most suitable candidature at the moment for the organic solar cell electrode because of its high work function and semi-transparent properties. It is widely used in OPVC and OLED and it can be easily obtained since it is commercially available. Others semitransparent conductors such as fluoride-tin-oxide (FTO) and aluminium zinc oxide (AZO) are also preferable choice of electrodes (Bernède, Cattin, Morsli, & Berredjem, 2008; Qiao, Beck, Lumpkin, Pretko, & McLeskey, 2006; Saarenpää, Niemi, Tukiainen, Lemmetyinen, & Tkachenko, 2010).

The single layer OPVC is often referred as Schottky type device or Schottky diode because a rectifying junction is formed at one of the organic-electrode interface which the charge separation mechanism take place here and another organic electrode formed an ohmic contact. The basic structure of a single layer organic photovoltaic cell is illustrated in Figure 2.7.

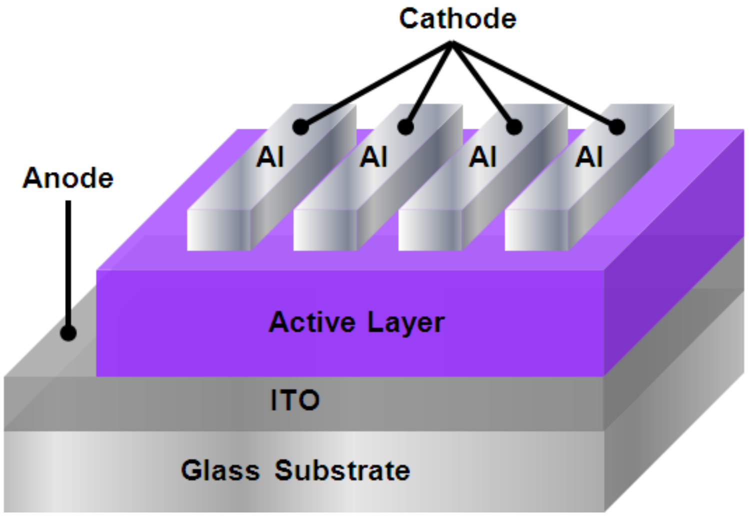

Figure 2.7 Schematic structure of an organic Schottky solar cell.

Typically, the single layer organic device is showing very low power conversion efficiency (≤1%) (Jain et al., 2008; Kwong, Djurišiĉ, Chui, Lam, & Chan, 2003; Takahashi et al., 2002) due to the dissociation of excitons can only occur at the interface between the conductor and organic semiconductor. Some researches claimed that the dissociation of excitons can be done by the electric field induced by the difference potential of work function of the two conductors. Exciton quenching at metal-organic interfaces can also reduce the photocurrent yields causing the lower efficiency in the single layer OPVC.

2.2.2 Bilayer (double layer) heterojunction organic photovoltaic cell

The bilayer heterojunction organic photovoltaic cell consists of two different layers of organic semiconductors sandwiched between the conductive electrodes. These two layers of organic semiconductors are donor (p-type) and acceptor (n-type) organic semiconductors that have different electron affinity and ionization energy. The organic semiconductor that has higher electron affinity and ionization potential is the electron acceptor and the organic semiconductor which has lower electron affinity and ionization potential will be the electron donor in the device. The interface between donor and acceptor layers creates the heterojunction where most of the dissociation of exciton takes place. The configuration of the bilayer organic photovoltaic cell is schematically depicted in Figure 2.8. For an efficient extraction of charge carriers, the work function of the conductive electrodes have to be match with the donor's HOMO and the acceptor's LUMO respectively. Proper and careful considerations are required for the selection of the donor and acceptor organic semiconductors so that the difference in the ionization potential and electron affinity of the adjacent materials are adequate to form a heterojunction with a strong electric field required to dissociate the excitons efficiently.

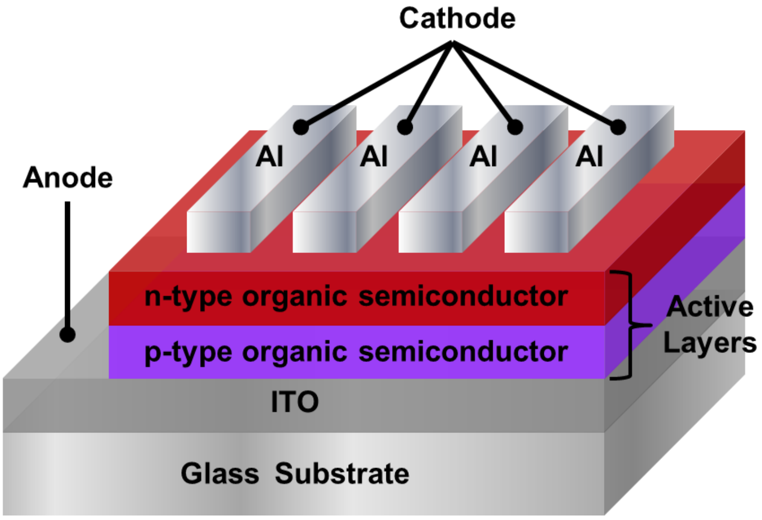

Figure 2.8 Schematic structure of a bilayer heterojunction OPVC.

The first bilayer organic photovoltaic cell appears to be reported by David Kearns and Melvin Calvin in 1958. They fabricated the photovoltaic devices by first pressing powdered the magnesium phthalocyanine (MgPc) into 1.5cm in diameter and 0.1cm thick disks. Then, they coated a thin layer of air oxidized tetramethyl p-phenylenediamine (TMPD) on one side of the disks and pressed contact the coated side with a conducting glass substrate. They reported these organic systems show photovoltaic effect with a maximum voltage of 200mV and a maximum power output of $3x10^{-12}$ W (Kearns & Calvin, 1958).

The first qualitative studied of bilayer heterojunction organic solar cell was done by Ching W. Tang in 1986. He reported his device has a fill factor as high as 0.65 and power conversion efficiency of 0.95% under stimulated air mass 2.0 (AM2.0) illumination. The device was fabricated by 30nm thick copper phthalocyanine (CuPc) layer as p-type organic semiconductor and a 50nm thick layer of perylenetetracarboxylicacid bis-benzimidazole as n-type organic semiconductor sandwiched between semi-transparent ITO substrate and Ag electrode with an active area of 0.1cm^2. He proposed that the absorption of light in both active layers created excitons which can diffuse in the bulk of the films. The interface or junction between the active layers was the active site for the dissociation of excitons to take place. After dissociation, the holes were transported and collected by ITO electrode while the electrons are transported towards Ag electrode. Tang made a hypothesis that the effectiveness of the exciton dissociation at the interface of the active layers may be associated with a high built-in electric field of “unknown origin” which he related to the dipole field or a field due to the trapped charges at the interface (Tang, 1986). This “unknown origin” later has been proved as the discontinuous electronic potential of the active layers. The achievement of Tang’s group was a breakthrough and outstanding benchmark since the previous first generation organic solar cell with the simplest single layer structure typically can only obtained the power conversion efficiency far less than 1%.

Considerable amount of research on the bilayer heterojunction organic solar cells have been conducted around the globe for the past few decades (Young Kim et al., 2008; Kymakis, Koudoumas, & Franghiadakis, 2006; Petritsch et al., 2000). For example, bilayer heterojunction based on pentacene/fullerene C_{60} bilayer heterojunctions have been fabricated by Yang et al. in 2007. They investigated the effect of the crystalline domain size of the pentacene on the device performance by controlling the deposition rate. Their devices showed improved power conversion efficiency from 0.49% to 1.2% in the evaporation rate range from 5Å/s to 0.5Å/s. The slower evaporation rate was suggested to create larger crystalline domains and less amorphous domains in the deposited film compared to the faster evaporation rate. This change in film morphology has given a great impact on the exciton dissociation at the donor/acceptor interface, charge mobilities, and hence directly affect the device performance (J. Yang & Nguyen, 2007).

In 2008, Sule Erten and Siddik Icli reported a bilayer heterojunction organic solar cell with a fill factor of 0.51 and power conversion efficiency of 0.54%. Their device composed of self-synthesised naphthalene bis-benzimidazole (N-CON) as electron acceptor (electron transport material) and zinc phthalocyanine (ZnPc) as electron donor (hole transport material). They deposited the active layers by successive evaporation on the glass substrates coated with ITO. Their device structure is ITO/PEDOT: PSS (80nm)/ZnPc (60nm)/N-CON (40nm)/Al (70nm). Due to the thermal and photostable properties of N-CON, the device was stable under illumination conditions. They found that the thickness of p-n heterojunction layers probably do not cause the extreme electrical shorting-out between two electrodes (Erten & Icli, 2008).

In 2011, Kekuda's group reported a fill factor 0.64 and power conversion efficiency up to 3.65% using regioregular poly(3-hexylthiophene) (P3HT) as electron donor and fullerene C_{70} as electron acceptor. Four types of solvents with different boiling point namely chloroform, xylene, 1, 2-dichlorobenzene (DCB) and 1, 2, 4-trichlorobenzene (TCB) were used for P3HT thin film growth. They suggested that high boiling point solvents provide sufficient time for the P3HT crystallisation process, which can facilitate a highly crystalline growth. The XRD results confirmed that the slow evaporation of the solvent has led to a better crystallisation, stronger inter-chain interaction and well defined crystalline peaks. Higher degree of crystallisation creates larger crystallite size in the processed films in which increases the surface roughness hence can provide larger interface area. They claimed their device with the device configuration ITO/PEDOT: PSS/P3HT/C_{70}/Al has the highest power conversion efficiency reported so far for the bilayer heterojunction OPVC (Kekuda et al., 2011).

2.2.3 Bulk heterojunctions organic photovoltaic cell

The bulk heterojunction OPVC is a single layer device similar to the organic Schottky solar cell. Nevertheless, the bulk heterojunction OPVC composed of the mixture of the donor and acceptor materials instead of one material in a single layer device. It still adapts the p-n junction concept as the bilayer heterojunction OPVC. This type of device can be achieved by either co-evaporation of donor and acceptor pigments (using thermal evaporation technique) or mixture of donor and acceptor (using solution based of spin coating technique). Figure 2.9 shows the schematic structure of a bulk heterojunction OPVC.

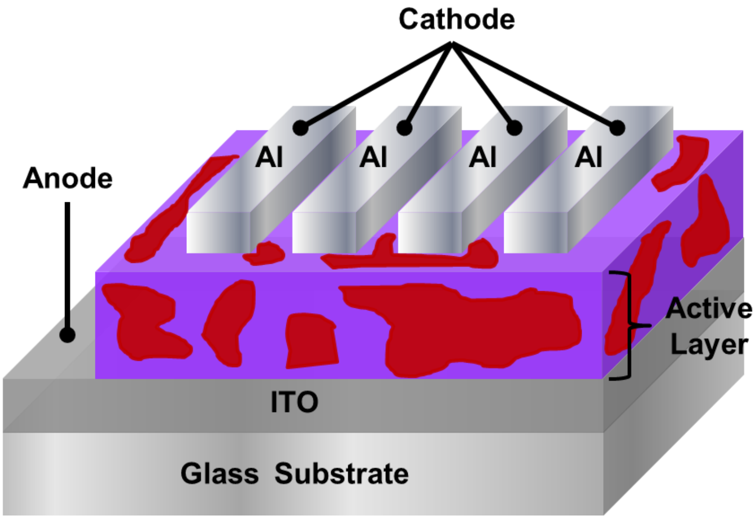

Figure 2.9 Schematic representation of a bulk heterojunction OPVC structure.

The primary advantages of this structure are the large donor-acceptor interface area (J. Yang & Nguyen, 2007) and relative short diffusion path of the charge carriers to the electrodes. The probability of exciton dissociation increases due to the large donor-acceptor interface area and therefore leading to a higher efficiency output. Unlike the bilayer heterojunction OPVC which the charge separation is limited to a single donor-acceptor interface region, the exciton dissociation can occur almost everywhere throughout the active layer of the bulk heterojunction OPVC. Most of the separated charges in the bulk heterojunction OPVC can diffuse to the electrodes within a relatively short distance compared to the bilayer heterojunction OPVC. Hence, better performance of bulk heterojunction OPVC over bilayer heterojunction OPVC can be expected. However, the disordered phase-separated interpenetrating network might trap or increase the recombination probability of the travelling charges. Besides that, the bulk heterojunction OPVC requires sensitive control over materials morphology since the surface morphology can have a drastic effect on the performance of the device. The choice of materials, solvents and donor-acceptor weight ratio are others factors that can dramatically affect the efficiency of the device. Therefore, optimisations of such great number of variables are the challenges to the researcher.

A lot of works have been done on the bulk heterojunction OPVC especially for the fullerene and polythiophene blend (Bricaud, Cravino, Leriche, & Roncali, 2009; Gupta, Bag, & Narayan, 2008; Kaur, Gopal, Davis, & Heflin, 2009; Zhou, Cheun, Choi, Fuentes-Hernandez, & Kippelen, 2011), since it has been considered as the most effective structure and device that currently available in organic photovoltaic cell.

In 2009, Park et al. reported a power conversion efficiency of 6.1% for their OPVC using poly[N-900-hepta-decanyl-2, 7-carbazole-alt-5, 5-(40, 70-di-2-thienyl-20, 10, 30-benzothiadiazole) (PCDTBT) in bulk heterojunction composites with the fullerene derivative [6,6]-phenyl C_{70}-butyric acid methyl ester ($PC_{70}BM$). They acquired a short circuit current density of $10.6mA/cm^2$, an open circuit voltage of 0.88V, a fill factor of 0.61 under air mass 1.5 global (AM1.5G) irradiation of $100mW/cm^2$. They claimed their device has the internal quantum efficiency approaching 100%. This implies that every photon absorbed leads to a separated pair of charge carriers and that every photogenerated mobile carrier was collected at the electrodes. Their achievement is attributed to the introduction of optical spacer between the photo-active layer and the top electrode. The optical spacer such as titanium suboxide (TiO_x) redistributed the maximum light intensity to be within the active charge separating bulk heterojunction layer (S. H. Park, et al., 2009).

A bulk heterojunction OPVC based on a poly[4, 8-bis-substituted-benzo [1, 2-b: 4, 5-b’] dithiophene-2, 6-diyl-alt-4-substituted-thieno [3, 4-b] thiophene-2, 6-diyl] (PBDTTT) polymer derivative and $PC_{70}BM$ was fabricated. Utilising this novel polymer of PBDTTT, the device with an active area of $\sim0.1cm^2$ produced a fill factor of 0.67 and achieved power conversion efficiency as high as 7.73% (Chen, et al., 2009). Such a high efficiency was reported to be associated with combining advantages of a low HOMO level (high V_{oc}) and long wavelength absorption (high J_{sc}) in the polymers.

2.2.4 Organic multilayer/tandem photovoltaic cell

An organic tandem photovoltaic cell is equivalent to a multilayer photovoltaic cell which is comprised of the superposition of two or more distinct devices forming multiple junctions with complementary absorption spectra. Each of the sub cells in the device is based on donor-acceptor composite and can be connected either in series or in parallel (Ameri, Dennler, Lungenschmied, & Brabec, 2009; Bruder et al., 2009; J. Y. Kim et al., 2007). Usually, a recombination layer is inserted between the two sub cells interface to provide a medium for the charges recombination in order to allow the charges to diffuse through the active layers and collect by the electrodes. The recombination layer is likely to be ultrathin layer (≤10nm) of conductive metal such as titanium suboxide (TiO_x) and silver (Ag) (J. Y. Kim, et al., 2007; Triyana, et al., 2005). Figure 2.10 represents a typical organic tandem solar cell.

The tandem approach offers a number of advantages over the other architectures device. First, the absorption spectrum of organic semiconductors usually is not made of a continuum like it is in inorganic semiconductors. Therefore, a combination of various different materials enables absorption over a broad range of photon energies within the solar emission spectrum which leads to higher power output. Secondly, an increase in the thickness of the active layer increases the internal resistance of the device due to the low mobility of the charge carriers in the organic semiconductors. The internal resistance reduces the open circuit and fill factor of the device. The tandem architecture is able to offer higher optical density over a wider range of absorption spectrum than a single cell without increasing the internal resistance of the device. Furthermore, as the two sub cells are connected in series, the open circuit is likely the sum of the open circuit of the individual cells (Ameri, et al., 2009; Bruder, et al., 2009; J. Y. Kim, et al., 2007).

In 1990, Hiramoto and his group did the pioneering work to introduce the organic tandem solar cell by stacking two heterojunction devices (Hoppe & Sariciftci, 2004; Persson & Inganäs, 2006; Spanggaard & Krebs, 2004). Later on, a numerous of research has been conducted on this type of device architecture and the results have shown promising progress. In 2000, Takahashi et al. fabricated a three layer organic tandem solar cell yielded an open circuit voltage of 0.39V, a fill factor of 0.51 and a power conversion efficiency of 3.51% when the device was irradiated with 445nm monochromatic light of 12µW/cm^2 intensity (Takahashi, Kuraya, Yamaguchi, Komura, & Murata, 2000). In 2005, Kuwat Triyana and his co-workers fabricated tandem devices using perylene derivatives and phthalocyanine derivatives. Their optimised device showed a fill factor of 0.34, an open circuit voltage of 1.10V and power conversion efficiency of 1.38% (Triyana, et al., 2005). Recently, a few researchers have made highly efficient organic tandem solar cells that achieved power conversion efficiency more than 5%. For example, Cheyns et al. in 2010 made a device with relatively high open circuit voltage of 1.92V, a fill factor of 0.62 and a power conversion efficiency of 5.15% (Cheyns, Rand, & Heremans, 2010). In the same year, Sista et al. successfully acquired a power conversion efficient of 5.84% for their device with an open circuit voltage of 1.25V and a fill factor of 0.63 (Sista et al., 2010).

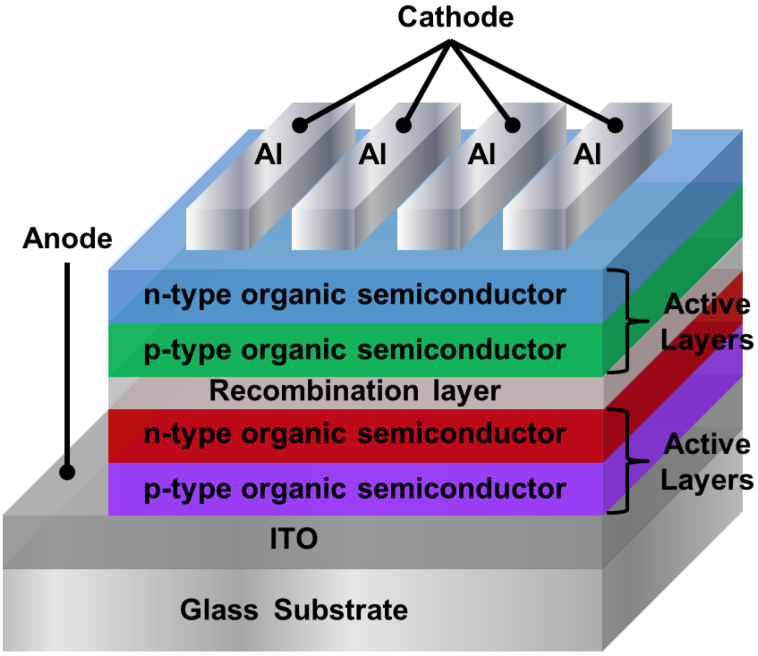

Figure 2.10 Schematic structure of a tandem OPVC.

2.3 Basic Working Principles of Organic Photovoltaic Cell

The process of photon energy conversion into electricity involved in four steps:

1. Light absorption and excitons formation
2. Excitons diffusion
3. Excitons dissociation
4. Transportation of charges to electrodes

The photoconversion mechanism of the organic photovoltaic cell is different from the conventional inorganic photovoltaic cell. Free electron hole pairs are generated immediately upon light absorption in inorganic photovoltaic cell while in organic photovoltaic cell, the light absorption causes the generation of excitons. It is not a free electron hole pair. An exciton or also called mobile excited state is a bound state of an electron and a hole which are attracted to each other by their electrostatic Coulomb attraction force. It is considered as an electrically neutral quasiparticle.

An exciton forms when a photon with energy, hν equal or larger than the energy band gap, E_g of a semiconductor absorbed in the organic semiconductor. The difference in the energy levels of the Highest Occupied Molecular Orbital (HOMO) and Lowest Unoccupied Molecular Orbital (LUMO) is the energy band gap of the organic semiconductors. The absorbed photon excites the electron from the HOMO to the LUMO of the organic semiconductor. As a result, this leave behind a localized positively charged hole. The electron in the LUMO is then bounded by the Coulomb attraction force of this localized hole. This attraction provides a stabilizing energy balance. Therefore, the exciton has slightly less energy than the unbound electron and hole. The exciton can be dissociated to free electron hole pair by a sharp drop of potential at the donor-acceptor interface (or called heterojunction) of the photovoltaic cell. In order to generate the separated positive and negative charges, the excitons need to diffuse through the active layer to the heterojunction where they can dissociate. Since the excitons are electrically neutral, their motion is not influence by any electric field and they diffuse by random hops. The excitons have short diffusion length (~10nm-20nm). It is importance for the excitons to reach to the interface before they decay back to the ground state. Hence, the thickness of active layers in the device plays a key factor in the performance of the solar cell.

Once the excitons have separated, the separated charges need to be collected at the electrodes to contribute as the photocurrent. As the active layers of the device are sandwiched between two electrodes with different work function, the built-in potential in the active layers results an electric field that assist the transport of the charges. By applying an external bias, the charge carriers can be collected with the efficiency depending on their mobility (Kippelen & Bredas, 2009). Electrons in the donor materials travel to the acceptor LUMO and then reach to the cathode. Holes in the acceptor in the other hand, firstly travel from HOMO of acceptor to the HOMO of donor and then collected at the anode.

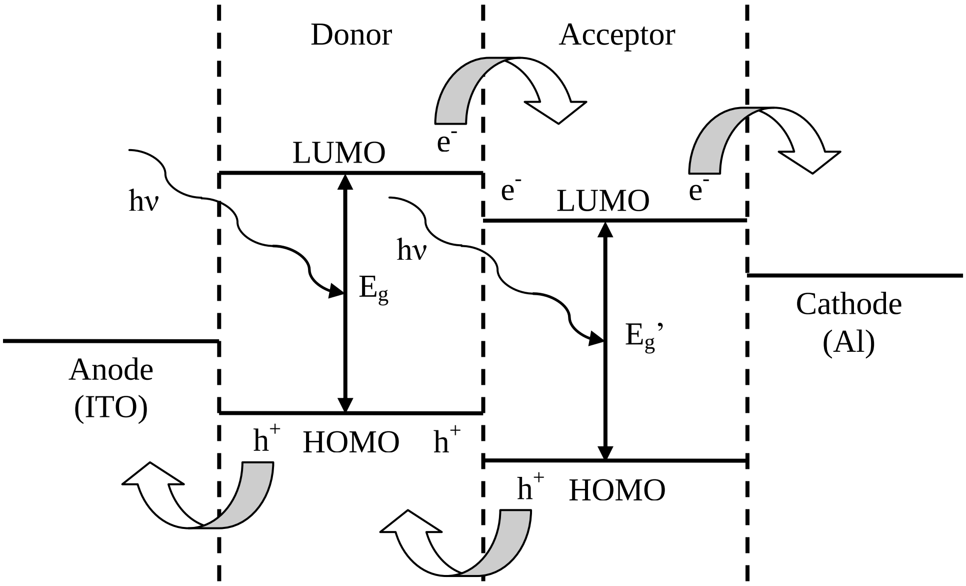

Figure 2.11 Photons with energy, hν equal or larger than the band gaps, E_g (Acceptor) or E_g' (Donor) excited the electrons from the HOMO to the LUMO leaving holes behind in the HOMO. Electrons are collected at the anode and holes transported to the cathode.

2.4 Performance Analysis

Although the working principle of organic photovoltaic cell is different from the inorganic counterpart but the performance analysis of the OPVC based on inorganic semiconductor photodiode still can be adapted. The current density-voltage characteristic (J-V curve) is used to analyse the performance of an OPVC. The scheme of typical J-V curve of an organic solar cell is shown in Figure 2.12. The OPVC shows diode behaviour in the dark condition. When the organic photovoltaic cells are exposed to light, the J-V curve is shifted downward generating a photovoltaic effect. Based on the characteristics represented in Figure 2.12, valuable information of the OPVC such as open circuit voltage, V_{oc}, short-circuit photocurrent density, J_{sc} and the largest power output, P_{max}, fill factor, FF and power conversion efficiency, PCE can be determined. The open circuit voltage, V_{oc} is the maximum voltage across an illuminated photovoltaic cell when no current is flowing (J_{sc}=0). The electrodes of the OPVC seem like open circuited device (zero current). Hence, the V_{oc} can be determined at the interception of *x*-axis in the J-V graph. The origin of the V_{oc} is still under intensive debate among the scientific community. Some scholars suggested that the V_{oc} of the cell depends on the energy difference between the ionization potential of the D component ($HOMO_D$) and the electron affinity of the A component ($LUMO_A$) forming the heterojunction (Brovelli, et al., 2007; Hoppe & Sariciftci, 2004; Kippelen & Bredas, 2009).

Open circuit voltage, $V_{oc} \approx \Delta(HOMO_D) - (LUMO_A)$ (Equation 2.1)

The short circuit current density, J_{sc} is the current that flow through an area per second when the solar cell is illuminated and the voltage applied across the device is zero (V=0) (i.e. the electrodes are short circuited). Therefore, the J_{sc} can be obtained at the interception of *y*-axis in the J-V graph. The largest power output, P_{max} of the OPVC is determined by the point where the product of voltage and current is maximized (V_{max} and J_{max}).

$$P_{max} = V_{max} \text{ x } J_{max} \qquad \text{(Equation 2.2)}$$

This can be done by plotting a power versus voltage (P-V) graph as shown in Figure 2.12 to search for the maximum power output, P_{max} at the maximum voltage, V_{max}. The power output of the OPVC firstly increases with the applied voltage until reaches a maximum point, then starts to decrease rapidly to zero around the value of V_{oc}. The maximum point in the P-V graph corresponds to the maximum power output, P_{max} and the maximum voltage, V_{max} of the device as shown in Figure 2.13. Division of P_{max} by the product of J_{sc} and V_{oc} yields the filling factor, FF as shown in Equation 2.3:

$$FF = P_{max} / (J_{sc} \text{ x } V_{oc}) \qquad \text{(Equation 2.3)}$$

The fill factor of the solar cell is defined as the ratio of the actual maximum obtainable power (V_{max} x J_{max}) to the theoretical power (J_{sc} x V_{oc}) of the cell. An ideal solar cell has a FF equally to 1. As a simple view, the FF is a parameter allows the researchers inspect the quality of the manufactured cell compare to the ideal cell.

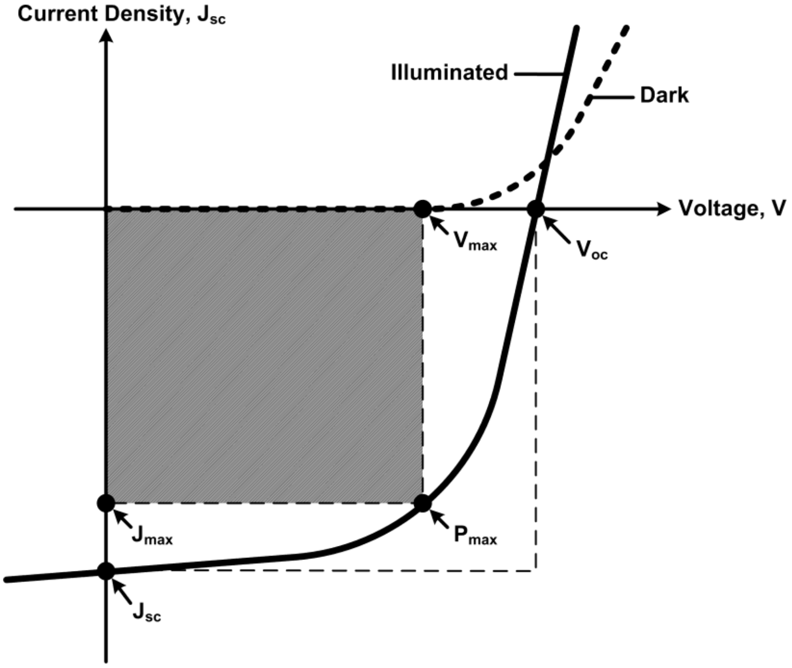

Figure 2.12 The current-voltage curve (J-V curve) of an organic photovoltaic cell under dark condition (dash line) and illuminated (full line).

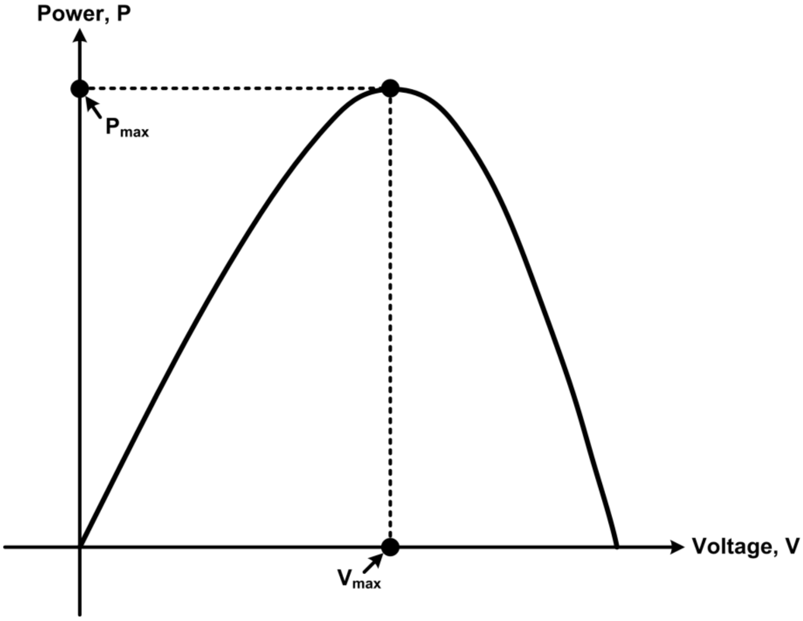

Figure 2.13 The power-voltage curve (P-V curve) of an organic photovoltaic cell under illuminated radiation.

The power conversion efficiency (PCE) is defined as:

$$PCE = P_{out} / P_{in} = P_{max} / P_{in} = (J_{sc} \times V_{oc} \times FF) / P_{in} \qquad \text{(Equation 2.4)}$$

To determine the PCE of an OPVC, the P_{max} needs to be compared with the power output of the incident light, P_{in}. PCE simply is a measurement the amount of power produced by a solar cell relative to the power available in the incident solar radiation, P_{in} (The ratio of power output to power input). For a standard measurement, a simulated air mass 1.5 (AM1.5) illumination with intensity of 100mW/cm^2 is utilised to determine the PCE of an OPVC. An AM1.5 illumination defines as the solar radiation travelled through 1.5 times atmosphere thickness corresponds to a zenith angle of z = 48.2° relative to the normal of the Earth's sea level.

Chapter 3

Experimental Techniques

3.0 Overview

Chapter 3 describes the processes involved in OPVC fabrication in this research including substrate preparation (cutting and etching), substrate cleaning, solution preparation, thin films deposition and electrodes deposition. The J-V characteristics' measurements to determine the performance of the device are also discussed. Measurements of the thin films are explained in this chapter including absorption properties, thickness and surface morphology by performing UV-VIS-NIR spectroscopy, AFM and FESEM. Furthermore the characterizations on the semicrystalline structure and chemical bonding of the prepared organic semiconductor thin films by XRD and FTIR spectroscopies are illustrated.

Figure 3.0 shows the flow of the OPVC fabrication procedures used in this research study. In this chapter, detail descriptions about the processes involving in OPVC fabrication will be discussed. Illustrations of device fabrication systems such as thermal evaporator and characterisation systems such as Jasco V-570 UV-VIS –NIR spectrometer, KLA Tencor P-6 Surface Profilometer, Siemens D5000 X-ray Diffractometer, et cetera will be shown. Furthermore, brief descriptions on the processes or mechanisms involved in the characterisation systems will be provided.

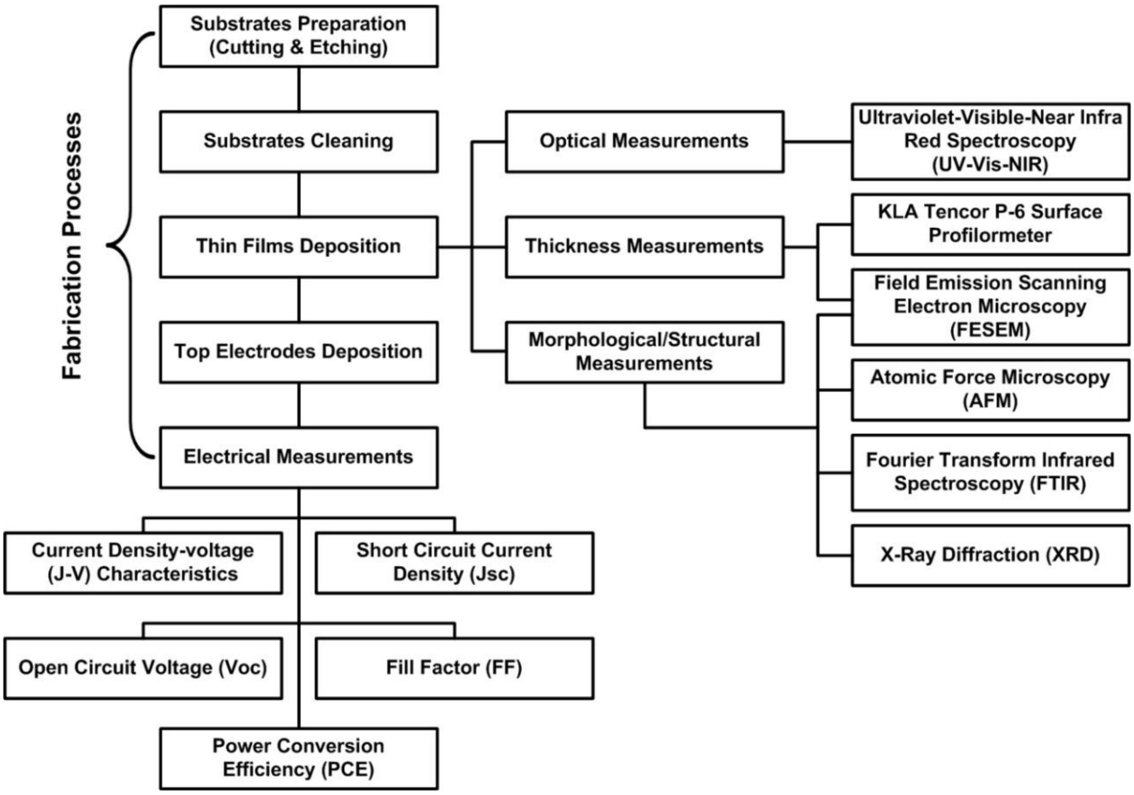

Figure 3.0 Flow chart of the OPVC fabrication processes and measurements.

3.1 Substrate Preparation: Cutting and Etching

OPVC requires a solid substrate to provide a base support for the organic thin films. It also provides some degree of protection to the device. Transparent glass and quartz substrates are being used to deposit the organic thin films for optical and surface morphology characterisations. Semitransparent indium-tin-oxide (ITO) coated glass substrates are being used to fabricate OPVC. The conducting ITO layer acts as an anode for the device. Those ITO substrates must be etched to form a pattern in order to avoid short circuit in the device. In the application of OPVC, transparent or semitransparent substrates are preferable in order to allow the light to be absorbed by the organic thin films. Nevertheless, opaque substrates such as silicon also have their usefulness in the organic thin films characterisation measurements for example Fourier Transform Infrared (FTIR) spectroscopy. Therefore, preparation of silicon substrates will be included in this section. In this research, all the glass, ITO and silicon substrates were cut into 2.5cm x 2.0cm in dimension. The reason to do so is because a specific device architecture had been designed as schematically shown in Figure 3.1. The shadow masks for electrodes deposition as shown in the Figure 3.9 and the sample holder for the J-V characteristics measurements as shown in Figure 3.2 were designed based on this device architecture. Consequently, a specific dimension of the substrates is required to fit into the designed masks and sample holder. The following sections elaborate the cutting technique for three types of substrates and etching process for the ITO substrates.

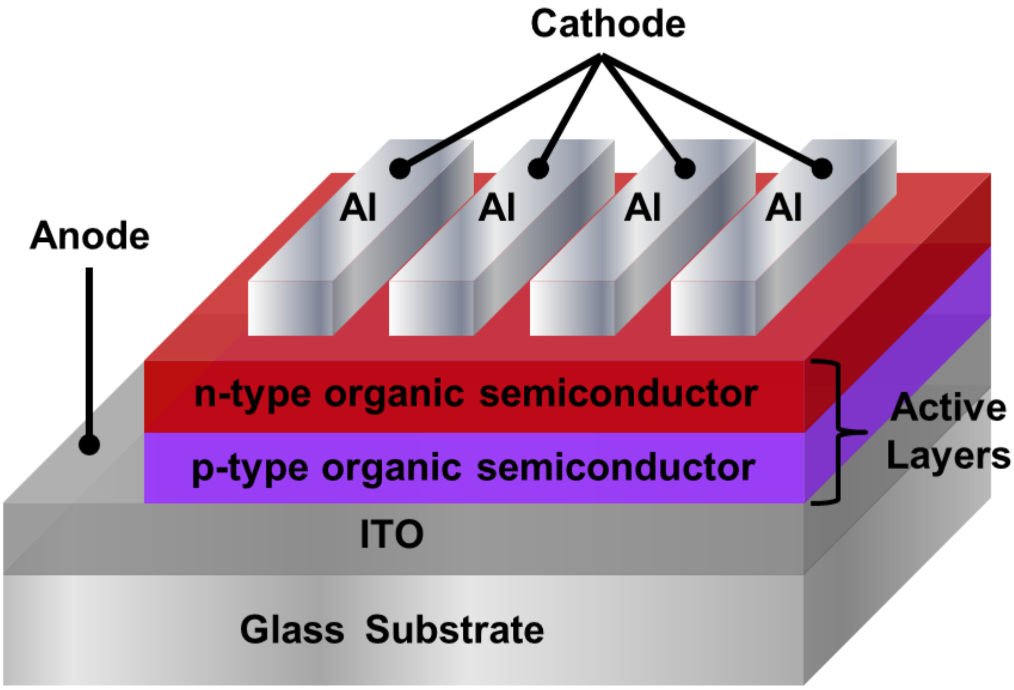

Figure 3.1 Schematic structure of a bilayer heterojunction OPVC.

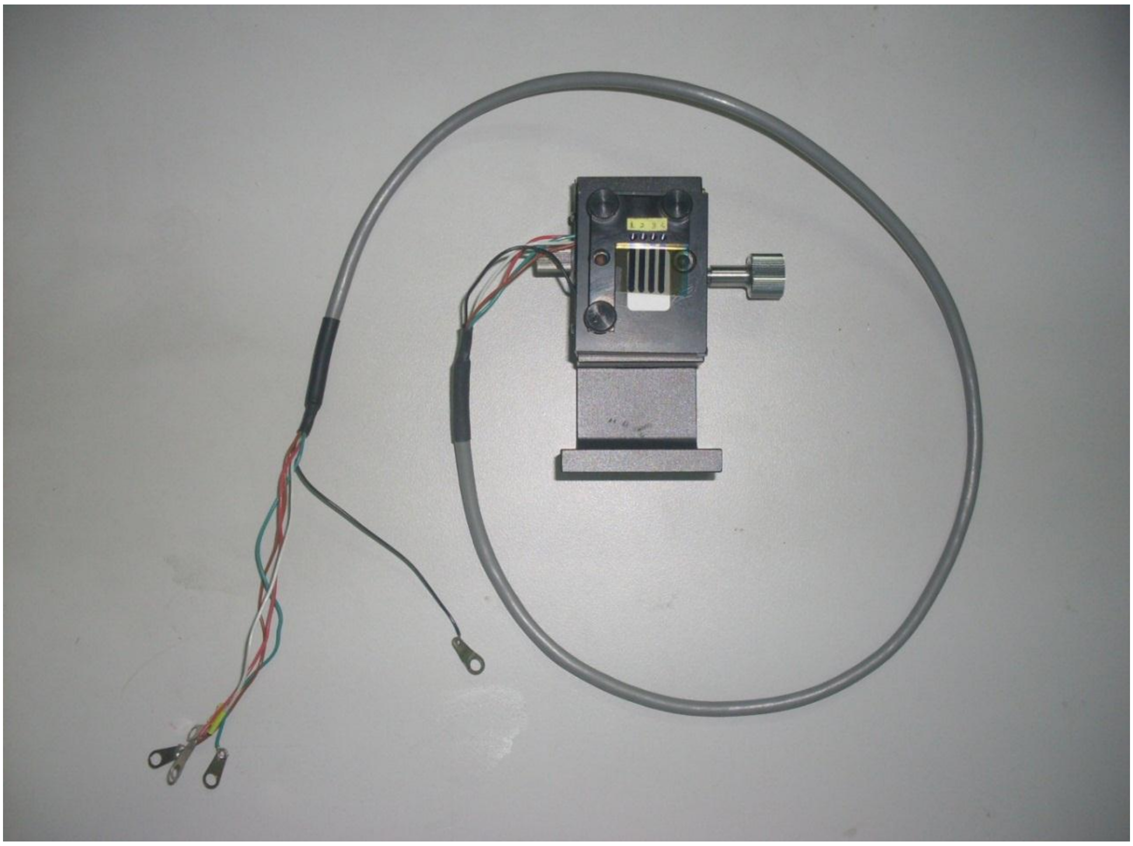

Figure 3.2 J-V characteristics measurement sample holder.

3.1.1 Substrates cutting techniques

Ordinary 7.6cm x 2.5cm microscope glass slides were used as the solid glass substrates for thin film deposition. Quartz substrates were prepared by 7.6cm x 2.5cm quartz slides that purchased from Magna Value Sdn. Bhd. ITO coated glasses purchased from LGC Scientific Sdn. Bhd. were about 47cm x 36.5cm in dimension. Therefore, extreme precautions are needed to prevent cracking the large area ITO glasses while cutting using a glass cutter. 6’ silicon wafers which purchased from Function Technologies Sdn. Bhd. were used to prepared silicon substrates. Three types of glass cutter are available in the market and use in this study: diamond glass cutter, tungsten carbide wheel glass cutter and pen-like tungsten carbide glass cutter. A pair of gloves, a mask and a goggle was used to protect any injury to eyes and hands that may cause by the glass shreds. Then a 2.5cm x 2.0cm rectangular shape or straight line was drawn on a piece of A4 size paper. This rectangular shape or straight line was used as a guide in the cutting process of the transparent glass and ITO substrates. The glass slide/quartz slide/ITO coated glass was located on the drawn shape/straight line. For silicon wafer, the desire shape can be drawn on the back side (rough surface) of the silicon wafer. By following the drawn line, the glass cutter's tip was pressed tightly against the glass/wafer and a straight line was scribed with the help of a ruler to form a split on the surface of the glass/wafer. This surface defection was used as the breaking point of the glass/wafer when an unbalance pressure was applied on the different sides of the glass/wafer surface along the scribe line. The different pressure was applied at the opposite side of the scribed line to bend and break the glass/wafer to the specific dimension of 2.5cm x 2.0cm substrates. Finally, the glass and silicon substrates were inserted in a clean container and stored in a dry box for cleaning process. The ITO substrates need to be etched to form a pattern before the cleaning process. The ITO etching procedure is described in the next section.

3.1.2 ITO substrates etching process

Initially, the ITO layer was coated with nail polish to cover an area of 2.5cm x 1.4cm in dimension as shown in Figure 3.3 (a). Then the coated ITO substrates were inserted into a beaker containing a diluted hydrochloric acid, HCl solution (H_2O: HCl =10: 1) and the solution was boiled at 70°C for 30 minutes on a hot plate. The boiling of the diluted HCl solution was taken place in a fume cupboard because the vapour of HCl was harmful. The exposed area (the uncoated area) of ITO layer was etched by the boiled HCl solution and therefore left behind a plain glass area as shown in Figure 3.4 (b). The purpose to have an etched area is to prevent short-circuiting the later fabricated device when taking the J-V characteristics measurements using the contact probes. After the etching process, the nail polish layer was rubbed off gently from the surface of glass using acetone solvent with the help of a cotton bud. The ITO area without went through the etching process was still intact coated onto glass substrate and act as the anode for the device. Then the ITO substrates were sonificated in the acetone for 5 minutes to remove the remaining traces of nail polish and this processes were repeated several times to remove the traces of nail polish completely. The etched ITO substrates can be stored in a clean container for further cleaning process.

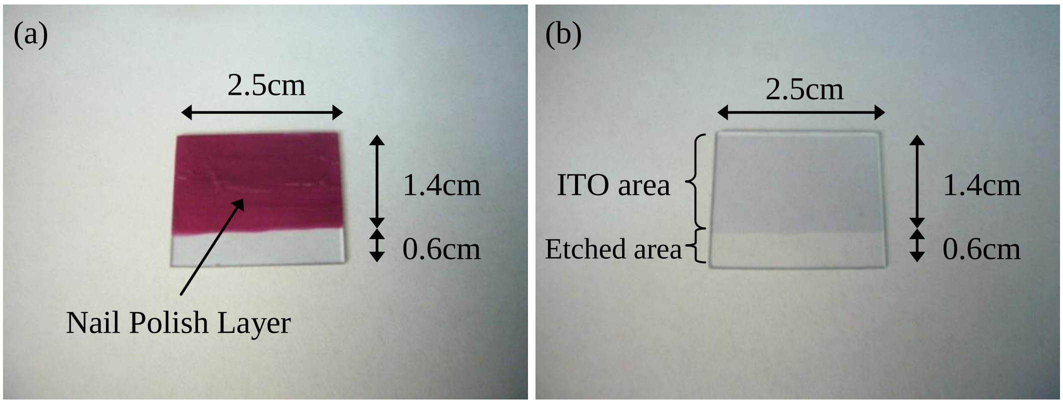

Figure 3.3 (a) ITO substrate coated with nail polish (red colour). (b) Etched ITO substrate.

3.2 Substrates Cleaning Process

All substrates must be considered as contaminated. Cleaning process is required to remove the traces of organic, inorganic and ionic contaminants. These contaminants can be oil, grease, dust particles, fabrics, oxide layer, ions, et cetera. They can give huge impact on the performance of the device by affecting the optical properties, electrical properties and surface morphology of the thin films and even may be alter the adhesiveness of the thin films on the substrates. Proper cleaning of substrates prior to OPV application is critical to the success of OPVC. Therefore, the following cleaning condition must be followed prior to application. It can be considered as the initial stage of the OPVC fabrication process and it is essential. Below are the descriptions of cleaning process for three types of substrates.

3.2.1 Glass, quartz and ITO substrates

The glass, quartz or ITO substrates were cleaned in a diluted Decon detergent (concentration of Decon: deionised water (DI) = 1: 300). The substrates were soaked in the diluted Decon solution about 5 minutes to remove particles and any organic substances. Then, the substrates were rinsed with DI water to remove the Decon detergent. After that, the substrates were sonificated in acetone solvent about 5 minutes to remove oil traces and residues from the substrates surface. The substrates were rinsed with DI water to remove acetone. Subsequently, the substrates were soaked in ethanol/isopropanol to remove any organic compounds that remaining on the substrates surface. Then, the substrates were rinsed again with DI water to remove ethanol/isopropanol. Finally, the substrates were cleaned by blowing the dry nitrogen gas (N_2). Those cleaned substrates were stored in a clean container in a dry cabinet for further use.

3.2.2 Silicon substrates

Firstly, the substrates were rinsed with DI water. After that, the substrates were immersed in the solution of H_2O: H_2O_2: NH_4OH (5: 1: 1) and boiled at 80°C for 10 minutes to remove organic contaminants. This treatment results in the formation of a thin silicon dioxide layer (≈10Å) on the silicon surface along with a certain degree of metallic (ionic) contamination that shall be removed in subsequent steps. The substrates then rinsed with DI water to remove the NH_4OH solution. Then, short immersion was carried out on the substrates in the H_2O: HF solution (50:1) to remove the thin oxide layer and some fraction of ionic contaminants. After that, the substrates were immersed and boiled in the solution of H_2O: H_2O_2: HCl (6: 1: 1) at 80°C to effectively remove the remaining traces of ionic contaminants. Immersion in the acids helps to neutralize NH_4OH which is alkaline. Finally, the substrates were rinsed with DI water to remove the acids and blew dry by N_2 gas. The silicon substrates were put in a clean container and stored in the dry cabinet for further use.

3.3 Solution Preparation

To prepare the solution for an organic semiconductor, the material was weighted using an analytical balance. Next, the weighted material was poured into a 10ml volumetric flask. The organic solvent was measured using a graduated cylinder/measuring cylinder. After precise volume was measured, the solvent was poured into the flask. Then the flask was inserted into a sonicator and let the sonification process took place for about 10-30 minutes. After the sonification, the organic semiconductor and the organic solvent should be mixed. The prepared solution was now ready to be used.

3.4 Thin Film Deposition

Among all the fabrication processes, thin films deposition can be considered as the most important process because the deposited thin films are used as the active layers. Various thin film deposition techniques are available for OPVC fabrications nowadays for example spin coating, vacuum thermal evaporation, molecular beam epitaxy (MBE), doctor blading, roll-to-roll printing, inkjet printing, et cetera. However, only two techniques were used throughout this study, namely spin coating and vacuum thermal evaporation techniques. Spin coating technique is highly recommended for the organic semiconductors that can be dissolved in organic solvents because the ease of use of this technique. In addition, this technique not only significantly shortens the process time (only a few second per coating), it also allows the user to deposit high uniformity films over the surface of the substrates. This technique is preferable for OPVC fabrication since the surface morphology of the thin film plays an important role in the performance of the device. Besides that, spin coating allows the user to precisely control the desire thickness easily by controlling the viscosity of the solutions, the rotational speed and duration of the substrates. The thickness of the active layers in the OPVC also affects the efficiency of the device due to the short mean free path of the electrons (≈10nm). Another advantage of spin coating is that this method consumes a very small amount of expensive organic semiconductors. It is a low cost and low volume operation. Therefore, large quantity of devices can be fabricated out of small amount of materials. This factor cut the production cost of the OPVC greatly. PEDOT: PSS layer and VOPcPhO layer were deposited by utilizing the spin coating technique.

PTCDA layer and Al top electrodes were deposited by vacuum thermal evaporation method. The reason the PTCDA layer was deposited by vacuum thermal evaporation instead of spin coating method due to the extremely poor solubility of PTCDA in any organic solvents. So far, none organic solvent that has been tested can completely dissolve PTCDA. The following section elaborates these two deposition methods' procedure step by step.

3.4.1 Spin coating procedure

A Laurell WS-400B-6NPP-Lite spin coater was used to deposit the thin films. The spin coating was performed in the 1K clean room environment. Figure 3.4 shows the schematic steps of the spin coating technique.

This spin coating process to form a thin film onto the substrate surface was started by mounting the substrate horizontally on the rotation platform of the spin coater. Then, the vacuum pump was turned on so that suction sucked the substrate on the platform to prevent it from dangerously spun off while high rotation speed was applied on the substrate. Using a syringe, an excess amount of the selected material solution (50ml-75ml) was dispensed onto the rotating substrate. The high rotation speed spread the solution by a centrifugal force. Such rotation continued for a duration set by the user on the spin coater. Usually, the applied solvent was volatile and simultaneously evaporated during the rotating process. After the solvent evaporated, a uniform thin film with the desired thickness has been coated onto the substrate. As mentioned before, the thickness of the thin film depends on its solution viscosity as well as the spin coater condition of rotation speed and spin duration. In this experiment, PEDOT: PSS was spun at 6000 rotations per minute (rpm) for 30 seconds. At this rotation speed and duration, PEDOT: PSS formed an ultrathin film around 20-40nm. VOPcPhO was spun at 2000rpm for 30 seconds to achieve ≈80nm thin film of VOPcPhO on the substrate. Finally, the vacuum pump was turned off and the material coated substrate was carefully picked up using a tweezers. Then, the thin film coated substrate was placed in a clean container for further process and characterization.

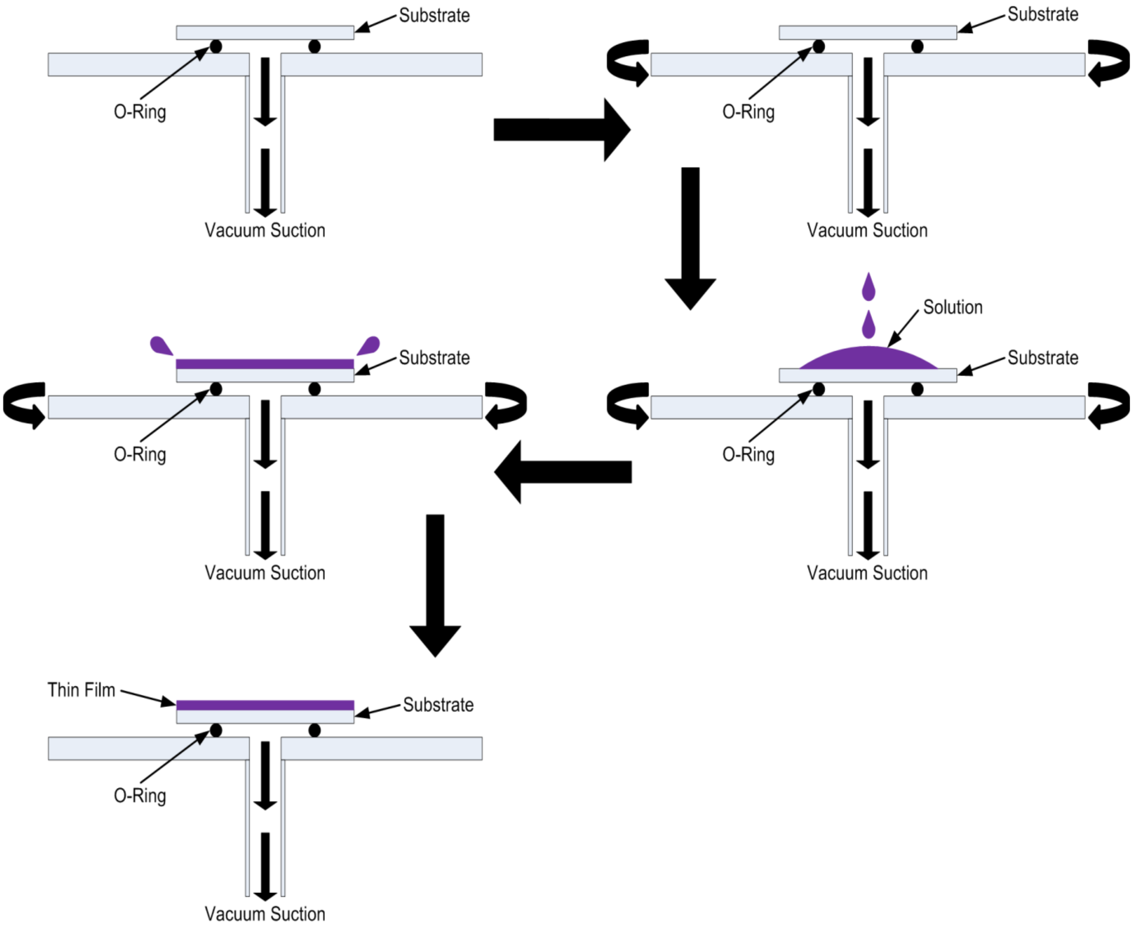

Figure 3.4 Schematic processes of the spin coating technique.

3.4.2 Vacuum thermal evaporation procedure

PTCDA was deposited onto the solid substrates by vacuum thermal evaporation technique. A new homemade thermal evaporator was specially built in order to perform the vacuum thermal evaporation of PTCDA to form thin films. The detailed description and illustrations of the homemade thermal evaporator are shown in section 3.4.3. The PTCDA was purchased from Sigma Aldrich in the powder form. This PTCDA powder was carefully weighted using an analytical balance. Only small quantity of powder was needed (10mg) to form PTCDA thin films. The correctly weighted powder was poured into a clean quartz evaporation boat and placed inside the thermal evaporator. In this case, a helical tungsten wire which was connected to the copper electrodes was used to heat up the quartz boat. The next was the preparation of the substrates onto the shadow mask/holder at the bottom of the top plate of the evaporator vacuum chamber. The distance between the evaporation source and the substrates play an importance role in the uniformity of the thin films coated onto the substrates. It was found that the ideal distance between the evaporation source and the substrates was around 12cm-15cm. After that, the chamber was closed and sealed properly. By turning on the pumps, the system started to increase the vacuum level. A high vacuum level below 5 x 10^{-5}mbar in the chamber was required to prevent the PTCDA powder oxidises during the heating process. When the pressure reached 5 x 10^{-5}mbar, then the evaporation process can be started by turning on the power source. A voltage regulator was utilised to supply sufficient current to the copper electrodes of the thermal evaporator. The current flow in the helical tungsten wire heated up the wire by a resistive heating. Through conduction and radiation, the heat transfer to the quartz boat and consequently heated up the PTCDA powder inside. The sublimation temperature of PTCDA was about 270°C. When the boat temperature reaches 270°C, PTCDA started to evaporate inside the chamber. The shutter was opened to allow the evaporating PTCDA particles travelled up to the substrates and condensed on the relatively cold surface of the substrates. The rate of the evaporation needed to be controlled to a very slow rate of 0.1-0.5Å/s. The evaporation rate can be controlled by controlling the vacuum level at around 5 x 10^{-5}mbar and the current at around 32A. The slow evaporation rate can assure no overheating occurred which might carbonise the PTCDA powder. Besides that, a uniform thin film can be obtained by utilising a slow evaporation rate. The thickness monitor was used to control the thin film thickness by a sensor. When the desire thickness was obtained, the shutter immediately closed. Then, the voltage regulator was tuned back to zero voltage to cut off the current flow into the tungsten wire and the power supply was turned off. The chamber should be allowed to cool down for about 20 minutes before it can be opened. Finally, the material coated substrates were taken out from the evaporator and placed in the electrodes deposition shadow mask for the electrodes deposition process.

3.4.3 Vacuum thermal evaporator

In this research project, a new homemade thermal evaporator was built and its photograph is shown in Figure 3.5 to deposit the PTCDA material. This section illustrates the architecture and the functionality of the various parts of the homemade vacuum thermal evaporator. Vacuum thermal evaporator is the system that being used to perform a thermal evaporation process that sublimates a material to form a thin film onto the substrates under a vacuum condition. Generally, a vacuum thermal evaporator consists of a chamber, a vacuum pump system and a power source system. The chamber is a hard casing make from either metal or glass with an enclosed space where the material is evaporated. In this study, a stainless steel metal was used to build a chamber. Either electrical component that was used to evaporate the materials (copper electrodes) or monitor the evaporation process (thickness monitor, thermocouple, et cetera) was built in this chamber. This vacuum system was equipped by the combination of two different types of vacuum pumps. The first pump was utilised to pump down the chamber from an atmospheric pressure to a low pressure state (< 10^{-2}mbar). This first pump of a dry diaphragm pump was used to achieve a pressure level of only about 10^{-2}-10^{-3}mbar. Hence, a second pump was required to pump the chamber to a high vacuum level (<10^{-4}mbar). In this case, a turbo molecular pump was utilised as the secondary pump. The total cost of this vacuum thermal evaporator was estimated to around RM60k.

The thermal evaporator chamber was designed with two round glass view ports for different angle viewing. The design of the chamber casing is illustrated in Figure 3.6. The top plate of the chamber consists of a shutter. A shadow mask or sample holder was screwed at the bottom centre of the top plate. The design of this shadow mask is shown in Figure 3.7. The bottom plate of the sample consists of two copper electrodes, a single front load crystal sensor (purchased from Kurt J. Lesker Company), a type K thermocouple (purchased from Kurt J. Lesker Company) and a Pfeiffer PKR 251 full range gauge (purchased from Pfeiffer Company). The crystal sensor was used to detect the thickness of the deposited thin film on the substrates and it was coupled with the multichannel quartz crystal monitor (purchased from Kurt J. Lesker Company) via an oscillator kit (a 15cm Bayonet Neill-Concelman (BNC) cable, an oscillator and a 10 meter BNC cable). The oscillator kit was purchased from Kurt J. Lesker Company. The oscillator is the electronic device that operates the crystal and it is not interchangeable because it is tuned to a specific monitor or controller. The Type K thermocouple is made by chromel (10% chromium and 90% nickel) and alumel (1% silicon, 2% aluminium, 2% manganese and 95% nickel). It is capable of sensing the change of temperature from -220°C to 1350°C. It was connected to a temperature controller. A Pfeiffer PKR 251 full range gauge was used to detect the change of pressure range from

1000mbar to 5 x10^{-9}mbar. A DN 63 ISO-K welding flange stainless steel host was made at the centre of the bottom plate for the pump system. A simple design stage was placed on top centre of the bottom plate to prevent the large particles from fell into the pump system.

The pump system of HiCube Eco Turbo Pumping Station was purchased from Pfeiffer Company. It consists of a Pfeiffer MPV 015-2 dry diaphragm vacuum pump, a Pfeiffer DN 63 ISO-K flange HiPace 80 turbo molecular pump, a Pfeiffer Vacuum Electronic Drive Unit (TC 110) and a Display and Control Unit (DCU). The diaphragm pump is able to pump to 2 x 10^{-2}mbar from the atmospheric pressure. The turbo pump can pump to below 1 x 10^{-5}mbar with a proper sealed chamber with the diaphragm pump as the backing pump. It possesses an air cooling system. The TC 110 is an integrated component of the turbo pump. Its purpose is to drive, monitor and control the turbo pump. The DCU is an operating unit for TC110. It enables control over all the main parameters of the unit. Additionally, the connection of the Pfeiffer PKR 251 full range gauge is possible to the DCU. The pressure of the chamber will display on the screen of the DCU and all commands are executed from the DCU. An unbraided hydraulic formed stainless steel bellow is used to connect the pump station to the host of the chamber. The bellow provides some flexibility and stretching space between the chamber and the pump station.

The power source of the vacuum thermal evaporator was constructed from a 250V contact voltage regulator, a 60A step-up transformer and a 100A ammeter. The voltage regulator was applied to maintain a constant voltage level to the step-up transformer (as the tuner for the current into the copper electrodes). This transformer was used to increase the current up to 60A, whilst an ammeter was employed to monitor the current supply to copper electrodes. This power supply was connected to the copper electrodes in the chamber by high current power cables. The actual constructed vacuum thermal evaporator is shown in Figure 3.5, while the schematic inner design is illustrated in Figure 3.8.

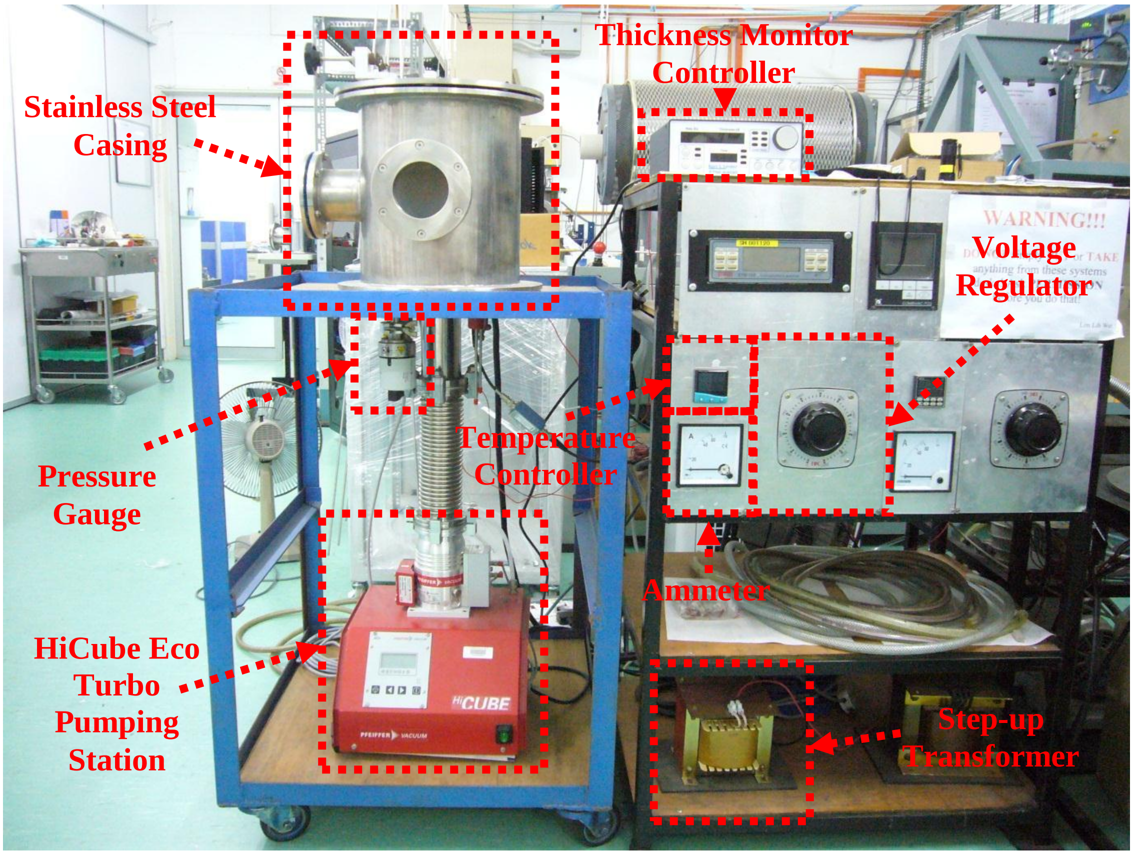

Figure 3.5 Home built vacuum thermal evaporators as indicated in red dashed box.

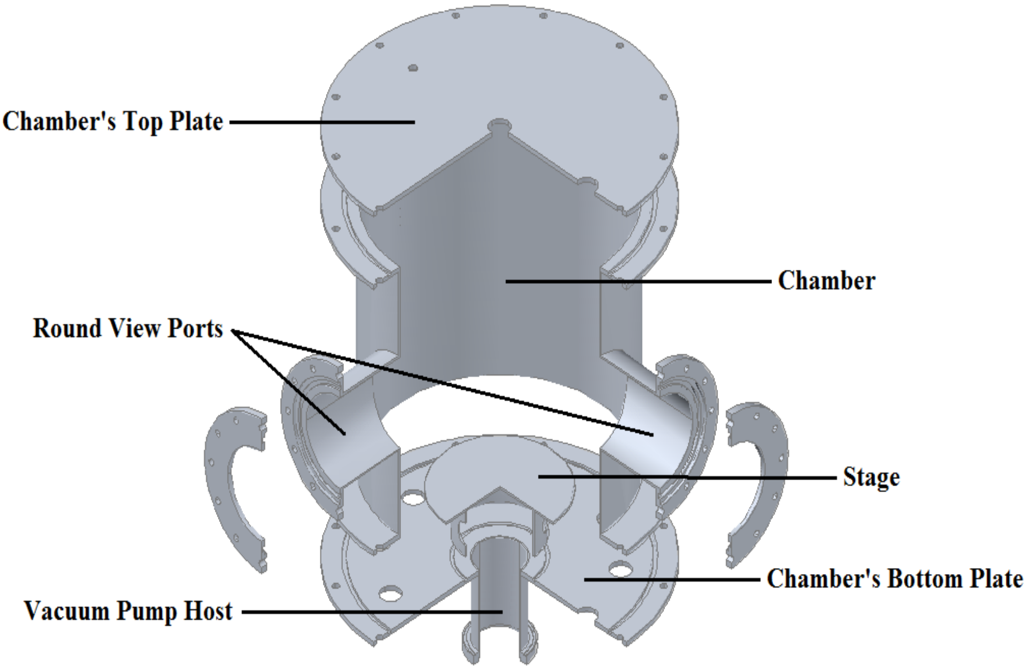

Figure 3.6 The design of the chamber casing.

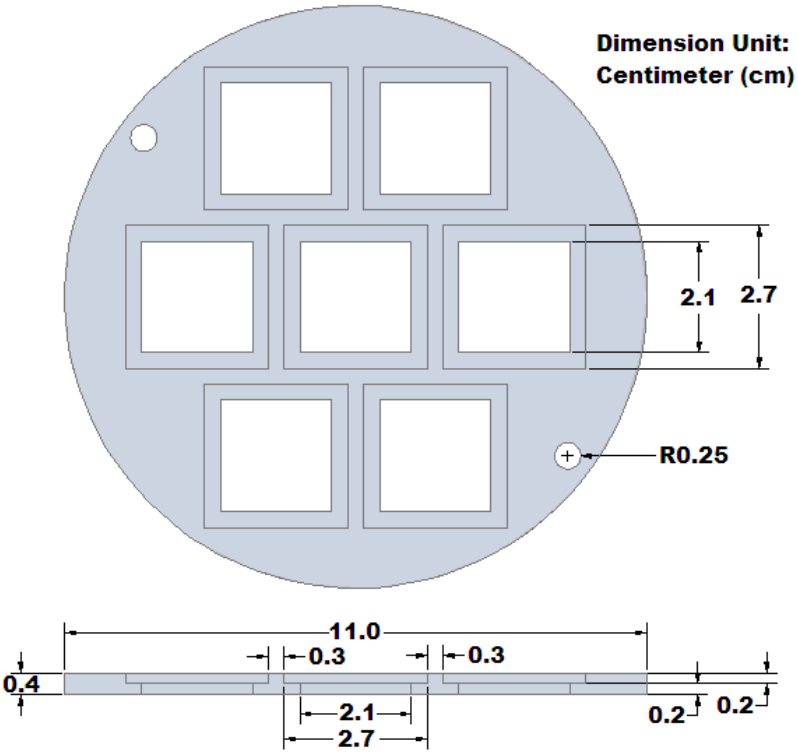

Figure 3.7 PTCDA thin film evaporation shadow mask.

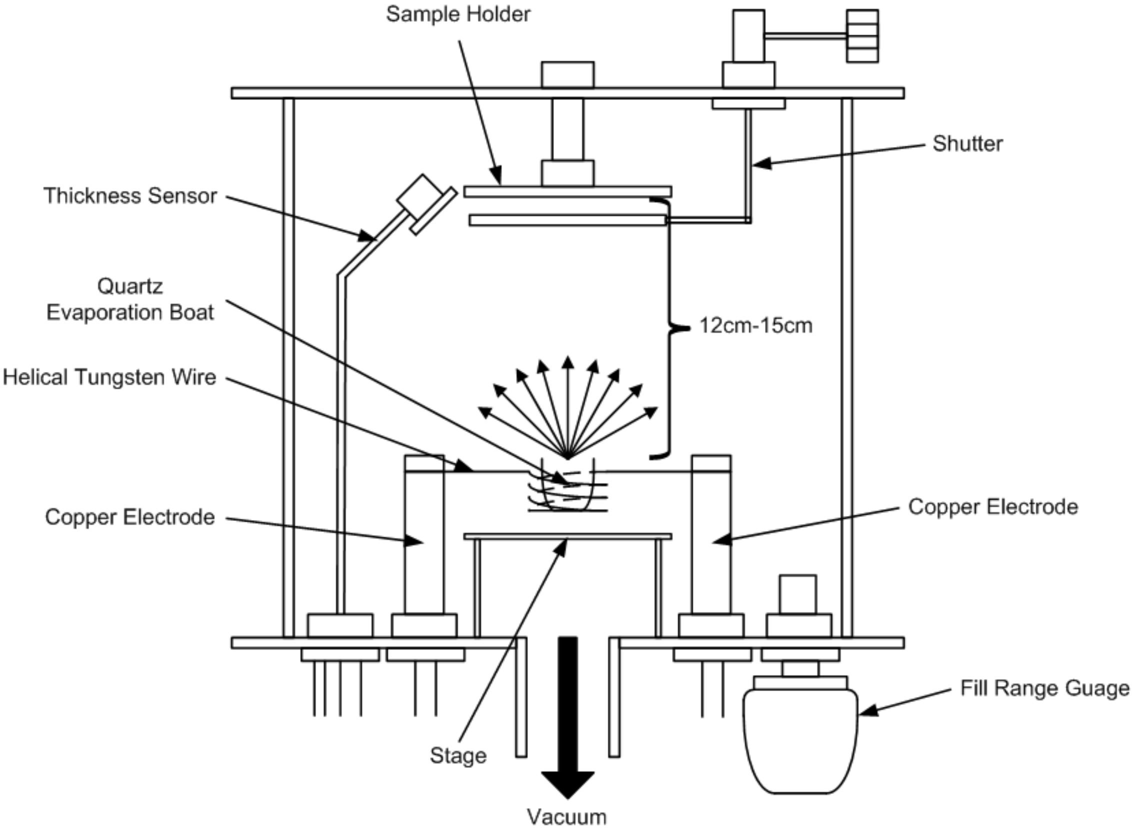

Figure 3.8 Schematic inner view of the custom-made thermal evaporator.

3.5 Top Electrodes Deposition

Electrodes deposition was considered as the final stage of the OPVC fabrication. In this work, the electrodes deposition was done in the 1K clean room environment using an Edward A-360 Thermal Evaporator. Aluminium (Al) was used as the top conductive electrodes for the OPVC. The purity of the Al wires is 99.99% purchased from Bumi Interactive Snd. Bhd. The small pieces of Al wires were placed on the helical tungsten wire in the vacuum thermal evaporator. Then the film coated substrates were placed onto a shadow mask/holder which was put inside the evaporator. The distance between the evaporation source and the substrates is important when depositing the top conductive electrodes onto the thin film. If the distance is too short, the high kinetic energy metal particles would travel and penetrate the thin film and causing the device to be short circuited. If the distance is too far, then most of the evaporated particles cannot reach the substrates surface and causing the thickness of the electrodes too thin and not sufficient for the measurements probes to make contact. Therefore, the ideal distance between the tungsten wire and the substrates should be around 12cm-15cm. The pressure inside the chamber should reach below 5.0×10^{-5}mbar before the evaporation process can be initiated. By increasing the current through the tungsten wire, aluminium started to melt and become molten beads. However, the current should not be increased too fast to prevent the melting aluminium dropped off from the tungsten wire. The current was slowly increased to 20 amperes. At this point, the molten Al beads started to evaporate when the heating temperature reaches around 1500°C. The shutter was opened to allow the evaporated Al particles to travel to the substrates and condensed. By utilising a shadow mask as illustrated in Figure 3.9, four stripes/pixels of aluminium top electrodes can be deposited onto the organic thin films. The rate of the evaporation was required to be controlled at less than 0.5Å/s. The slow evaporation rate prevents the penetration of metal particles into the thin film and therefore preventing it from short circuit. When the desire thickness of the Al electrodes was reached, the shutter was closed immediately and the chamber was cooled down in 20 minutes. The photovoltaic cells as shown in Figure 3.10 were ready to be collected and tested.

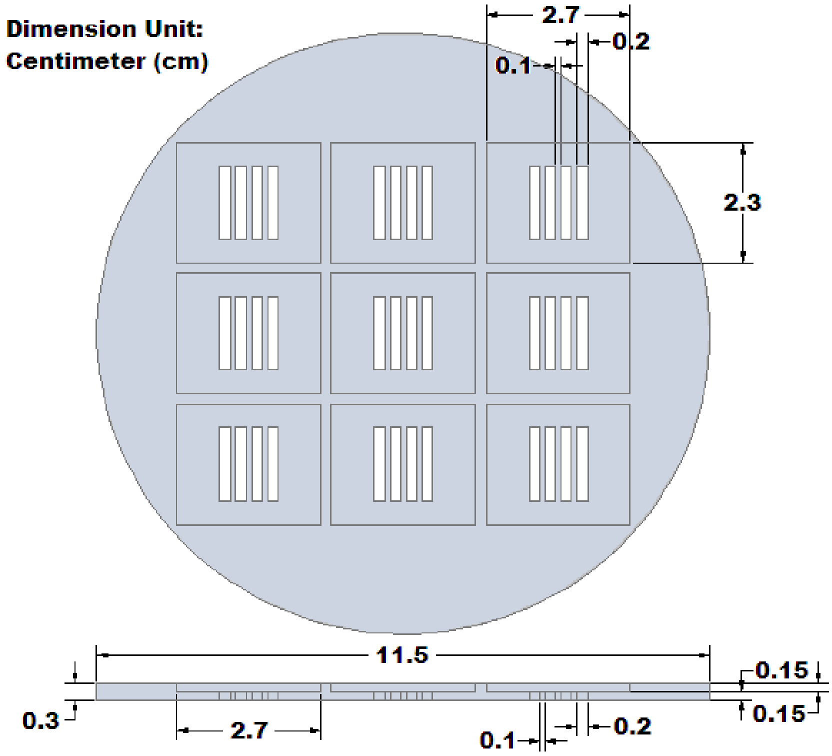

Figure 3.9 Top electrodes evaporation shadow mask.

3.6 Device Structure

The OPVC devices in this research were made into bilayer heterojunction OPVC. The active layers of p-type and n-type material were sandwiched between two electrodes of ITO and Al. The final device configuration consists of ITO/p-type/n-type/Al is shown schematically in Figure 3.1. Figure 3.10 shows the photograph of an actual OPVC consists of p-type/n-type active layers with the size of 2.5cm x 2.0cm. The active area is around 0.28 cm^2, which defined as the coverage area of a top Al electrode over the ITO electrode. Therefore the active area of a pixel can be calculated as the length times the width of a top Al electrode which is cover above the ITO electrode. The portion of the Al electrode that cover over the etched area is not consider as active area. This device was then placed into a sample holder for J-V measurement as shown in Figure 3.2.

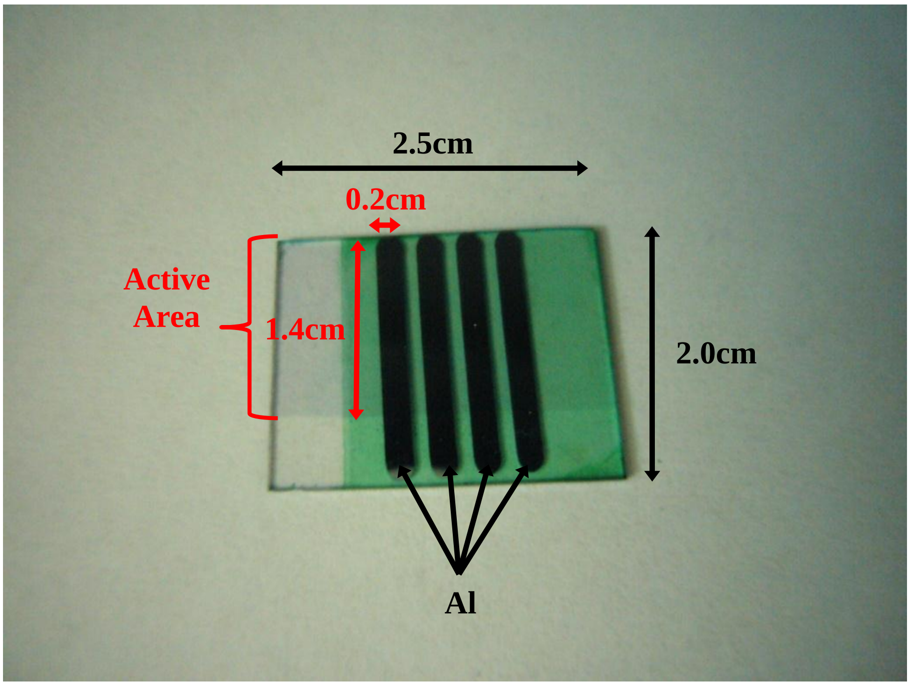

Figure 3.10 A functional OPVC device.

3.7 Characterisation Methods

Ultraviolet-visible-near infrared (UV-Vis-NIR) spectroscopy was used to determine the absorption spectrum and estimating the optical band gap whilst Fourier Transform Infrared (FTIR) spectroscopy was employed to determine the chemical bonding of the tested materials. Besides, X-ray diffraction (XRD) was utilised to obtain the information on the crystallography structure, crystallite size, chemical composition and physical properties of the material in either the powder or thin film form. The microscopy measurements were performed by means of Atomic Force Microscopy (AFM) and Scanning Electron Microscopy (SEM) in order to investigate the structure, layer ordering, thickness, surface morphology and homogeneity of the organic thin films.

Current density-voltage (J-V) characteristic measurement was performed to determine the electrical properties and performance of the OPVC. A lot of information can be obtained from the J-V characteristic curve for example the short circuit current density (J_{sc}), open circuit voltage (V_{oc}), fill factor (FF) and power conversion efficiency (η).

The subtitles below elaborate all the methods and system models that applied throughout this research project.

3.7.1 Ultraviolet-visible-near-infrared (UV-VIS-NIR) spectroscopy

The optical absorption spectra of PTCDA and VOPcPhO thin films coated on glasses/quartz/ITO substrates were obtained by performing UV-Vis-NIR spectroscopy. The spectrophotometer model used in this project was a Jasco V-570 UV-VIS-NIR spectrophotometer. The absorption spectra were scanned within the wavelength range of 300nm to 1100nm (UV region to NIR region) in the ambient air. A deuterium discharge tube supplies the ultraviolet region radiation from wavelength 300nm to 350nm whereas a tungsten iodine lamp provides the visible to near-infrared region light source from wavelength 350nm to 1100nm. The light from the light source is first converged and entered the monochromator. It is then dispersed by the grating in the monochromator and the light passing through the exit split is monochromated. This light is split into two light paths by a sector mirror. One light incident on the sample to be measured and the other on the reference sample. The light that has passed through the sample or reference sample is detected by the photomultiplier tube or lead (II) sulphide (PbS) photoconductive cell. The light detected by the photomultiplier tube or PbS photoconductive cell is converted into an electrical signal. The electrical signal is synchronously rectified and converted into a digital form and enters the microcomputer. The signal processed by the microcomputer is displayed on the output device (computer) as digital data or spectrum.

Baseline correction has been performed at the beginning of the absorption measurements. Glass and quartz have its own absorption wavelength which considered as the background signal. Therefore, a baseline correction must be done in order to eliminate this background absorption spectrum. The absorption measurements on thin films were carried out by placing a clean substrate either glass or quartz or ITO into the reference holder of the spectrophotometer whilst the organic thin film coated on the similar solid substrates as used in the reference cell was placed in the sample holder. On the other hand, the quartz cuvettes were employed for the absorption measurement of materials in solution form.

3.7.2 Fourier transform infrared (FTIR) spectroscopy

The FTIR spectroscopy was used to obtain the transmission spectrum of a material in the range of the infrared region. In this study, the transmission spectra of the PTCDA and VOPcPhO thin films were measured by a Perkin Elmer System 2000 FTIR Spectrophotometer. Silicon substrates were used in the FTIR spectroscopy and the baseline correction also must be carried out at the beginning of the measurement.

A Michelson interferometer is adapted in FTIR spectrophotometer. In this Perkin Elmer System 2000 FTIR Spectrophotometer, the interferometer is named Dynascan^{TM} interferometer capable of achieving a resolution of 0.15cm^{-1}. In the interferometer, a light beam is split into two paths by a beam splitter (a configuration of mirrors) and creates an optical path difference. The optical path difference of the light beams induces interference fringes when pass through a material and detect by detectors as an interferogram (raw data). The raw data acquired from the measurement is required to undergo Fourier Transform (a mathematical algorithm) to covert the data into actual a spectrum. A series of digital signal processing boards that built in the spectrophotometer performs the Fourier Transform on the raw data.

3.7.3 Atomic force microscopy (AFM)

A Veeco Dimension 3000 Atomic Force Microscope (AFM) was utilised to measure the surface morphology of the organic thin films. AFM is a very high resolution scanning microscopy that enables the user to details on the surface of the scanned object by giving a very clear three dimensional (3D) view. The resolution can go up to nanometre which is 1000 times better than optical microscopy. The first AFM was invented by Binning, Quate and Gerber in 1985.

The AFM consists of a cantilever with a microscopic tip at its end. It is made from silicon or silicon nitride. This cantilever moves like a spring over the surface of the specimen in the x, y and z directions via piezoelectric elements. The microscopic tip with tip radii of 10nm to 30nm served as the probe and is used to scan the specimen surface. The size of the tip and the flexibility of the cantilever contribute to the high resolution of the image. When the tip is brought into proximity of a specimen surface, force between the tip and the specimen leads to a deflection of the cantilever according to the Hooke's Law. A laser beam deflection system is used to detect the deflection of the cantilever. A laser is reflected off the end of the cantilever onto a position sensitive detector (an array of photodiodes). The photodiodes detect the reflected laser and produce an image of the surface topography.

3.7.4 Field emission scanning electron microscopy (FESEM)

FESEM images a sample by scanning it with a high energy beam of electrons instead of using light. The electrons beam is produced by an electron gun fitted with a tungsten filament cathode via thermionic emission. This beam travels in a vertical path through lenses and electromagnetic fields which focus the beam down towards the sample. When the electrons beam hit the surface of the sample, the electrons interact with the atoms near to the surface of the sample to produce signals that contain information about the sample’s surface topography. The types of signals being produced include primary backscattered electrons (caused by elastic scattering), secondary electrons (caused by inelastic scattering), light and X-rays (emission of electromagnetic radiation). These signals are detected by detectors in the microscope and convert them into an image to display on the computer monitor.

Magnification of a FESEM can be controlled over a wide range from about 10 times to more than 50,000 times. This is about 250 times better than an optical microscope. In this work, the Leica S440 model was used to visualise the images of SEM.

3.7.5 Thickness measurements

The PTCDA and VOPcPhO thin films were coated on the glass substrates and the thicknesses were measured by using a KLA Tencor P-6 Surface Profilometer. All the thickness measurements were taken under an atmospheric condition. Initially, the samples were positioned at the centre of the disk holder inside the profilometer. Then the scanning parameters were set in the profilormeter’s command software as tabulated in Table 3.0.

Table 3.0 Scanning parameter of KLA Tencor P-6 Surface Profilormeter.

Scan type	Two dimensional (2D)
X Scan size	2000µm
Scan speed	100µm/s
Sampling rate	20Hz
Multi scan average	1
Applied forced	0.50mg
Range/resolution	327µm/0.1953Å
Profile type	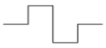

After the parameters have been set up, a command was given to the profilometer through the software to manual load the sample. Then the probe of the profilometer started to move downward until it touched the surface of the sample. A minimum scanning force of 0.5mg was applied to the sample because of the soft material in nature of organic thin films. After the scanning was done, the data was saved and manual load the probe to move upward.

3.7.6 X-ray diffraction (XRD)

XRD measurements were performed by a Siemens D5000 X-ray Diffractometer. The obtained results in this study were used to determine the crystallinity and crystallite size of the PTCDA powder and thin films. X-ray Diffraction (XRD) technique is a versatile, non-destructive analytical technique which can reveal detailed information about the structural, chemical and physical properties of the materials and thin films. This technique is based on observing the scattered intensity of a monochromatic x-ray beam incident on a sample as a function of the wavelength, incident angle and scattered angle.

In the x-ray diffractometer, the x-ray beam is generated by a cathode ray tube by heating a filament to produce electrons, accelerating the electrons by applying a high voltage and bombards the high velocity electrons to a target material. The high velocity electrons which have sufficient energy to dislodge the inner shells electrons of the target material produce x-rays. The target material such as copper, iron, molybdenum, chromium, et cetera decides the specific wavelength of the x-ray. The Siemens D5000 X-ray Diffractometer use copper as the target material. The x-ray is $CuK_{\alpha 1}$ radiation with a wavelength of 1.5418Å. The x-ray is filtered by a monochromator to produce monochromatic radiation. After that, the monochromatic x-ray is collimated to concentrate and direct to the sample that placed on a platform at a certain angle. The incident ray interacts with the crystal lattice to produce constructive interference according to the Bragg's Law:

$$n\lambda = 2d\sin\theta \qquad \text{(Equation 3.1)}$$

Bragg's Law relates the wavelength of electromagnetic radiation, λ to the diffraction angle, θ and the lattice spacing, d in the crystalline sample. The monochromatic x-ray beam is used to produce the diffraction because their wavelength is typically the same order of magnitude as the same spacing between the planes in the crystal lattice. The interference pattern is detected by the x-ray detector and process. By scanning the sample through a range of 2θ angles, all possible diffraction directions of the lattice can be obtained.

3.7.7 Current density-voltage (J-V) characteristic measurements

The J-V characteristic measurement was done in the ambient condition in a custom made dark box. The dark box was made to effectively block out the background light. In this dark box, a 150W Newport solar simulator equipped with a 1.5 Air Mass filter is located. It acts as the light source for the OPVC. The solar simulator has been calibrated to provide an input power of 100mW/cm^2 to the OPVC. To measure the J-V characteristic, the OPVC was attached on a sample holder. This custom made sample holder was described previously (see Figure 3.3). One probe of this sample holder provided a contact to the anode electrode (ITO) and whilst the other four probes were connected to the cathode electrodes (Al) of the OPVC. The OPVC was connected to a Keithley 236 System Measuring Unit (SMU) via the sample holder. The SMU works as a voltage source and current measure unit. It provides the applied voltage to the device prior set by the user and measures the photocurrent induced in the OPVC. The SMU was connected to the computer through General Purpose Interface Bus (GPIB) cable and a *Labview* J-V programme. The parameters used in this J-V measurement are tabulated in Table 3.1.

Table 3.1 Parameters of Labview J-V Programme.

SMU Address	18
Initial Voltage/V	-1.0
End Voltage/V	1.0
Number of Points	200
Sweep Delay/s	0
Filter	4 Readings
Integration	50Hz (20msec)

Chapter 4

Characterisations of Organic Semiconductors VOPcPhO and PTCDA Thin Films

4.0 Overview

In this chapter, the results obtained are presented from the spin-coated p-type vanadyl 2, 9, 16, 23-tetraphenoxy-29H, 31H-phthalocyanine (VOPcPhO) thin films using the material solution onto glass substrates. Besides, the results of thin films are depicted from the n-type 3, 4, 9, 10-perylenetetracarboxylic dianhydride (PTCDA) deposited by thermal evaporation technique using a homebuilt thermal evaporator. Furthermore, the physical characterisations of optical and morphological properties are discussed based on the prepared thin films. The results of absorption spectra, optical band gap, et cetera extracted from the ultraviolet-visible (UV-VIS) spectroscopy are presented and co-related with the thin films structures, crystallinity feature and crystallite size obtained from X-Ray Diffraction (XRD) spectroscopy. Additionally, FTIR spectra are presented to determine the chemical structure of the organic compounds. Finally, Atomic Force Microscopy (AFM) and Field Emission Scanning Electron Microscopy (FESEM) images are shown to provide detail morphological information of the thin films.

4.1 Ultraviolet-Visible (UV-VIS) Spectroscopy

Figure 4.0 shows the absorption spectrum of VOPcPhO, PTCDA and bilayer heterojunction VOPcPhO/PTCDA thin films coated on glass. As can be seen from the absorption spectrum, the VOPcPhO thin film possesses two distinct transition bands. One of the VOPcPhO band occurs in the visible spectrum which corresponds to radiation wavelength ranged from 380nm to 750nm. The other transition band is located in the ultraviolet (UV) region within 350nm to 500nm with a shoulder at around 400nm - 415nm. Another transition band with a broader coverage appears as a volcano mountain shape around the wavelength of 570nm to 900nm (yellow-infrared region) with the first peak at 711nm and the second peak at around 673nm. The VOPcPhO thin film covers a large portion of the visible spectrum except the region around 500nm-570nm which is corresponding to the green colour region. That is the reason the colour of VOPcPhO powder, solution and thin film appear in dark green. The absorption spectrum of the spin coated VOPcPhO thin film is almost identical to the reported of the thermally evaporated VOPc thin film deposited by other research groups (Teodosio Del Caño, et al., 2003; T. Del Caño, et al., 2005; Y. L. Pan et al., 1998). They showed that the VOPc exhibited two transition bands in the UV-VIS range. The lowest energy transition in the visible range (between 1.45eV - 2.0eV that corresponds to 570nm-900nm) is called Q-band. This transition is common in all phthalocyanines. This band is believed related to the packing density and orientation of the VOPc molecules. Another band located at higher energy transition which is in the UV region is known as B or Soret band. Both bands, Q and B correspond to the π-π^* transition and their dipoles lie in the plane of the molecule (Kolotovska, et al., 2006). It is not surprising that the absorption spectrum of soluble VOPcPhO thin film displays high similarity as the absorption spectrum of the insoluble VOPc thin film since VOPcPhO is a derivative of VOPc. Therefore, the absorption bands of VOPcPhO thin film also can be attributed as the VOPc thin film absorption bands.

According to the literature, the phases of the VOPc can be identified by looking at the strongest absorption peak and its shoulder in the Q-band. The phase-I VOPc layer has the strongest absorption peak at around 720nm (≈1.7eV) and a shoulder at 660nm (≈1.85eV). This is due to a stacking structure of co-facial packing in phase-I. This phase of VOPc is known as amorphous form. The phase-II of the VOPc layer can be identified by the maximum absorption at 800nm (≈1.55eV) and a shoulder at 700nm (≈1.8eV). Furthermore, the unique near-IR absorption in the Q band indicates the VOPc thin film transform from phase-I to phase-II, which is characterised by a triclinic crystal structure or “head to tail” arrangement (Danziger, et al., 1991; Kolotovska, et al., 2006; Law, 1985, 1988; Nakano, et al., 2001; Santos & et al., 2008; Yamashita, et al., 1993). Obviously, the absorption spectrum of a 90nm in thickness of VOPcPhO film coated on glass as shown in Figure 4.0 appears to be in the phase-I structure. Therefore, it is suspected that this VOPcPhO thin film spin coated on glass in the ambient atmospheric condition is in amorphous form.

As for the PTCDA, the absorption spectrum of PTCDA coated by thermal evaporation technique on glass absorbs photon in a broad visible region which ranged from 400nm-600nm. It absorbs very well in blue and green colour region except in red colour region thus the PTCDA powder and thin film appear in red colour. The absorption spectrum of PTCDA film shows a peak at 475nm with a shoulder at 555nm. The PTCDA thin film absorption band is in complimentary spectral region to the VOPcPhO thin film. Since the VOPcPhO does not absorb photon in the red colour region but the PTCDA do and the VOPcPhO absorbs wavelength that PTCDA does not, suggesting these two materials can be couple together to form a bulk or bilayer thin film so that the mixture can absorb the whole range of visible wavelength to provide good coverage of the solar spectrum. Therefore attempts have been made to deposit the bilayer heterojunction of VOPcPhO/PTCDA thin films on glass to measure the absorption spectrum of this combination. Figure 4.0 shows that the absorption spectrum of this bilayer film is a simple superposition of two spectra; one for the VOPcPhO and the other for PTCDA. The bilayer heterojunction of VOPcPhO/PTCDA thin films shows the domination of VOPcPhO thin film in the absorption spectrum except there is a small “bump” appears around the red colour region. The absorption ability in the red colour region has slightly improved. This phenomenon is associated with the low absorption of the PTCDA thin film. The section below discussed about the absorption ability of the thin films using absorption coefficient parameter. The absorption coefficient is independent of the thickness of the material. Therefore, it is more suitable to use as a comparative quantity to show the absorption ability in the thin films.

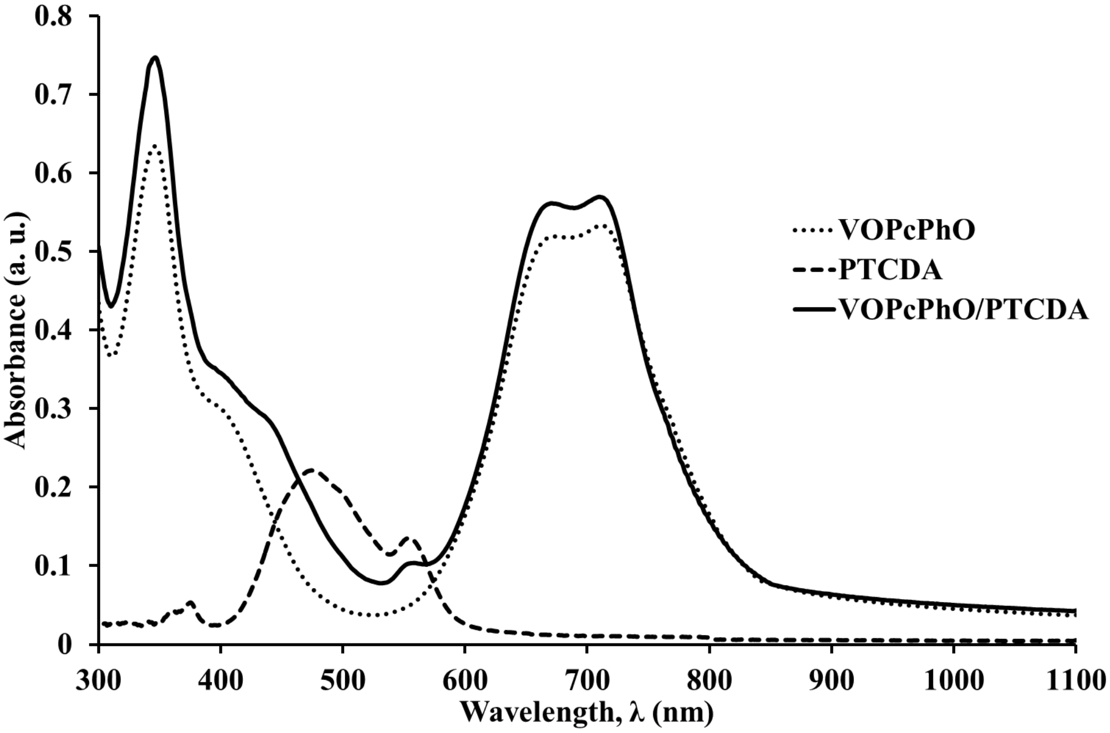

Figure 4.0 The absorption spectrum of VOPcPhO, PTCDA and bilayer heterojunction VOPcPhO/PTCDA thin films coated on glass.

4.1.1 Absorption coefficient, α

The absorption coefficient is the fraction of incident radiant energy absorbed per unit mass or thickness of an absorber. A large absorption coefficient of a material means that the beam is quickly absorbed as it passes through the material. A small absorption coefficient of a medium indicates that the beam can transmit through the medium relatively efficient. The absorption coefficient is derived from the Beer-Lambert Law. Beer-Lambert Law states that the measured transmitted intensity, *I* through a layer of material with a thickness of *d* is proportional to the inverse exponential power of the incident intensity of the beam, I_o. The derivation of absorption coefficient equation from Beer-Lambert Law is shown below:

From the Beer-Lambert Law,

$$I = I_o e^{-\alpha d} \qquad \text{(Equation 4.1)}$$

Convert the both sides in the Equation 4.1 to logarithm,

$$\log_{10} I = \log_{10} I_o + \log_{10} e^{-\alpha d}$$

$$= \log_{10} I_o - \alpha d \log_{10} e \qquad \text{(Equation 4.2)}$$

Rearrange the equation,

$$\alpha d \log_{10} e = \log_{10} I_o - \log_{10} I$$

$$= \log_{10} \frac{I_o}{I} \qquad \text{(Equation 4.3)}$$

In the spectroscopy, the absorbance, Abs. is defined as:

$$\text{Absorbance, } Abs. = \log_{10} \frac{I_o}{I} \qquad \text{(Equation 4.4)}$$

Therefore,

$$\alpha d \log_{10} e = Abs. \qquad \text{(Equation 4.5)}$$

Finally, divides both sides with $d \log_{10}$ e,

$$\text{Absorption Coefficient, } \alpha = \frac{1}{\log_{10} e} \bullet \frac{Abs.}{d} \qquad \text{(Equation 4.6)}$$

Figure 4.1 shows the absorption coefficient, α versus photon energy, hv of corresponding photon wavelength for the VOPcPhO, PTCDA and VOPcPhO/PTCDA thin films. The single layer VOPcPhO thin film shows relatively high absorption coefficient compared to the single layer PTCDA thin film and the bilayer VOPcPhO/PTCDA thin films. It indicates that the VOPcPhO thin film possesses relatively effective absorption ability compared to the single layer PTCDA thin film. Note that the thermally evaporated PTCDA thin film has an absorption coefficient several times lower compared to the spin coated VOPcPhO thin film. This result confirms that the VOPcPhO absorption is more dominant compared to the PTCDA due to the relatively less efficient absorption of the PTCDA thin film. Therefore when VOPcPhO coupled with PTCDA, not much alteration can be seen on the absorption spectrum of this bilayer structure. Nevertheless, the addition of PTCDA into the structure has slightly improved the absorption in the red colour region. However, the PTCDA thin film affected the bilayer structure by causing the bilayer structure in terms of lower absorption coefficient due to greater thickness contributed by PTCDA layer.

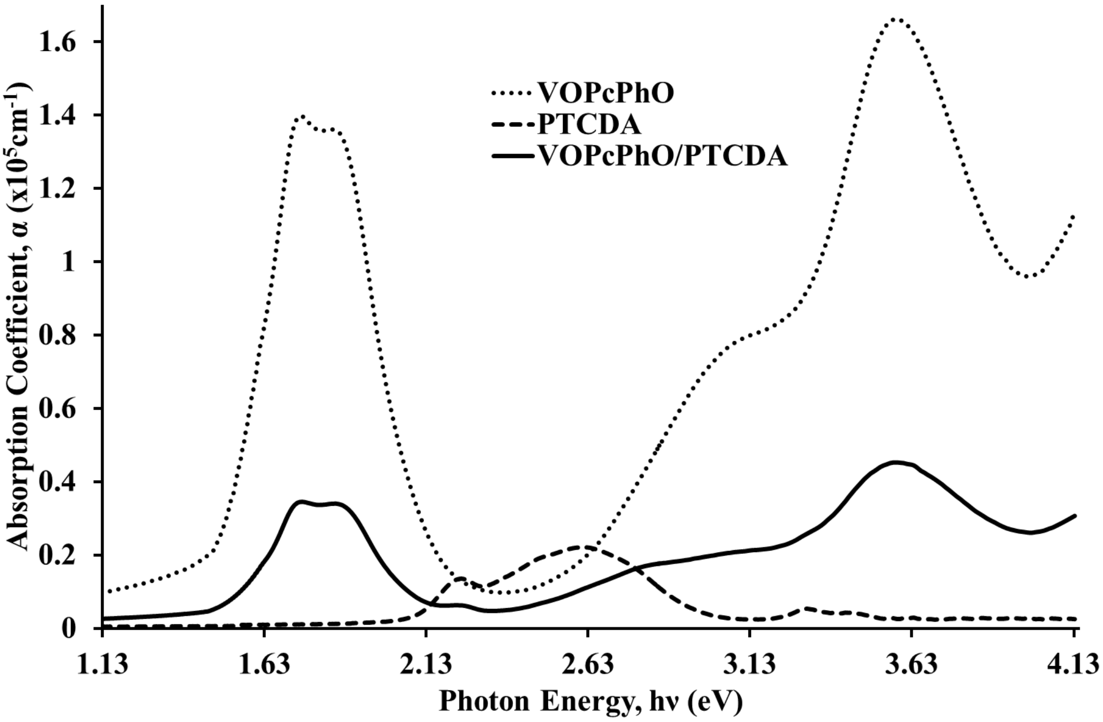

Figure 4.1 Graph of absorption coefficient, α versus photon energy, hν of corresponding photon wavelength for the VOPcPhO, PTCDA and VOPcPhO/PTCDA thin films.

4.1.2 Optical band gap, E_g

From the UV-VIS absorption spectra, another important optical property of the thin films is accessible. By applying Tauc plot pioneered by J. Tauc, the optical band gap or Tauc gap, E_g of the materials in the thin film form can be determined. The Tauc plot shows the quantity of $h\nu$ (the photon energy) on the abscissa and the quantity $(\alpha h\nu)^n$ on the ordinate. The value of the exponent, n denotes the nature of the transition in the materials. The direct transition materials have the n value of 2 while the indirect transition has the value of ½. The resulting plot will have a distinct linear slope which denotes the onset of absorption. Thus, extrapolating the linear region to the abscissa

[$(\alpha h\nu)^2$=0] yields the x-interception. This x-interception is the E_g, the energy of the optical band gap of the material.

Before the determination of optical band gap of the material can be done, the nature of the transition should be determined first. The section below shows the brief derivation of Tauc relation to determine n value and E_g of the material.

From the Tauc relation,

$$(\alpha h\nu) = \alpha_o (h\nu - Eg)^n \qquad \text{(Equation 4.7)}$$

where α is the absorption coefficient of the material, h is the Plank's constant, v is the corresponding wavelength of the light, n denotes the nature of the transition in the material, α_o is a constant which is different for different transition, E_g is the optical band gap of the material.

Log both sides of the Equation 4.7 and the equation shall become,

$$\ln(\alpha h\nu) = n \ln(h\nu - E_g) + \ln \alpha_o \qquad \text{(Equation 4.8)}$$

where lnα_o is a constant.

By dividing both sides with n,

$$\ln(\alpha h\nu) = n \ln(h\nu - Eg) + \text{ constant} \qquad \text{(Equation 4.9)}$$

Derivation of the Equation 4.9 will get,

$$\frac{d \ln(\alpha h\nu)}{dh\nu} = \frac{n}{h\nu - E_g} \qquad \text{(Equation 4.10)}$$

By plotting the graph of d ln($\alpha h\nu$)/d $h\nu$ versus photon energy, $h\nu$, a curve with a maximum should be observed. The maximum is being utilised to estimate the E_g of the material. Figure 4.2 (a), Figure 4.2 (b) and Figure 4.2 (c) show the plots of the d ln($\alpha h\nu$)/d $h\nu$ versus photon energy, $h\nu$ for the VOPcPhO, PTCDA and VOPcPhO/PTCDA thin films respectively. From the results, the estimated optical band gap, E_g of VOPcPhO, PTCDA and VOPcPhO/PTCDA thin films are around 1.67eV, 2.14eV and 1.67eV respectively. By utilising this estimated E_g, the graph of $\ln(h\nu\text{-}E_g)$ versus $\ln(\alpha h\nu)$ was then plotted to determine the value of n. It is very obvious that the Equation 4.9 is a linear equation. The value of n can be estimated by determining the slope of the linear region of the graph. Figure 4.3 (a), Figure 4.3 (b) and Figure 4.3 (c) show the graphs of $\ln(\alpha h\nu)$ versus $\ln(h\nu\text{-}E_g)$ for VOPcPhO, PTCDA and VOPcPhO/PTCDA thin films respectively. From the graphs, it is found that the closest values for the n values for these three thin films are ½. Therefore, it can be concluded that all three materials in thin films form are direct transition. This finding is in agreement with the previously reported organic materials (Güllü, Çankaya, Biber, & Türüt, 2008; Mathew, Sudarsanakumar, & Menon, 2010; Rejitha & Menon, 2012).

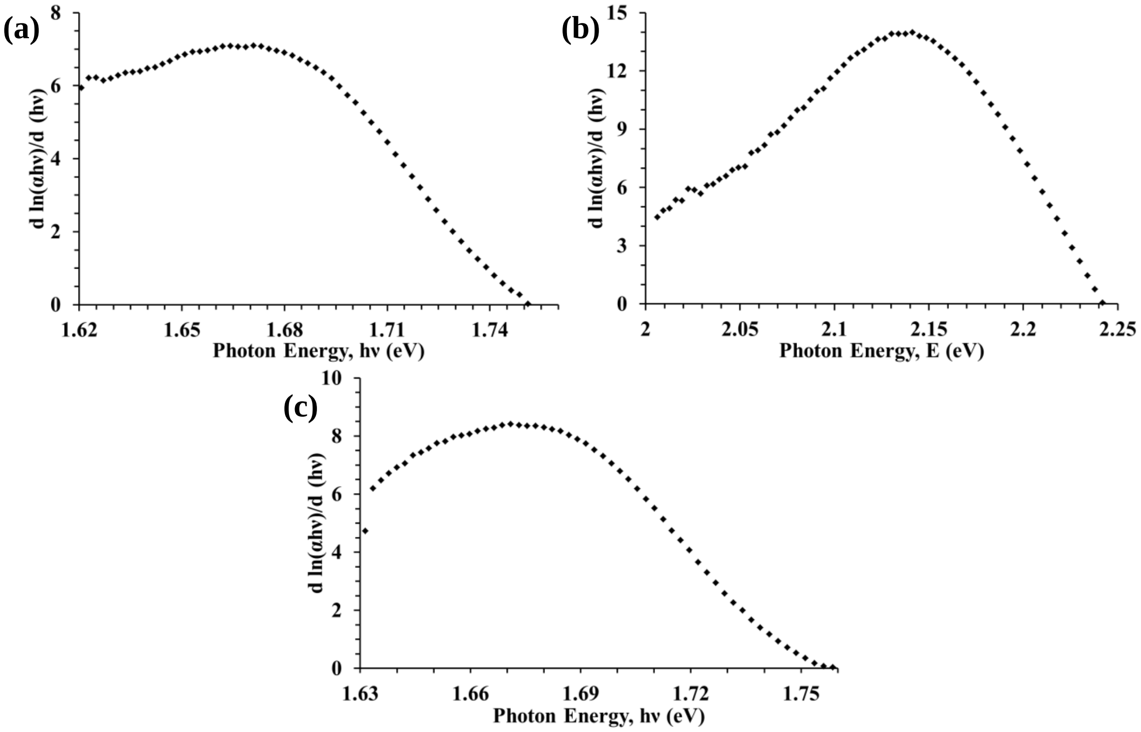

Figure 4.2 The graph of d ln(αhν)/d hν versus photon energy, hν of (a) VOPcPhO thin film, (b) PTCDA thin film and (c) VOPcPhO/PTCDA thin film.

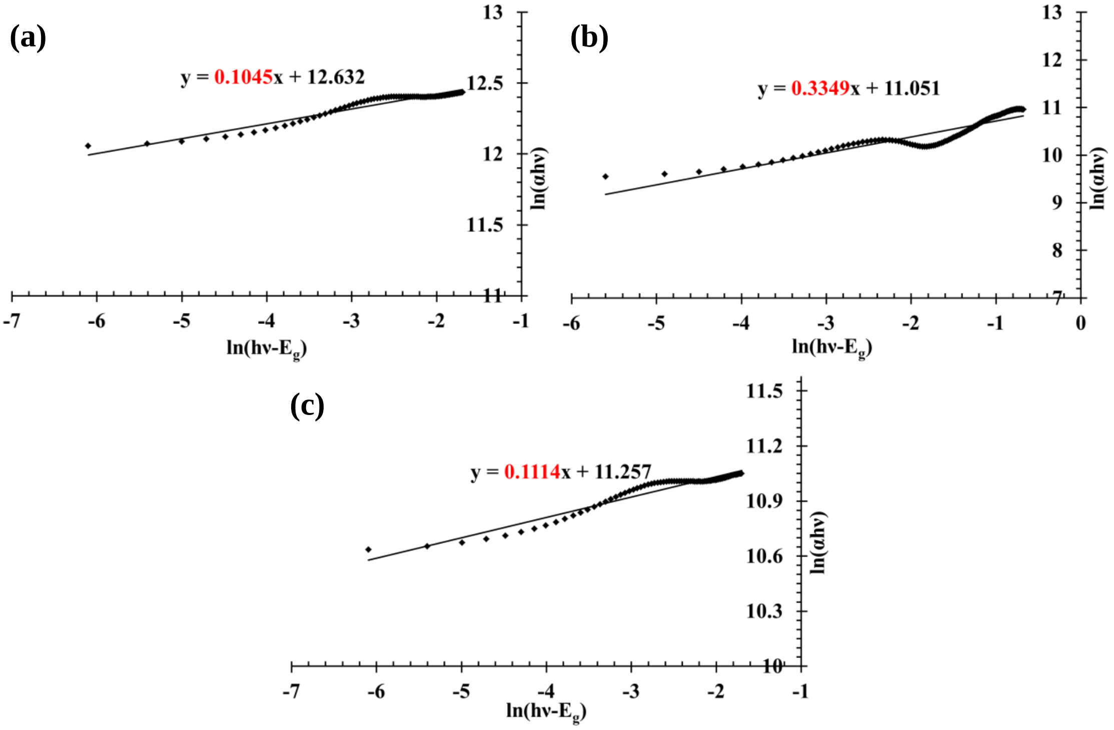

Figure 4.3 Graph of ln(hν-E_g) versus ln(αhν) of the (a) VOPcPhO thin film, (b) PTCDA thin film and (c) VOPcPhO/PTCDA thin film.

After the *n* value of the material has been estimated, substitute the *n* value to the Equation 4.7 and plot a graph of $(\alpha h\nu)^{1/n}$ versus photon energy, $h\nu$. From the graphs as shown in Figure 4.4 (a), Figure 4.4 (b) and Figure 4.4 (c), the optical band gap determined are 1.6eV, 2.13eV and 1.62eV for the VOPcPhO, PTCDA and VOPcPhO/PTCDA thin films respectively (Muhammad, Abdul Hapip, & Sulaiman, 2010). This is the first in determining the optical band gap of VOPcPhO since there is no report can be found on this subject so far. Therefore, the band gap of VOPc was utilised to make the comparison. It is found that, the determined VOPcPhO optical band gap is comparable with the band gap of VOPc (≈1.4eV) which determined by a few researchers (Bamsey, et al., 2011; Teodosio Del Caño, et al., 2003). The optical band gap of VOPcPhO is slightly higher than the optical band gap of VOPc probably is due to the β-peripheral substitution of phenoxide ions. The optical band gap of PTCDA obtained in this study also consistent with the results reported by other researchers using cyclic voltammetry and ultraviolet photoemission spectroscopy (UPS) measurements to determine the band gap of PTCDA (Brovelli, et al., 2007; Maruyama, et al., 2000; Pérez-Merchancano, et al., 2008). The mixture of VOPcPhO/PTCDA thin film has a similar optical band gap value as VOPcPhO thin film. The small optical band gap of VOPcPhO and PTCDA is one of the essential parameter for the organic photovoltaic cell. Since small optical band gap requires relatively low photon energy to excite the electron in the material to form exciton therefore the probability of exciton creation in the device become relatively high. Radiation with energy higher than 2.13eV (orange radiation) is sufficient to cause the excitation of the electrons in the VOPcPhO, PTCDA or VOPcPhO/PTCDA thin films. As a brief conclusion, the well coverage of solar spectrum, possible direct transition nature and low optical band gap of the VOPcPhO and PTCDA thin films make these materials suitable to fabricate OPVC.

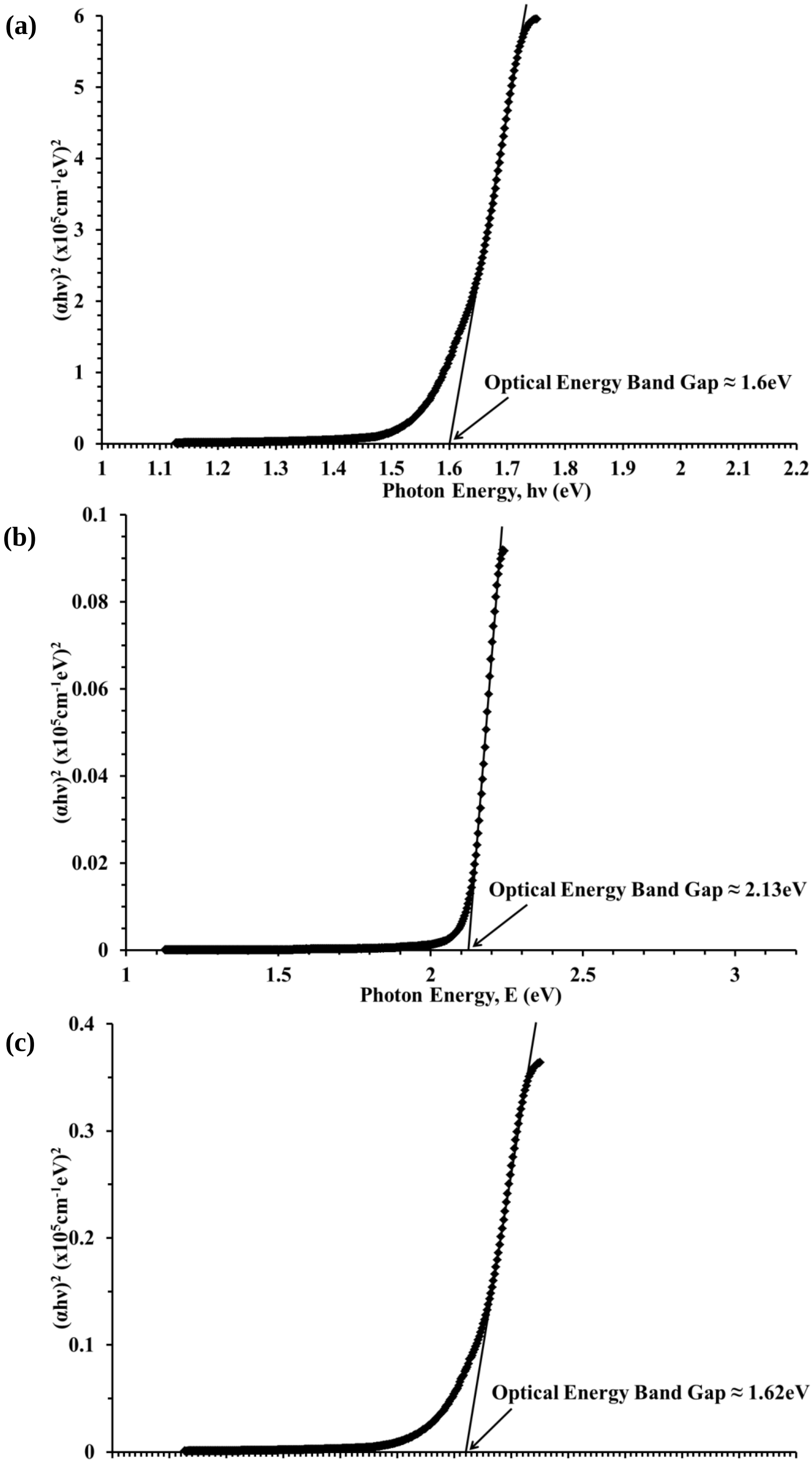

Figure 4.4 Graph of ln(hν-E_g) versus ln(αhν) of the (a) VOPcPhO, (b) PTCDA and (c) VOPcPhO/PTCDA thin films.

4.2 X-Ray Diffraction (XRD) Spectroscopy

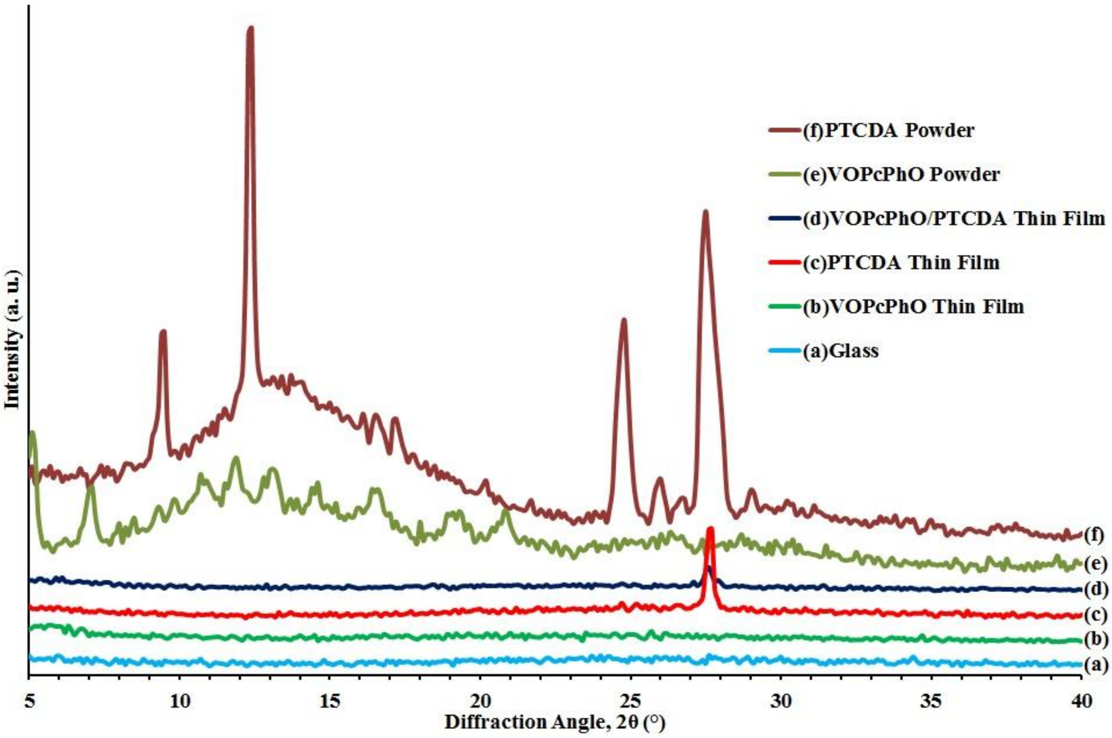

Figure 4.5 The XRD spectrum of the (a) glass, (b) VOPcPhO thin film, (c) PTCDA thin film, (d) VOPcPhO/PTCDA thin film, (e) VOPcPhO powder and (f) PTCDA powder.

In order to achieve a better assessment of the crystallography of the thin films, X-ray diffraction (XRD) measurements were carried out. Figure 4.5 shows the XRD spectra of a plain glass and the respective organic semiconductors thin films deposited on the glass substrates as well as their powder form. The bottommost spectrum, indicated by Figure 4.5(a), is the XRD spectrum of plain glass, which was used as a reference. Similar to the glass spectrum, the pristine VOPcPhO thin film deposited on glass substrate indicated by Figure 4.5(b) does not show any diffraction peak. All the diffraction crystalline peaks shown in the VOPcPhO powder which indicated by Figure 4.5(e) vanished in the spin coated VOPcPhO thin film indicating that the spin-coated pristine VOPcPhO thin film produces only amorphous structure. The XRD spectra of VOPcPhO confirmed the hypothesis previously made based on the UV-VIS spectra which speculated that the VOPhPhO thin film spin coated in the ambient atmospheric condition is in amorphous structures (phase-I).

At least four diffraction peaks are clearly visible in the XRD spectra of the PTCDA powder as shown in Figure 4.5(f). However, only two peaks can be identified: (102) plane located at 2θ = 24.8° and (110) plane located at 2θ = 27.5° (Heutz & Jones, 2002; Hudej & Bratina, 2002). All these diffraction peaks in powder form except the (102) peak vanish after the PTCDA powder has been thermally evaporated to form PTCDA thin film on the glass substrate held at room temperature as shown in Figure 4.5(c). The same angular position of the (102) peak indicates that both films and powder exhibit the same crystalline phase. The existence of the (102) peak suggesting that relatively ordered PTCDA layers can be obtained by the vacuum thermal evaporation process on glass substrates. S. Heutz and T. S. Jones suggested that PTCDA deposited on an amorphous substrate such as glass will lead to α polymorph and form small spherical crystallites (Heutz & Jones, 2002). Further investigations were conducted to obtain the average crystallite size of the thermally evaporated PTCDA thin film. For this purpose, the Scherrer equation is used:

$$\text{Mean crystalline size, } \tau = \frac{\kappa\lambda}{\beta\cos\theta} \qquad \text{(Equation 4.11)}$$

where κ is the shape factor (0.89), λ is the x-ray wavelength (1.54Å), β is the full width at half maximum intensity of the peak (FWHM) in radians and θ is the Bragg angle. Using Lorenztian lineshapes for the curve fitting shown in Figure 4.6(a), the FWHM of the (102) peak in the single layer PTCDA thin film is about 0.1969°. The calculated average crystallite size, τ for the diffraction peak at 2θ = 27.65° in the single layer PTCDA thin film is about 41.08nm.

The bilayer heterojunction VOPcPhO/PTCDA also exhibit a diffraction peak at 2θ=27.6 as shown in Figure 4.5(d). However, the intensity of the peak decreased significantly. The reduction in the intensity suggesting that the second layer of PTCDA film probably does not form crystallise structure on the first layer of VOPcPhO thin film. It may be argued that after a few tenths nanometer thick of the PTCDA molecules covered on top of the VOPcPhO layer then the PTCDA molecules only able rearrange themselves to form crystalline structure. Consequently only small portion on the top of the characterised layer consist of crystalline structures which might explain the intensity change in Figure 4.5. In Figure 4.6(b), the FWHM of the (102) peak in the bilayer VOPcPhO/PTCDA was estimated to be 0.2857°. The calculated average crystallite size, τ for the diffraction peak at $2\theta = 27.65°$ in the bilayer VOPcPhO/PTCDA thin film is around 28.32nm.

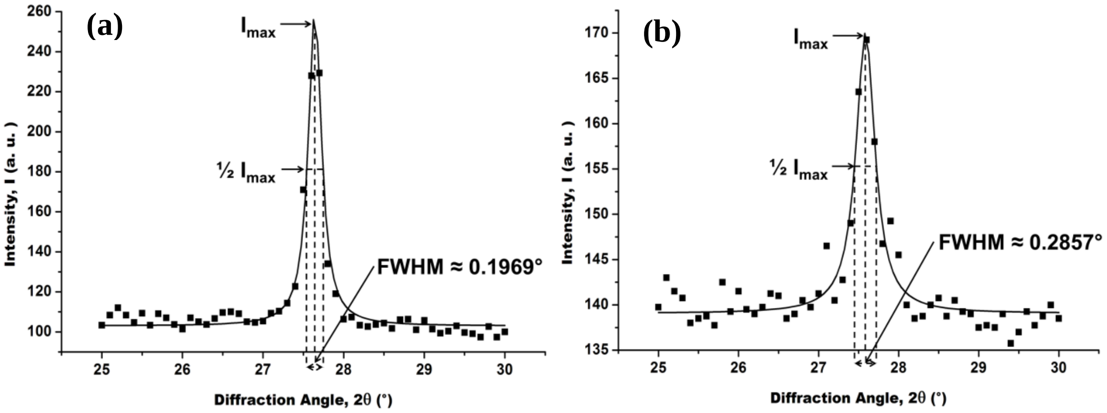

Figure 4.6 Estimated FWHM values of the diffraction peaks for (a) single layer PTCDA and (b) bilayer VOPcPhO/PTCDA thin films.

4.3 Fourier Transform Infrared (FTIR) Spectroscopy

Figure 4.7 shows the FTIR spectrum of the single layer VOPcPhO, PTCDA and bilayer VOPcPhO/PTCDA thin films. Two regions of the infrared spectra of aromatics distinguish aromatics from organic compounds that do not have an aromatic ring. These two regions are located at 675cm^{-1}-900cm^{-1} (caused by the aromatic C-H out-of-plane bending modes) and at 1665cm^{-1}-2000cm^{-1} (weak bands known as "overtones"). Not only can these bands help in distinguishing aromatics, but they can also be useful in determining the number and positions of substituents on the aromatic ring. The pattern of overtone bands in the region of 1665cm^{-1}-2000cm^{-1} reflects the substitution pattern on the ring. The pattern of the C–H out-of-plane bending bands in the region of 675cm^{-1}-900cm^{-1} is also characteristic of the aromatic substitution pattern. All the thin films show the C-H out-of-plane bending bands and the overtones confirm that all the thin films are indeed aromatic organic compounds.

For the single layer VOPcPhO thin film as shown in the Figure 4.7(a), the vanadium-oxygen double bond, V=O stretching perpendicular to the molecular plane shows a peak at 951cm^{-1}. Peaks with a relatively strong intensity, positioned near to 1004cm^{-1}, 1080cm^{-1}, 1120cm^{-1} and 1233cm^{-1} are governed by the C-O-C stretching vibrations. The peaks at 1052cm^{-1}, 1161cm^{-1}, 1203cm^{-1} and 1334cm^{-1} are due to C-N in-plane stretching vibration and C-H in-plane bending. The peaks from 1400cm^{-1} to 1680cm^{-1} are caused by the aromatic carbon to carbon skeletal (single bonding or double bonding) stretching vibrations. C-N in-plane stretching may also contribute near the 1400cm^{-1}, while C=N stretching vibration may also cause the peak at 1590cm^{-1}.

For the single layer PTCDA thin film as shown in Figure 4.7(b), the strong peaks at 1236cm^{-1} and 1301cm^{-1} can be assigned to the C-O-C stretching vibrations of the anhydride in the PTCDA molecules. The peaks at 1120cm^{-1} and 1411cm^{-1} are probably due to the δ(C-H) in-plane vibrations. Aromatic C=C vibrations lead to the peak at 1517cm^{-1} and 1595cm^{-1}. The absorption due to carboxylic dianhydride consists of –CO-O-CO- characterised at 1018cm^{-1}. The peaks at 1630cm^{-1} to 1815cm^{-1} is caused by the carboxylic acid of C=O stretching vibrations. The peak at 1746cm^{-1} is caused by the asymmetric carbonyl vibration while the peak at 1773cm^{-1} is due the symmetric carbonyl vibration (Berger, Heimer, Mack, & Ziegler, 2005; Hara, Satoh, Takami, & Ohsaki, 1995; Kaiser et al., 1999). The FTIR spectra of the bilayer VOPcPhO/PTCDA thin film is therefore the combination of the single layer VOPcPhO and PTCDA thin films as can be seen in Figure 4.7(c). The bilayer VOPcPhO/PTCDA thin film shows all the absorption peaks exist in the single layer VOPcPhO and PTCDA thin films. Summary of the chemical features of VOPcPhO and PTCDA thin films are tablulated in Table 4.0 and Table 4.1 respectively.

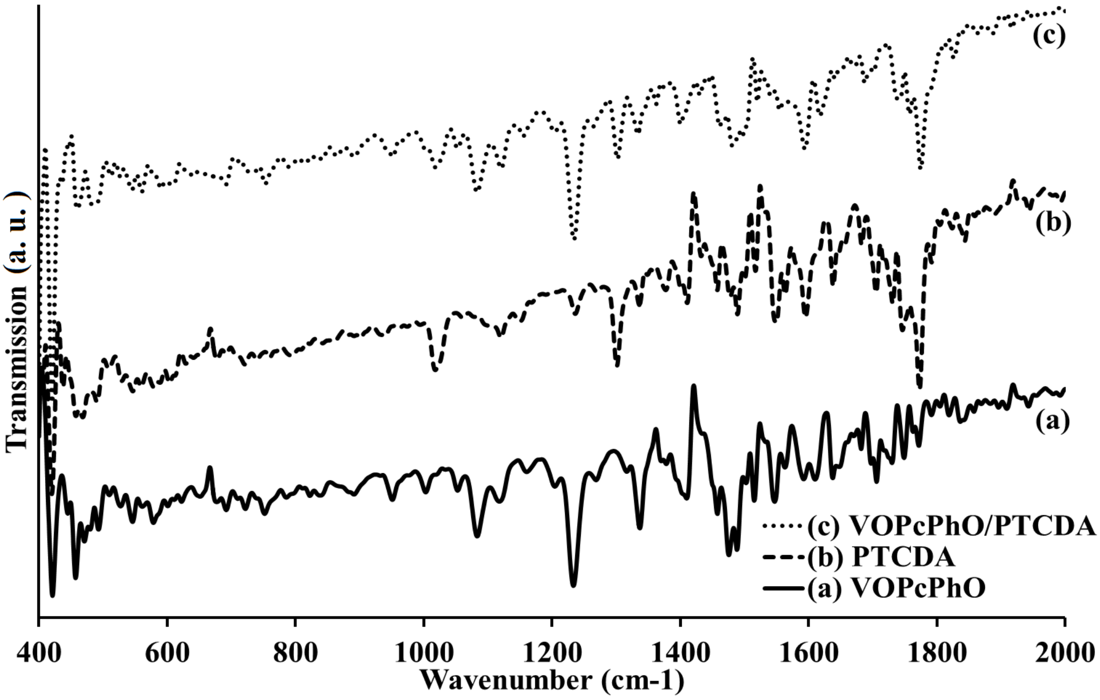

Figure 4.7 The FTIR spectrum of (a) VOPcPhO, (b) PTCDA and (c) VOPcPhO/PTCDA thin films.

Table 4.0 Summary of the chemical features of VOPcPhO thin film.

Possible vibrations	VOPcPhO
Aromatic C-H out-of-plane bending	675cm^{-1} to 900cm^{-1}
V=O stretching	951cm^{-1}
C-O-C stretching	1004cm^{-1}, 1082cm^{-1}, 1119cm^{-1} and 1233cm^{-1}
C-N and C–H in-plane bending	1052cm^{-1}, 1161cm^{-1}, 1202cm^{-1} and 1339cm^{-1}
Aromatic rings C-C or C=C stretching, C-N in-plane stretching	1397cm^{-1}
Aromatic C-C or C=C stretching	1481cm^{-1}
Aromatic C=C stretching vibration	1589cm^{-1}, 1618cm^{-1}

Table 4.1 Summary of the chemical features of PTCDA thin film.

Possible vibrations	PTCDA
Aromatic C-H out-of-plane bending	675cm^{-1}-900cm^{-1}
-CO-O-CO- vibration	1018cm^{-1}
δ(C-H) in-plane vibration	1120cm^{-1} and 1411cm^{-1}
C-O-C stretching vibrations (anhydride)	1236cm^{-1} and 1301cm^{-1}
Aromatic C=C vibrations	1595cm^{-1} and 1517cm^{-1}
C=O stretching vibrations (carboxylic dianhydride)	1630cm^{-1} to 1815cm^{-1}

4.4 Atomic Force Microscopy (AFM) and Field Emission Scanning Electron Microscopy (FESEM)

4.4.1 Single layer VOPcPhO thin film

The single layer VOPcPhO thin film displayed very uniform and smooth surface as shown in the AFM two dimensional (2D) and three dimensional (3D) images in Figure 4.8(a) and Figure 4.8(b) respectively. The root mean square roughness (Rq) and the mean roughness (Ra) measured for this VOPcPhO layer were 0.905nm and 0.737nm respectively. The values indicate that the VOPcPhO thin film is extremely smooth and flat. In order to visually observe the surface morphology of the VOPcPhO thin film, surface images of the VOPcPhO thin film were taken by the FESEM measurements. The 20k times magnification of FESEM image as shown in Figure 4.9(a) reveals a protrusion located at the center of the image. This protrusion was being utilized to make the focusing adjustments. It is thought that this protrusion is either a contaminant particle or an undissolved VOPcPhO powder particle. The size of the particle is around 200nm. The image surrounding of the particle displays a very smooth and homogenous surface. The higher magnification up to 80k times as shown in Figure 4.9(b) displays flat surface without any feature on it. Therefore, the FESEM images are consistent with the AFM results. As a simple conclusion, an extremely smooth and homogenous VOPcPhO thin film can be obtained by spin coating technique under ambient atmospheric condition using chloroform as solvent.

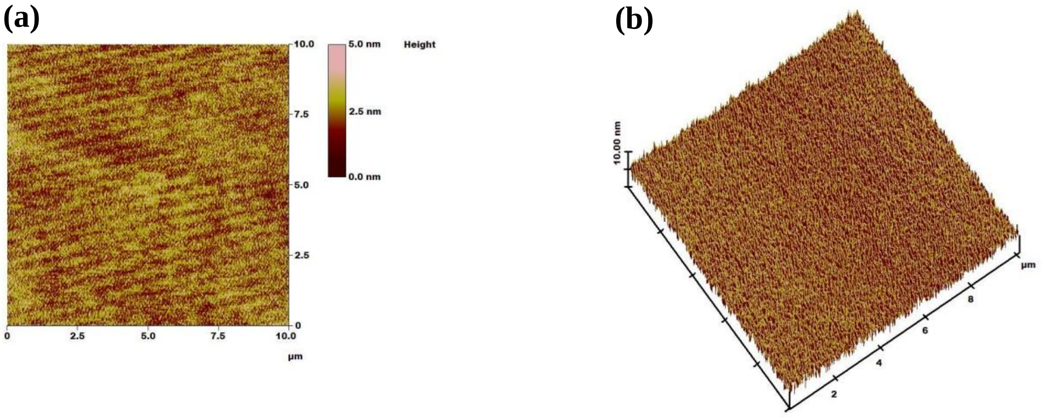

Figure 4.8 (a) 2D and (b) 3D AFM images of VOPcPhO single layer thin film.

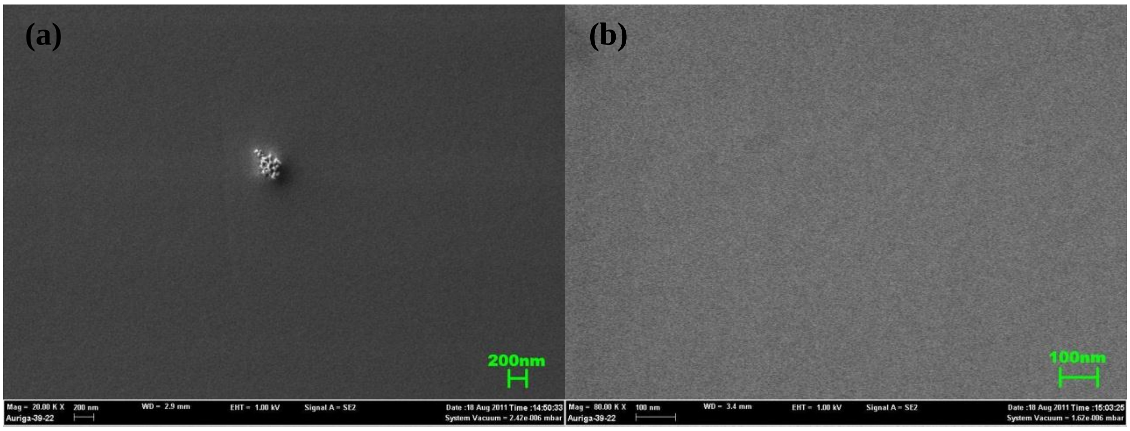

Figure 4.9 (a) 20k times magnification and (b) 40k times magnification FESEM images of VOPcPhO single layer thin film.

4.4.2 Single layer PTCDA thin film

However, the surface morphology of the PTCDA thin film deposited by thermal evaporation technique in a base pressure of 5.0 x 10^{-5} mbar and the substrate temperature held at room temperature is completely different. The surface images of PTCDA thin film scanned by AFM as can be seen in the Figure 4.10(a) and Figure 4.10(b) are considerably rough and uneven. The root mean square roughness (Rq) and mean roughness (Ra) measured are 18.722nm and 14.228nm respectively. There are several protrusions grown on the substrate surface. These protrusions typically have approximately height of 90nm and width of less than 100nm. Further inspections of the surface morphology of PTCDA single layer thin film was done by FESEM imaging.

Figure 4.11(a) is the 20k times magnification FESEM image of the PTCDA thin film. Identical to the AFM results, the FESEM image displayed a rough surface that full with small particles as seen in Figure 4.11(b) with 80k times magnification. The particles size was estimated to be less than 80nm. It is suggested that the thin film consist of these small PTCDA particles that evaporated and stack together to form a single layer on the substrate surface. Figure 4.11(c) is the in-lens (immersion lens) FESEM image. In-lens FESEM image gives higher resolution and extra information of the surface morphology. From the in-lens image, it is obvious that the particles packed and stacked themselves together to form a dense layer. As a conclusion, the surface of thermally evaporated PTCDA single layer thin film is relatively rough compared to the spin coated VOPcPhO single layer thin film.

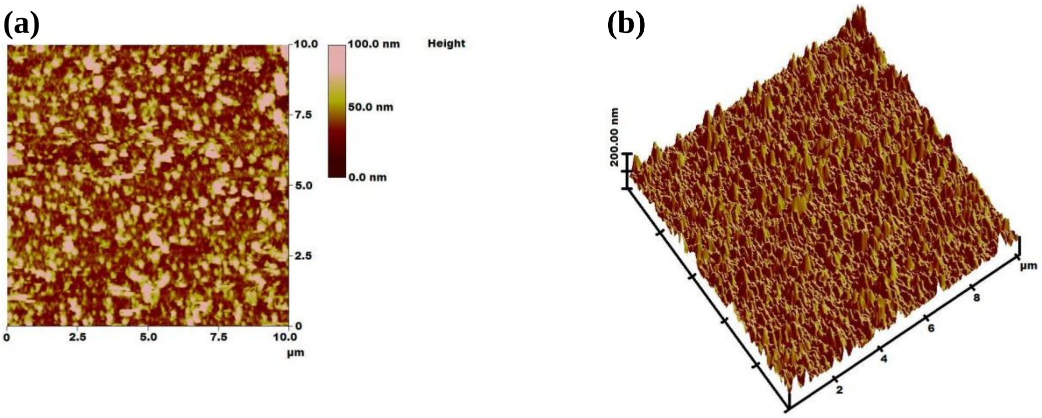

Figure 4.10 (a) 2D and (b) 3D AFM images of PTCDA single layer thin film.

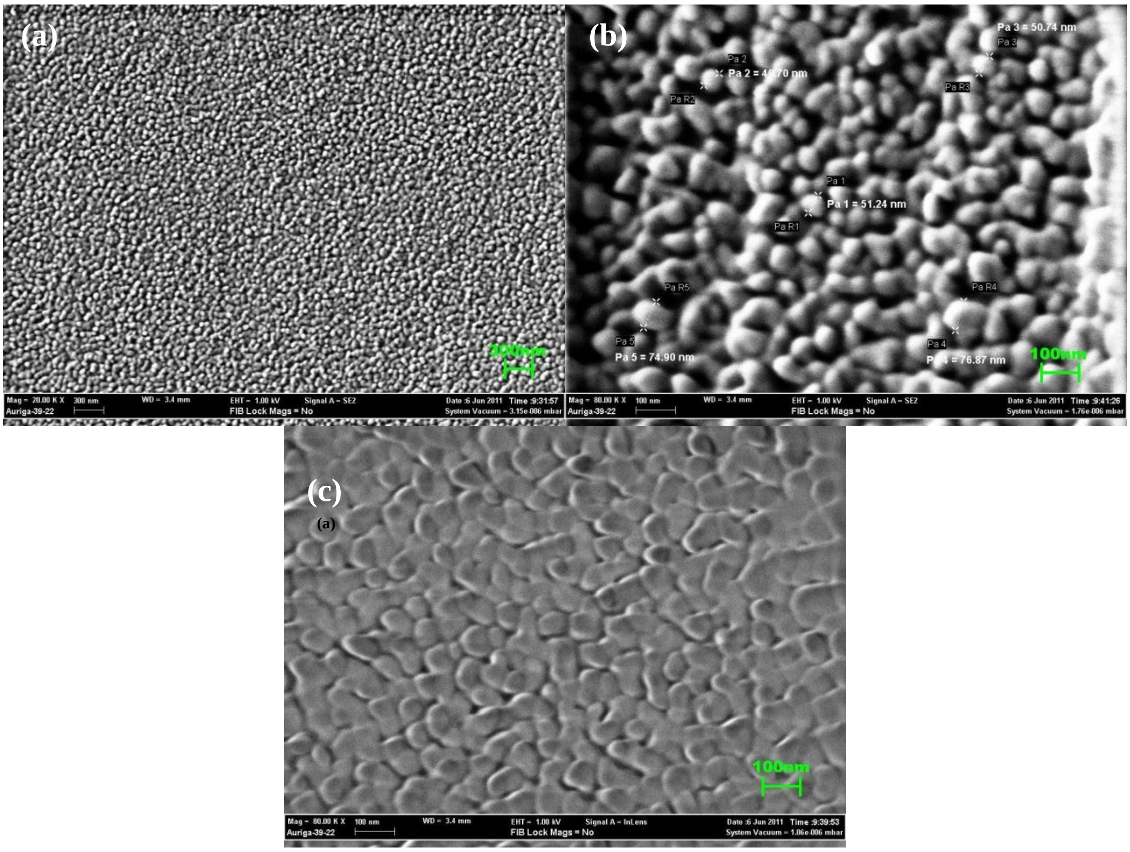

Figure 4.11 FESEM images of PTCDA single layer thin film. (a) 20k times magnification, (b) 80k times magnification and (c) 80k times magnification in-lens scanning.

4.4.3 Bilayer VOPcPhO/PTCDA thin film

Figure 4.12(a) and Figure 4.12(b) show the AFM images of bilayer VOPcPhO/PTCDA thin film in 2D and 3D respectively. The root mean square roughness (Rq) and mean roughness (Ra) measured are 9.355nm and 7.071nm respectively. The roughness of the bilayer structure is intermediate of the single layer VOPcPhO thin film and single layer PTCDA thin film. The AFM images show that needle-like structures with height less than 100nm and width smaller than 50nm grown on the substrate surface. Figure 4.13(a) is the below-the-lens FESEM image of bilayer thin film scanned at 40k times magnification. Initially, blur images were obtained when the bilayer thin film was scanned by means of below-the-lens technique. Then, fortunately, in-lens scanning technique was able to produce clearer images for the bilayer thin film. Interestingly, from the in-lens FESEM images as shown in Figure

4.13(b) and Figure 4.13(c), the structure of the PTCDA particles was different from the single layer PTCDA thin film. The deposited PTCDA layer formed rod like nanostructure over the VOPcPhO layer. Furthermore, the PTCDA structures seem like embedded into the VOPcPhO layer with a shallow depth. This morphology is preferable for the organic photovoltaic cell because the embedded structure will increase the heterojunction interface area thus will increase the probability of the exciton separation. As a preliminary conclusion, the AFM and FESEM images confirm the bilayer structure is preferable in the fabrication of the OPVC.

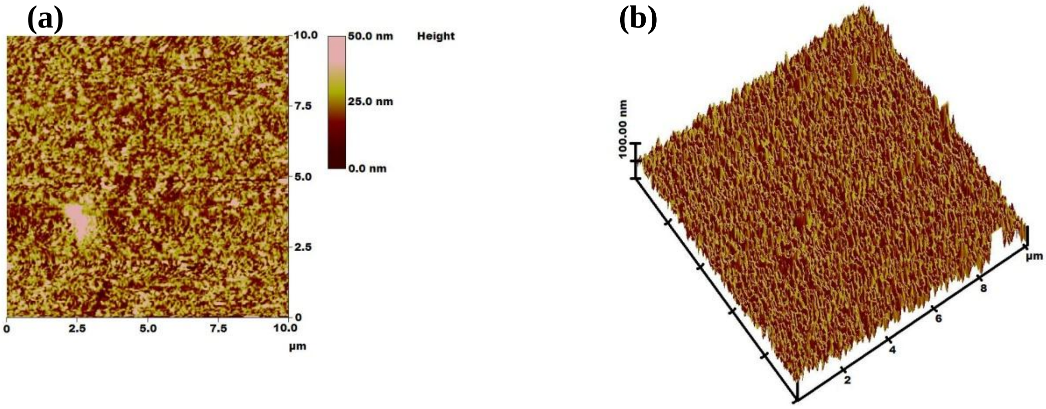

Figure 4.12 (a) 2D and (b) 3D AFM images of VOPcPhO/PTCDA bilayer thin film.

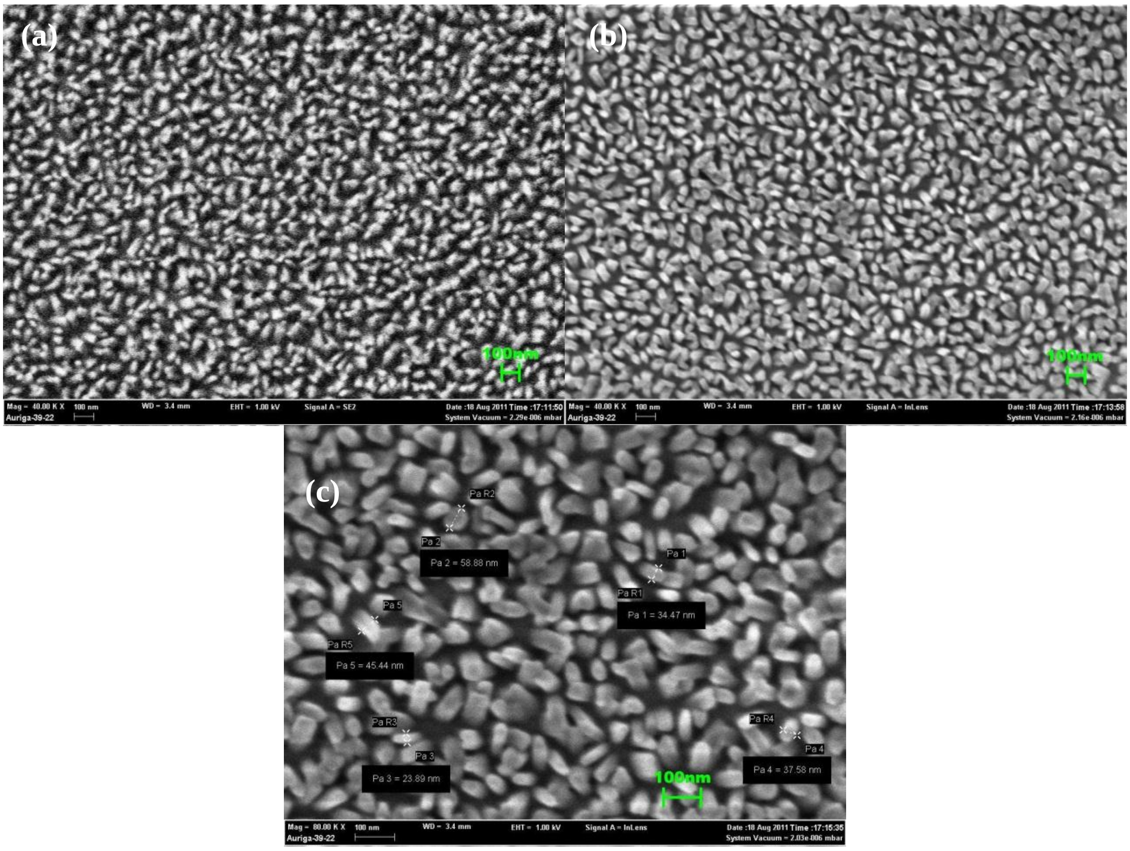

Figure 4.13 FESEM images of VOPcPhO/PTCDA bilayer thin film: (a) 40k times magnification, (b) 40k times magnification in-lens scanning and (c) 80k times magnification in-lens scanning.

Chapter 5

Electrical Properties and Improvements

5.0 Overview

The results presented from Chapter 4 on the single layer VOPcPhO, single layer PTCDA and bilayer VOPcPhO/PTCDA thin films are used in fabrication of OPVC. Hence the results on the fabricated devices with the structure of ITO/VOPcPhO/Al, ITO/PTCDA/Al and ITO/VOPcPhO/PTCDA/Al, are presented in Chapter 5. The electrical properties of these devices are illustrated in the J-V characteristics curves. In order to improve the performance of these devices, several methods have been employed: namely the inclusion of anode buffer layer, oxygen plasma treatment of anode, thickness optimisations, post annealing treatment and solvent vapour treatment. Results and discussion about each optimisation methods are provided in the following sections respectively.

5.1 Single Layer VOPcPhO and Single Layer PTCDA OPVCs

Either the single layer VOPcPhO or the single layer PTCDA OPVC shows any photovoltaic effect as shown in Figure 5.0 and Figure 5.1 respectively when the devices were illuminated under a simulated air mass 1.5 (AM1.5) illumination with the intensity of 100mW/cm^2. The illuminated J-V curves for both the single layer VOPcPhO and PTCDA OPVCs were slightly shifted compared to the dark condition. However, the fourth quadrants of the J-V characteristics for both devices do not show any changes upon light illumination. These phenomena can be clearly seen in the insets of the Figure 5.0 and Figure 5.1. The minimum of the V-shape in the illuminated curve located at the same position as the dark curve. No shift presents indicating no photovoltaic effect. Given typical value for the exciton Borh radius which is usually less than 10nm (Agranovich, Basko, Rocca, & Bassani, 1998; Polimeni et al., 2004), and exciton binding energy 0.15eV-1.0eV (Franceschetti & Zunger, 2001; Huang et al., 2009), a field of > 10^7 V/m would be required to cause the exciton to dissociate.

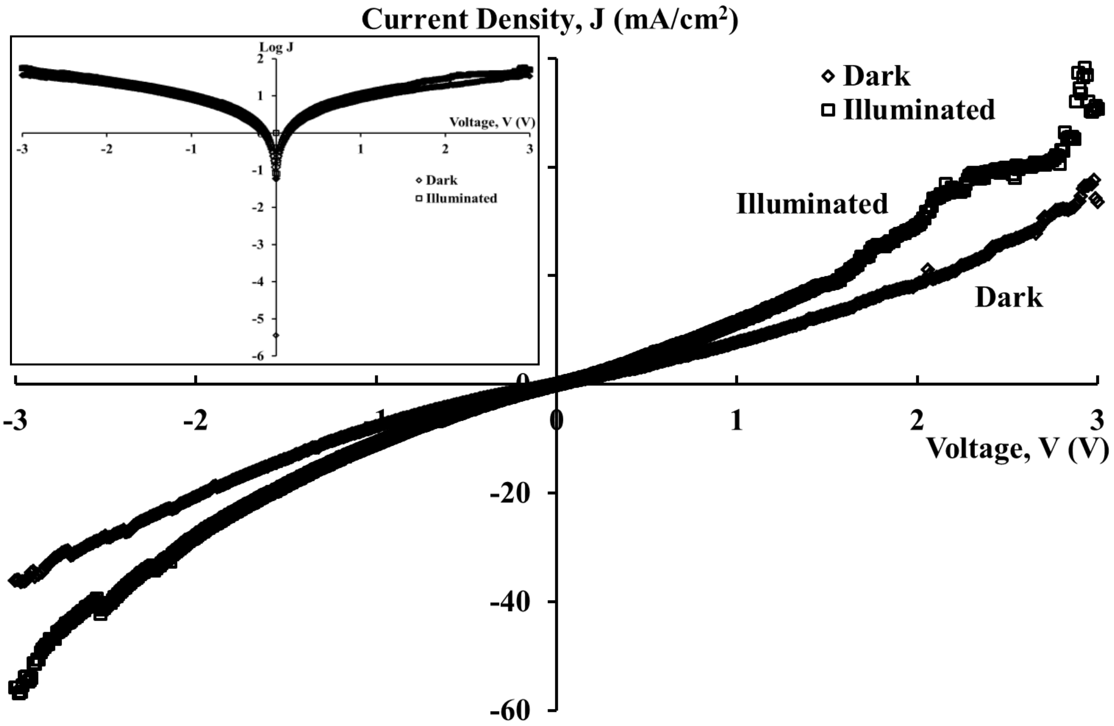

Figure 5.0 The J-V characteristic curves of ITO/VOPcPhO/Al OPVC. The inset shows the log J-V curves of the device.

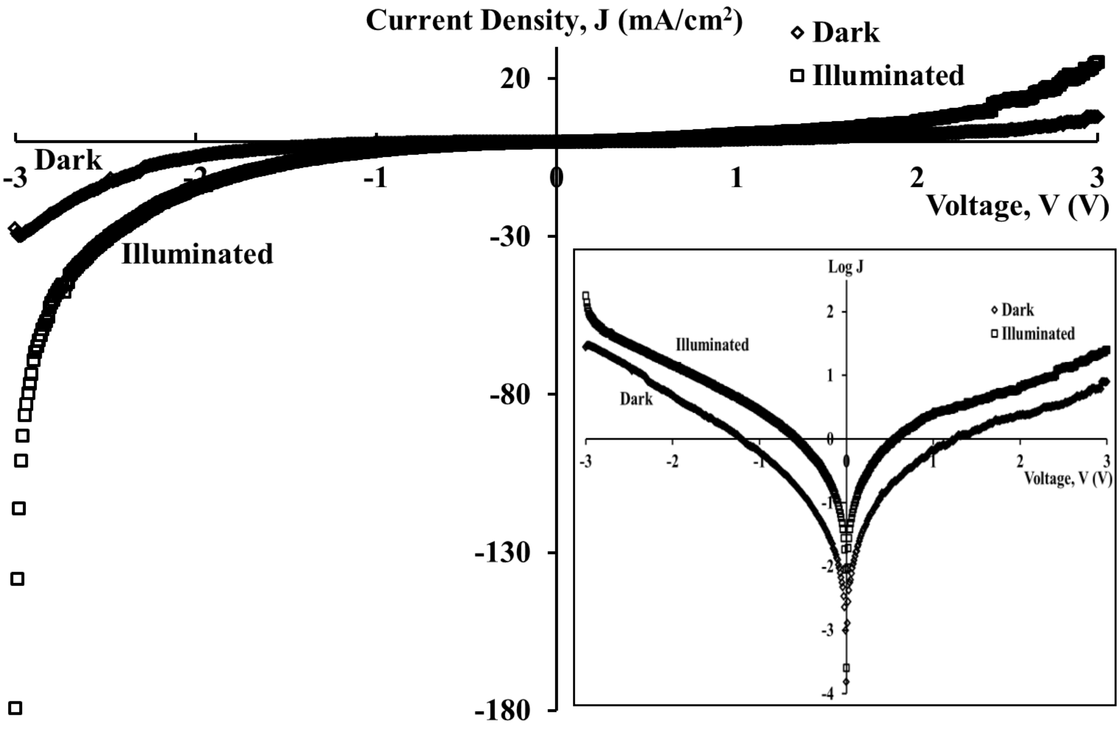

Figure 5.1 The J-V characteristic curves of ITO/PTCDA/Al OPVC. The inset shows the log J-V curves of the device.

However, the internal electric field that induced in the active layers (~200nm) between the anode and cathode when applied an external voltage normally less 2V for OPVC is typically in the range of ~ 106 V/m. It is suggested that the electric field induced by the difference in the work function of anode (ITO) and cathode (Al) is not strong enough to dissociate the excitons created in the active layers (Gregg & Hanna, 2003).

5.2 Bilayer VOPcPhO/PTCDA Organic Photovoltaic Cell

Figure 5.2 shows the J-V curves for the bilayer heterojunction VOPcPhO/PTCDA organic photovoltaic cell under dark and illumination condition. Unlike the single layer VOPcPhO or single layer PTCDA OPVCs which do not exhibit photovoltaic effect, the bilayer herojunction device clearly shown interesting photovoltaic effect when light beam shined upon it. When the device was illuminated by a simulated air mass 1.5 (AM1.5) illumination with the intensity of 100mW/cm^2, the curve shifted downward indicating the photovoltaic effect. The inset of Figure 5.2 is the semi-log J-V curves of the device which is able to provide extra information of the PV effect of the cell. From the semi-log J-V curves, the V-shape of the dark curve centred nearly at 0V. However, the illuminated curve shifted upward and the V-shape curve centred at 0.21V. This minimum point of 0.21V is actually the open circuit voltage, V_{oc} of the device. As briefly discussed in the section 2.4 in chapter two, the photovoltaic parameters of the cell such as the short current density (J_{sc}), the open circuit voltage (V_{oc}), the fill factor (FF) and the power conversion efficiency (PCE) can be extracted from the J-V graph for the analysis of the performance of the cell. All these parameters of the simple structure ITO/VOPcPhO/PTCDA/Al cell are summarised in Table 5.0. The negative short-circuit current flows from ITO electrode to Al electrode ($I < 0$) in a manner as expected. That is, the excitons created in the VOPcPhO and PTCDA layers upon illuminated and diffused to the VOPcPhO/PTCDA interface where the exciton dissociations take place. The exciton dissociations produced free charge carriers of holes and electrons. The produced holes transported across VOPcPhO and the produced electrons transported across PTCDA layer. These holes and electrons travelled to ITO and Al electrodes respectively generated a direct current through an external circuit in the direction from ITO to Al electrodes, $I < 0$. The photovoltaic effect detected in the bilayer structure device but not in the single layer devices proves that the exciton dissociations can only take place at the VOPcPhO/PTCDA interface hence directly conform the speculation made in the section 5.2 that the internal electric field induced by the electrodes is not strong enough to dissociate the exciton. However, the device has low power conversion efficiency due to the fabrication and characterisation processes are all done in the ambient atmospheric condition of un-encapsulated device. The organic semiconductors were easily degraded in the ambient atmospheric condition due to the moisture, oxygen, light et cetera (H. B. Yang, Song, Gong, & Li, 2010). Therefore, the highest PCE obtained for the simple structure ITO/VOPcPhO/PTCDA/Al device is 0.0025% with FF of 0.31, J_{sc} of 0.0025mA/cm^2 and V_{oc} of 0.21V.

The parallel shunt resistance, R_{sh} and series resistance, R_s of the cell are determined from the J-V curves. In general, R_{sh} arises from charge recombination at the donor/acceptor interface and surface current leakage while R_s is affected by the bulk resistance of the active layer and the contact resistance between the active layer and the electrode. R_{sh} is calculated from the inverse slope around the bias voltage, ~0V and R_s from the inverse slope at a positive bias voltage over V_{oc} in the J-V curves. For this simple structure ITO/VOPcPhO/PTCDA/Al, the R_{sh} and R_s estimated from the J-V curve are $10.87\times10^4\Omega$cm^2 and $5.65\times10^4\Omega$cm^2 respectively. The R_{sh} is rougly twice of the R_s. For an ideal solar cell, the R_{sh} would be infinite which indicated that there is no alternate path for current to flow, while R_s would be zero, resulting in no further voltage drop before the load. Drop in R_{sh} and rise in R_s will decrease the FF. If R_{sh} is excessively decreased, V_{oc} will drop, while excessive increment in R_s can cause J_{sc} to drop instead.

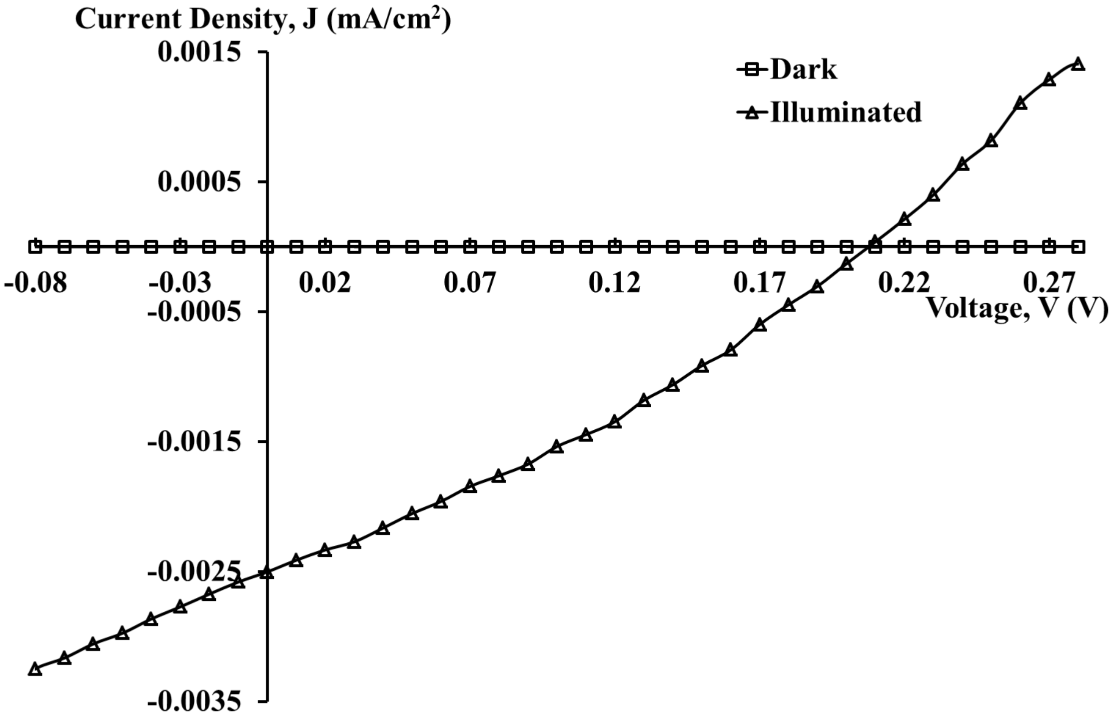

Figure 5.2 The J-V characteristic curves of ITO/VOPcPhO/PTCDA/Al OPVC. The inset shows the log J-V curves of the device.

Table 5.0 Photovoltaic parameters for the ITO/VOPcPhO/PTCDA/Al organic device.

Device	J_{sc} (mA/cm^2)	V_{oc} (V)	FF	PCE ($\times10^{-3}$%)	R_{sh} ($\times10^4\Omega$cm^2)	R_s ($\times10^4\Omega$cm^2)
ITO/VOPcPhO /PTCDA/Al	0.0025	0.21	0.31	0.16	10.87	5.65

5.3 Improvements and Optimisation of Organic Solar Cell

5.3.1 Hole transport layer - PEDOT: PSS

Poly(3,4-ethylenedioxythiophene): poly(styrenesulfonate) (PEDOT: PSS) is a conjugated polymer made up of two ionomers: poly(3,4-ethylenedioxythiophene) (PEDOT) and poly(styrenesulfonic acid) (PSS). Figure 5.3 shows the molecular structure of the PEDOT: PSS molecule. It is widely used in organic optoelectronics due to its high conductivity, good optical transparency in thin film and high stability

(Friedel et al., 2009; Hu, Zhang, Hao, & Zhao, 2011; Youngkyoo Kim, Ballantyne, Nelson, & Bradley, 2009). This conjugated polymer is commercially available therefore making it highly accessible. Most importantly, PEDOT: PSS possesses high water solubility and can be easily deposited as thin films via relatively inexpensive and easy method such as spin coating technique.

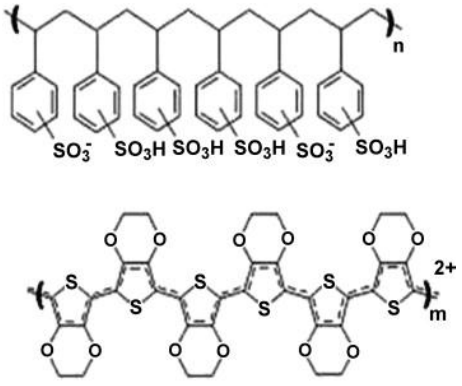

Figure 5.3 The molecular structure of PEDOT: PSS.

In this research work, PEDOT: PSS was used as the anode buffer layer to enhance the performance of the OPVC. It was sandwiched between the transparent ITO electrode and the bilayer VOPcPhO/PTCDA light absorbing layer. The PEDOT: PSS thin film then went through thermal annealing process at 100°C for 30 minutes under the ambient atmospheric condition to remove the water molecules before the active layer was deposited onto it. The removal of water molecule in the PEDOT: PSS layer is essential because it can decrease the acidic property of the PEDOT: PSS and prevent the potential cause of the degradation of the adjacent active layer. (Friedel, et al., 2009). The J-V curves in Figure 5.4 and the data in Table 5.1 show the device performance has been improved significantly by inserting the PEDOT: PSS layer into the OPVC. The increased J_{sc} by 952% of the device after inclusion of the PEDOT: PSS layer can be attributed to the enhanced efficiency of the holes transfer between the VOPcPhO layer and the PEDOT: PSS layer compared to the holes transfer between the VOPcPhO layer and the ITO anode layer. Improved surface smoothness of the anode/active layer contact may also facilitate the holes transfer in the device. The V_{oc} was also found to be increased from 0.2V to 0.5V in the device consists of PEDOT: PSS layer. The increment in V_{oc} can be attributed to the effect of increased work function relative to the ITO. Better matching work function of the electrodes with the HOMO level of the active materials in the active layer may allow the V_{oc} approaches the theoretical value (Youngkyoo Kim, et al., 2009). The FF decreased as a result of drastic decreases in R_{sh} and R_s. The ratio of R_{sh} over R_s (R_{sh}: R_s) is 0.82 which is close to 1 may be causing the forth quadrant of the J-V curve of the device to be ohmic. As a consequent, the FF decreased from 0.31 to 0.20 after inclusion of PEDOT: PSS into the OPVC. However, the decline in the FF does not affect much on the overall performance of the OPVC. As a result, the insertion of the PEDOT: PSS as a buffer layer on the ITO electrode significantly improved the PCE of the device by one order of magnitude. This result is in agreement to the other reports by Yoo and Xi (Xi et al., 2010; Yoo et al., 2005).

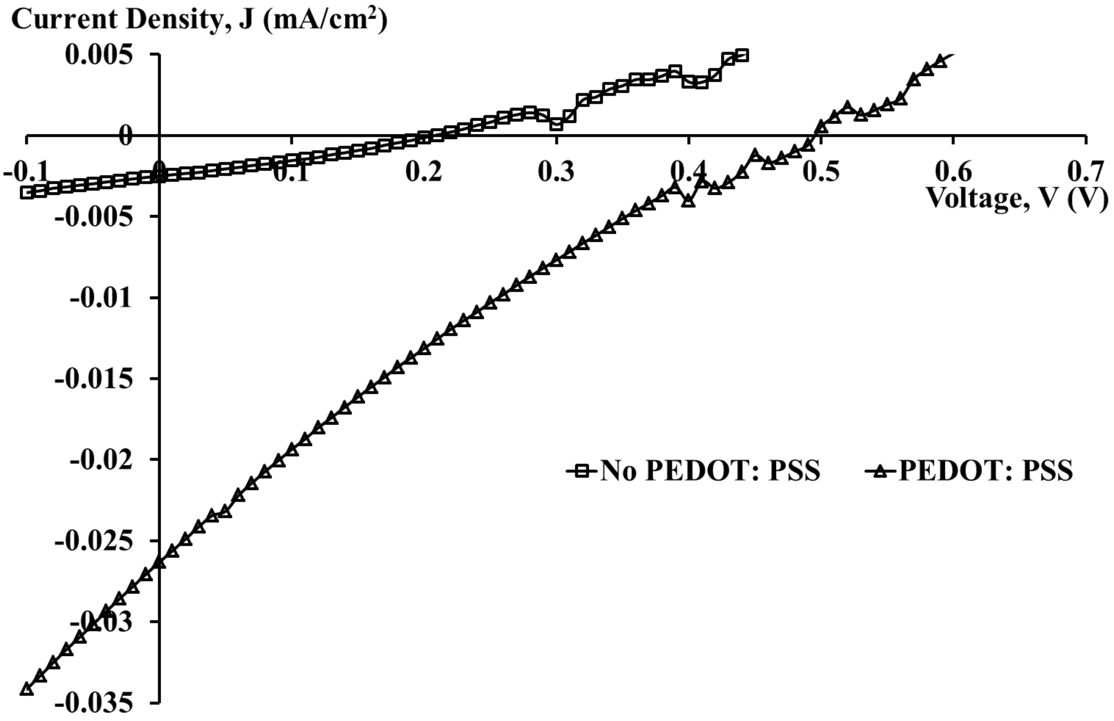

Figure 5.4 The J-V curves comparison of the OPVC without PEDOT: PSS and OPVC with PEDOT: PSS.

Table 5.1 Photovoltaic parameters for the ITO/VOPcPhO/PTCDA/Al and ITO/PEDOT: PSS/VOPcPhO/PTCDA/Al organic devices.

Device	J_{sc} (mA/cm^2)	V_{oc} (V)	FF	PCE ($\times10^{-3}$%)	R_{sh} ($\times10^4\Omega cm^2$)	R_s ($\times10^4\Omega cm^2$)
ITO/VOPcPhO/ PTCDA/Al	0.0025	0.21	0.31	0.16	10.87	5.65
ITO/PEDOT: PSS/VOPcPhO/ PTCDA/Al	0.0263	0.50	0.20	2.64	1.35	1.65

5.3.2 Oxygen (O_2) plasma treatment

Oxygen (O_2) plasma treatment on the ITO surface was reported to have improved the performance of the OPVC (Hashimoto & Hamagaki, 2006; Young Kim, et al., 2008). Therefore attempts were made to improve the bilayer VOPcPhO/PTCDA OPVC based on this technique. The ITO substrates were treated by O_2 plasma for 5 minutes at a radio frequency (RF) power of 35W. The pressure of the chamber was maintained at 1.0mbar during the treatment. Obviously, from the J-V curves and table data shown in Figure 5.5 and Table 5.2, all the OPVC properties enhanced after the ITO substrate went through O_2 plasma. Compared to the untreated OPVC coated with PEDOT: PSS, the J_{sc} increased from 0.0263mA/cm^2 to 0.0301mA/cm^2 and the V_{oc} increased from 0.50V to 0.53V. FF of the O_2 plasma treated OPVC also increased from 0.20 to 0.23. Consequently, the PCE of the O_2 plasma treated OPVC uplifted to 3.71×10^{-3}% from 2.64×10^{-3}% of the untreated OPVC. Note that both the R_{sh} and R_s also increased slightly resulted from the O_2 plasma treatment. However, the ratio of R_{sh} to R_s is 0.76 (≈ 1) hence the FF of the device still remains low.

The O_2 plasma treatment is thought to be able to improve the stoichiometry of the ITO surface by removing the surface contaminants such as hydrocarbon contaminants. Hydrocarbon contaminants caused low surface energy. The removal of hydrocarbons can leads to an increase of the surface energy. In the addition, oxide bonds can form onto the ITO surface during the O_2 plasma treatment. The oxide bonds lead to higher surface energy and the surface become more hydrophilic. The increase of surface energy of ITO substrates provides better adhesion of the PEDOT: PSS thin film and reduces the interfacial energy between the PEDOT: PSS layer and the ITO layer (You & Dong, 2007). More hydrophilic surface is favorable for the PEDOT: PSS because PEDOT: PSS is water based solution. All these factors caused the increase of the effective area and improvement of a better electronic contact between the PEDOT: PSS thin film and the ITO layer. Furthermore, O_2 plasma treatment may alter ITO function to be higher and reduced the barrier height of the ITO/organic layer interface (You & Dong, 2007). This leads to better charge transport and therefore improved the performance of the OPVC.

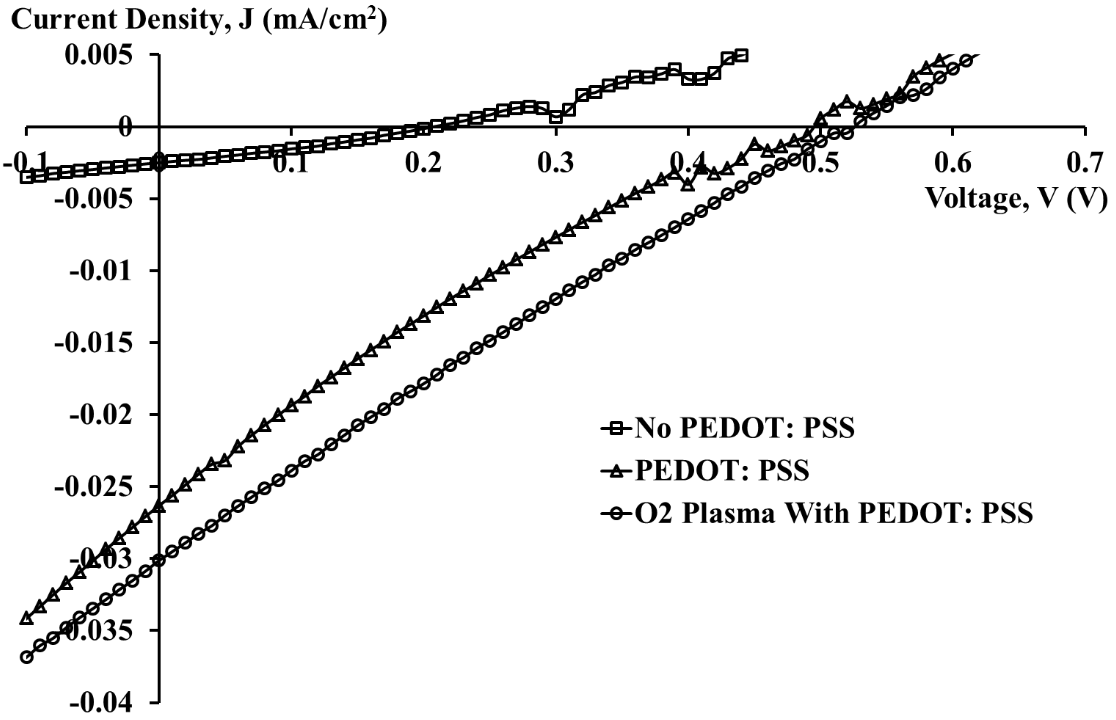

Figure 5.5 The J-V curves comparison of the OPVC without PEDOT: PSS, OPVC with PEDOT: PSS and OPVC treated by O_2 plasma.

Table 5.2 Photovoltaic parameters for the OPVC without PEDOT: PSS, OPVC with PEDOT: PSS and OPVC treated by O_2 plasma.

Device	J_{sc} (mA/cm^2)	V_{oc} (V)	FF	PCE ($\times10^{-3}$%)	R_{sh} ($\times10^4\Omega$cm^2)	R_s ($\times10^4\Omega$cm^2)
Without PEDOT: PSS	0.0025	0.21	0.31	0.16	10.87	5.65
With PEDOT: PSS	0.0263	0.50	0.20	2.64	1.35	1.65
O_2 Plasma	0.0301	0.53	0.23	3.71	1.55	2.04

5.3.3 PEDOT: PSS layer thickness optimisation

Thickness variation of the PEDOT: PSS layer was carried out to find out the optimum thickness of PEDOT: PSS for the bilayer OPVC. PEDOT: PSS was spun at four different spin rates which were 2000 rotation per minute (rpm), 4000rpm, 6000rpm and 8000rpm for 30 seconds onto the O_2 plasma treated ITO substrates. Then, the thickness of PEDOT: PSS thin films were measured using KLA Tencor P-6 Surface profilormeter. As expected, a higher spin rate produces a thinner film and the results are displayed in Figure 5.6 and Table 5.3. It is found that by applying these four spin rates in preparing PEDOT: PSS thin films, the thickness varied from 23nm to 75nm.

Subsequently, OPVCs based on these four different spin rates were fabricated. All the others parameters suchs as effective active area, deposition condition et cetera were kept constant. The effect of PEDOT: PSS thickness on the current density, J_{sc} and open circuit voltage, V_{oc} of the bilayer OPVC is shown in Figure 5.7 whereas, Figure 5.8 presents such variation on the fill factor and efficiency. The summary of the results are tabulated in Table 5.3. The overall performance of the OPVCs initially enhanced from the spin rate of 2000rpm and peak at the spin rate of 6000rpm but decreased after 6000rpm. The highest OPVC efficiency is achieved at the spin rate of 6000rpm corresponds to the PEDOT: PSS thickness of 31.27nm. Therefore, this optimum spin rate of 6000rpm (thickness of ~30nm) is adopted for all the following experiments.

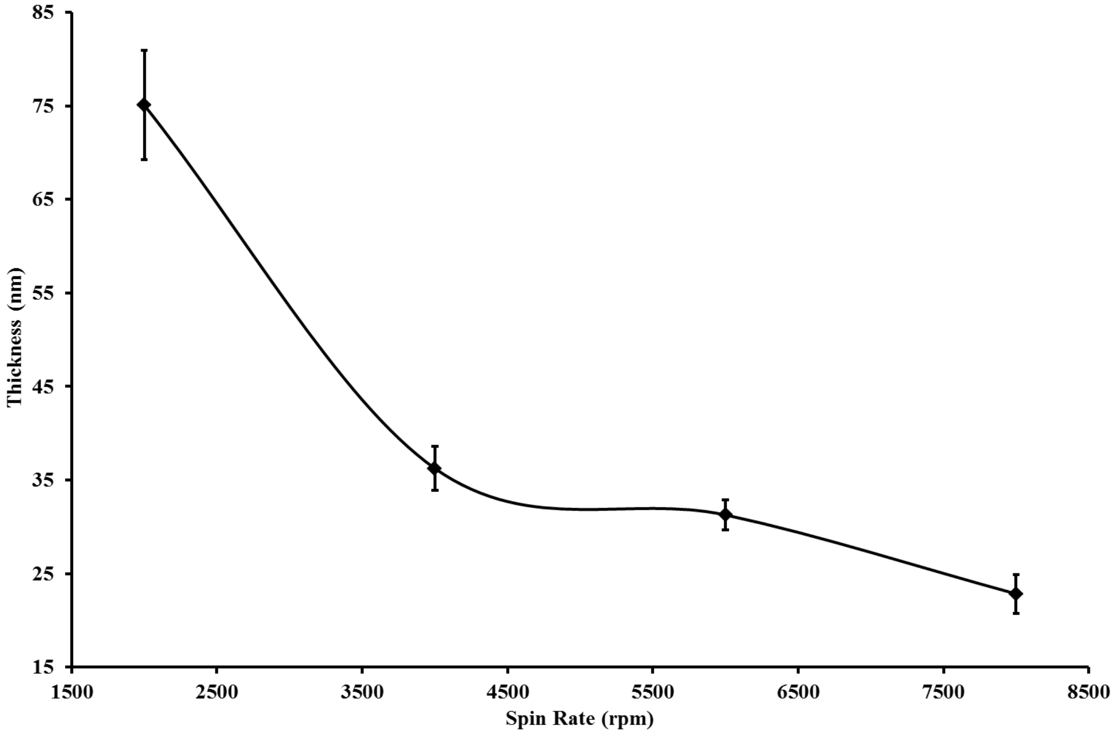

Figure 5.6 The thickness of PEDOT: PSS thin films spun at four different spin rates.

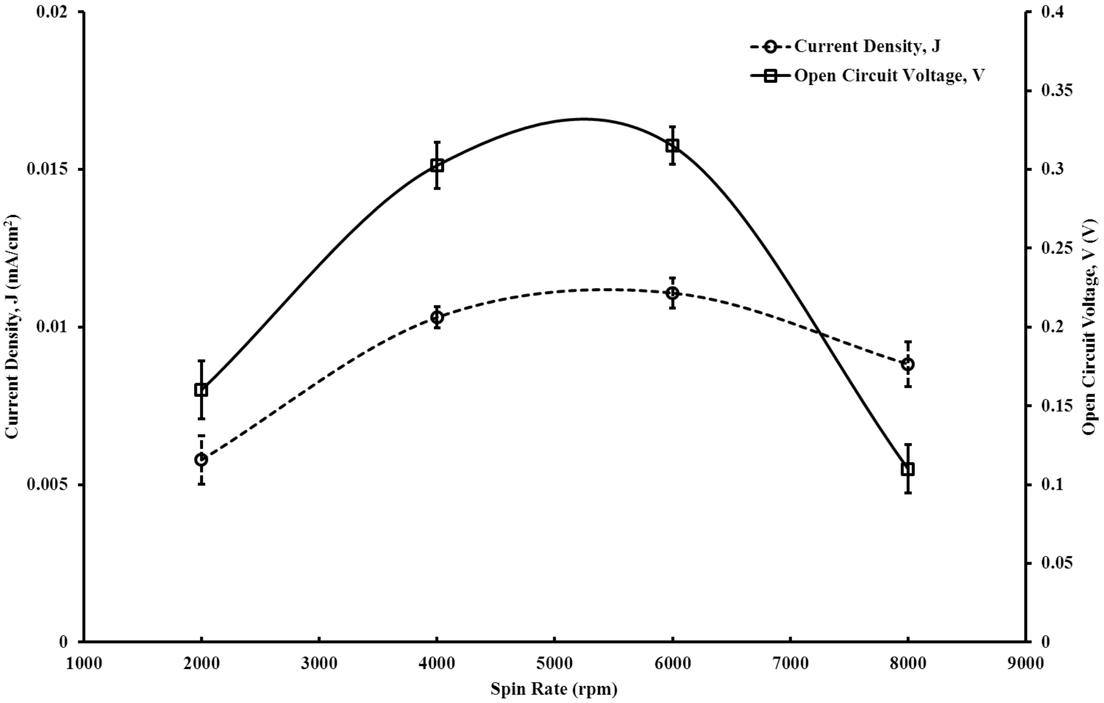

Figure 5.7 The graph of J_{sc} and V_{oc} versus spin rate for different PEDOT: PSS thickness OPVC.

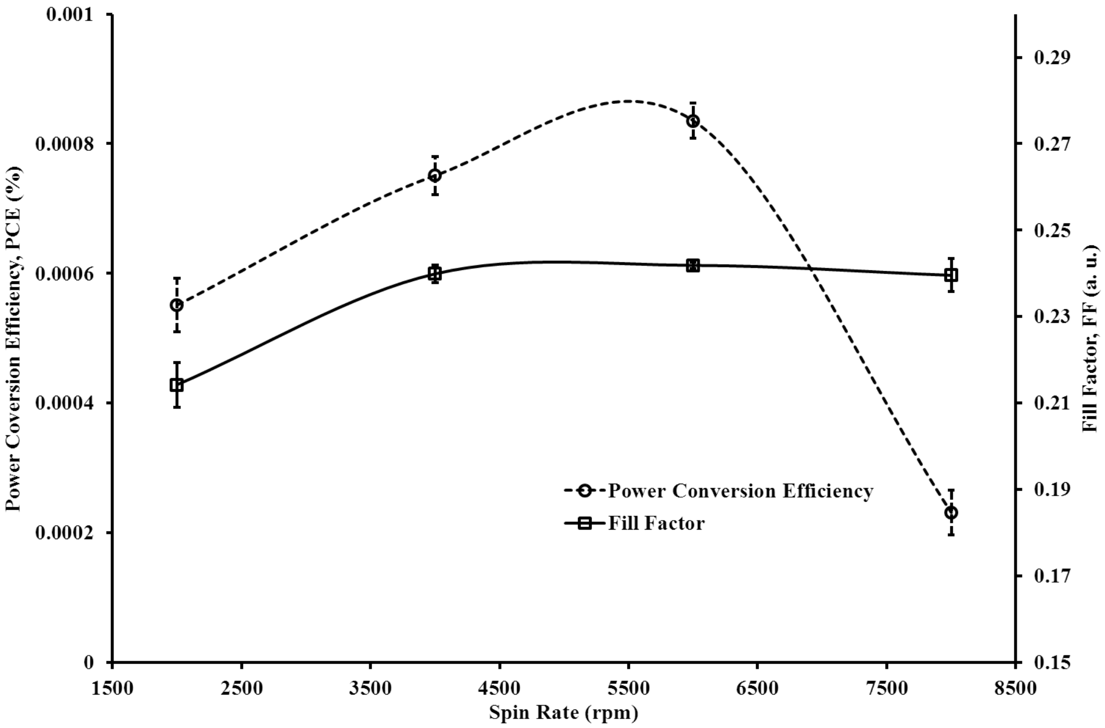

Figure 5.8 The graph of PCE and FF versus spin rate for different PEDOT: PSS thickness OPVC.

Table 5.3 Photovoltaic parameters for the OPVC with different PEDOT: PSS thickness.

Spin Rate (rpm)	Thickness (nm)	J_{sc} ($\times 10^{-2}$mA/cm^2)	V_{oc} (V)	FF	PCE ($\times 10^{-3}$%)
2000	75.07	0.58	0.16	0.21	0.55
4000	36.24	1.03	0.30	0.24	0.75
6000	31.27	1.11	0.32	0.24	0.84
8000	22.84	0.88	0.11	0.24	0.23

5.3.4 VOPcPhO layer thickness optimisation

Thickness optimisation of the VOPcPhO layer was performed out to discover the optimum thickness of VOPcPhO for the bilayer OPVC. Initially, VOPcPhO solution was spun at four different spin rates; 1000rpm, 2000rpm, 3000rpm and 4000rpm for 30 seconds onto the 30nm thick PEDOT: PSS layer. After that, the VOPcPhO thin films were brought to measure the thickness using KLA Tencor P-6 Surface profilormeter. The thickness of the VOPcPhO thin film displays almost linearity in the thickness versus spin rate as presented in Figure 5.9. Overall results are displayed in Table 5.4, in which can be observed that higher spin rate produces thinner films. Thickness range from 23nm to 75nm of VOPcPhO thin films can be deposited using those four spin rates. As can be seen in Figure 5.10, higher spin rates which corresponds to the thinner thin films generate higher current densities and open circuit voltages in the devices. In Figure 5.11, the fill factor of the devices show variation corresponding to the different spin rates. Higher FF can be obtained from the films prepared at lower spin rates and a maximum FF occurs at 2000rpm. FF of the devices drops for the spin rates higher than 2000rpm. However, the FF of the devices do not give any distinct effect on the PCE of the devices compared to the J_{sc} and V_{oc} therefore the increment in PCE trend follows the J_{sc} and V_{oc} variations. The increased PCE of the devices correspond to lower thickness of the VOPcPhO thin films are understandable if we look into the nature of the excitons. As mentioned in the section 2.3 of chapter 2, the excitons have short diffusion length (~10-20nm) (Bergemann & Forrest, 2011; Lunt, Giebink, Belak, Benziger, & Forrest, 2009; Y.-l. Pan et al., 1998b). Besides, the exciton dissociation can occur only near the interface of the VOPcPhO/PTCDA as discussed in the earlier section 5.3 and 5.4. Therefore it is understandable that the thickness of the VOPcPhO and PTCDA thin films should be thin enough hence excitons can diffuse to the VOPcPhO/PTCDA interface. Furthermore, the probability of the excitons to recombine in the active layer is lower for the thinner organic thin films. This leads to better chance of the exciton dissociations at the VOPcPhO/PTCDA interface, therefore increase the PCE of the devices. The VOPcPhO thin film thickness optimisation experiment shows that the highest PCE obtained at thickness 23nm which corresponds to the spin rate of 4000rpm. This spin rate will adopted for all the following experiments.

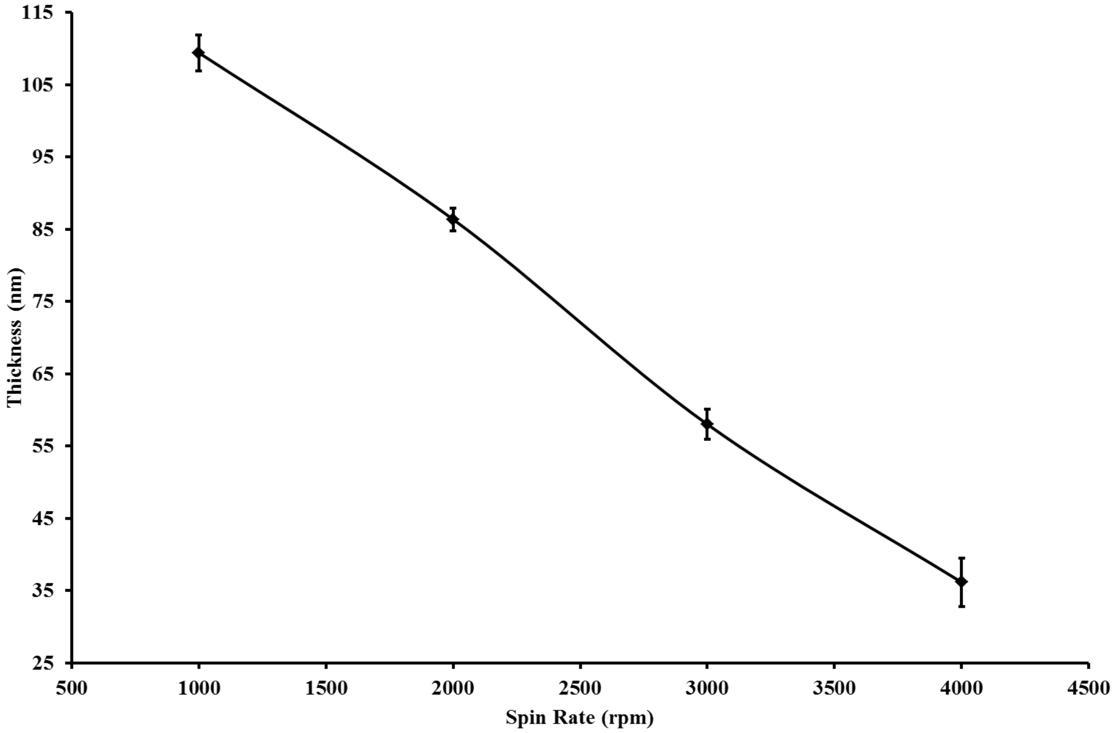

Figure 5.9 The thickness of VOPcPhO thin films spun at four different spin rates.

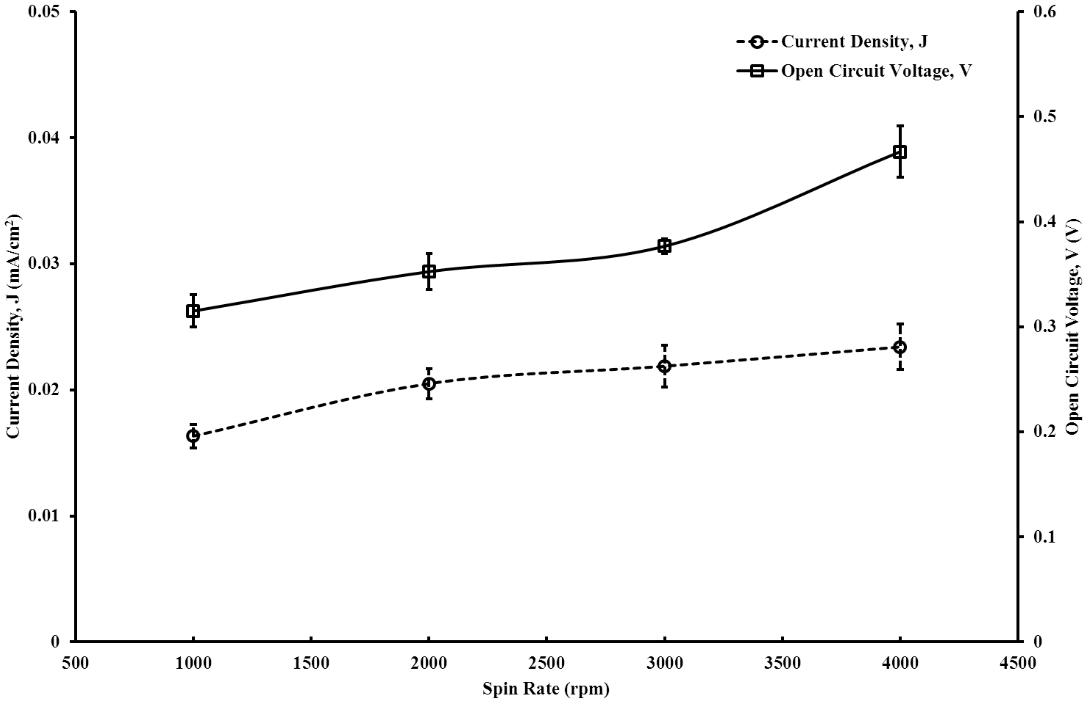

Figure 5.10 The graph of J_{sc} and V_{oc} versus spin rate for different VOPcPhO thickness OPVC.

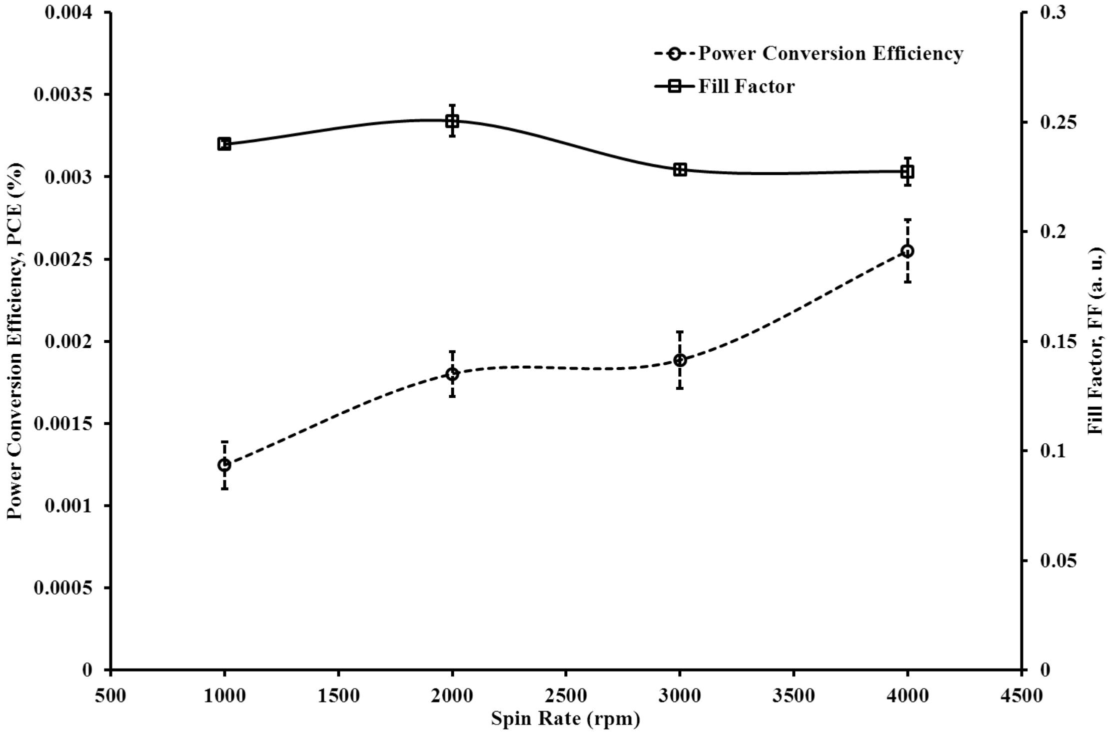

Figure 5.11 The graph of PCE and FF versus spin rate for different VOPcPhO thickness OPVC.

Table 5.4 Photovoltaic parameters for the OPVC with different VOPcPhO thin films thickness.

Spin Rate (rpm)	Thickness (nm)	J_{sc} ($\times 10^{-2}$mA/cm^2)	V_{oc} (V)	FF	PCE ($\times 10^{-3}$%)
1000	94.35	1.63	0.32	0.24	1.25
2000	79.15	2.05	0.35	0.25	1.80
3000	74.16	2.19	0.38	0.23	1.89
4000	36.15	2.34	0.47	0.23	2.55

5.3.5 Post thermal annealing and vapour treatments

Many studies have shown that the *in situ* thermal treatment of the substrate temperature (inside a thermal evaporator) is an effective method to induce the crystallization of VOPc from phase-I to phase-II (T. Del Caño, et al., 2005; Nakano, et al., 2001; Yamashita, et al., 1993). Therefore, in this research study, several attempts were made to induce a similar crystallisation process in the spin-coated VOPcPhO thin films using a post thermal annealing approach on a hot plate at 100°C for 30 minutes. The effect of crystallisation in the OPVC then studied by comparison to the amorphous device. Figure 5.12 shows the effects of post thermal annealing and solvent vapour treatments onto the VOPcPhO thin films in UV-VIS spectrum. It can be noticed that absorption intensity has been reduced either by annealing or treating with vapour.

According to the literature, the thermally evaporated VOPc has been reported to form at least in two phases: phase-I and phase-II. Phase-I VOPc has been reported as having an amorphous structure, whilst phase-II VOPc is characterised by a triclinic crystal structure (T. Del Caño, et al., 2005; Nakano, et al., 2001; Yamashita, et al., 1993). The two different phases of the VOPc thin film can be identified by unique near-infrared (IR) absorption in the Q band of the absorption spectrum. In this study, the spin-coated VOPcPhO thin film and then annealed, show a broader Q band and shifted towards red region of the absorption spectrum as presented in Figure 5.12. One can noticed that the absorption peak, λ_{max} of the annealed VOPcPhO has shifted to 800nm, compared to the pristine VOPcPhO thin film with λ_{max} = 711nm. Note that the λ_{max} of the B band also has red shifted to λ_{max} = 355nm and λ_{max} = 347nm for the annealed and vapour treated VOPcPhO thin films, respectively. The results of the UV-VIS absorption spectra indicate that the post thermal annealing approach under ambient atmospheric conditions may transform the VOPcPhO thin film from a phase-I (amorphous) to a phase-II (semi-crystalline) structure.

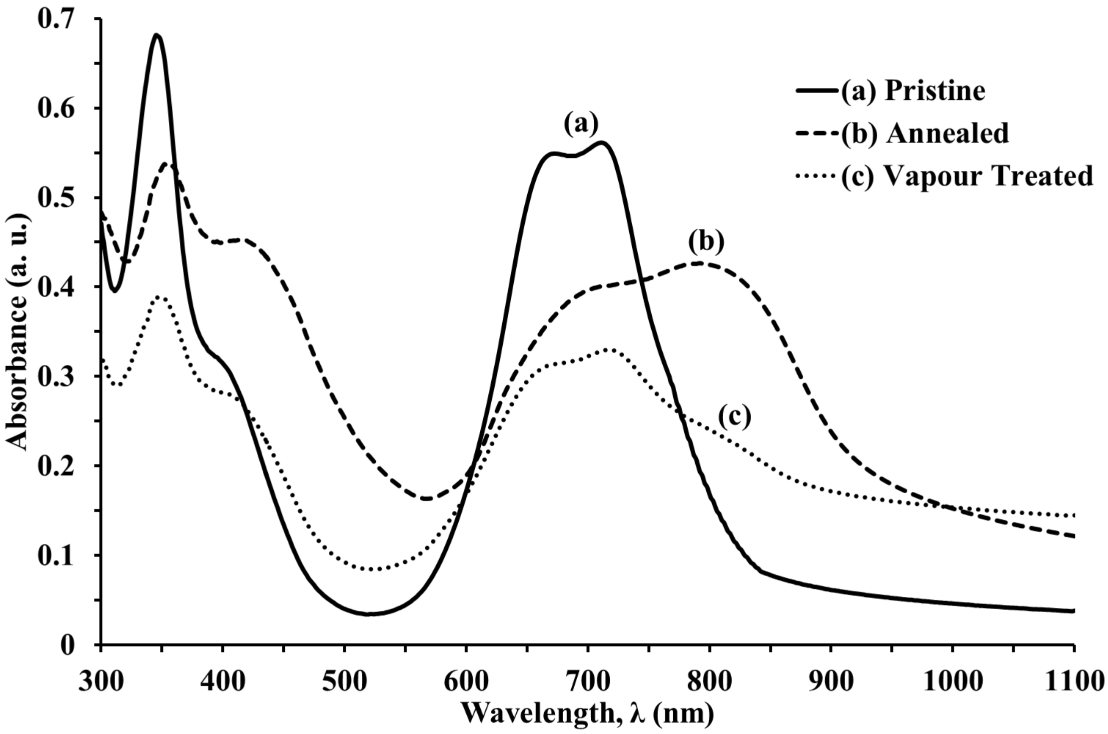

Figure 5.12 The UV-VIS spectra of the pristine, annealed and vapour treated VOPcPhO thin films.

The second method employed was the solvent vapour treatment, in which the VOPcOhO thin film was exposed to chloroform vapour inside a completely sealed container for about 30 minutes, in order to induce the crystallization in the VOPcPhO film. The absorption spectrum of this vapour treated film was found to be in agreement with reported results of tert-butyl-substituted vanadyl phthalocyanine dye (Law, 1985).

A unique near-IR absorption shoulder appears at λ ≈ 800nm for the chloroform vapour treated VOPcPhO film, may leads to a small phase transition from phase-I to phase-II. However, unlike the post thermally annealed VOPcPhO thin film, there is no red shift in the peak of the Q band in the absorption spectrum, indicating that the structural change in the VOPcPhO films induced by the vapour treatment method is different from that caused by the post thermal annealing process. This difference will be discussed further in the surface morphology analysis.

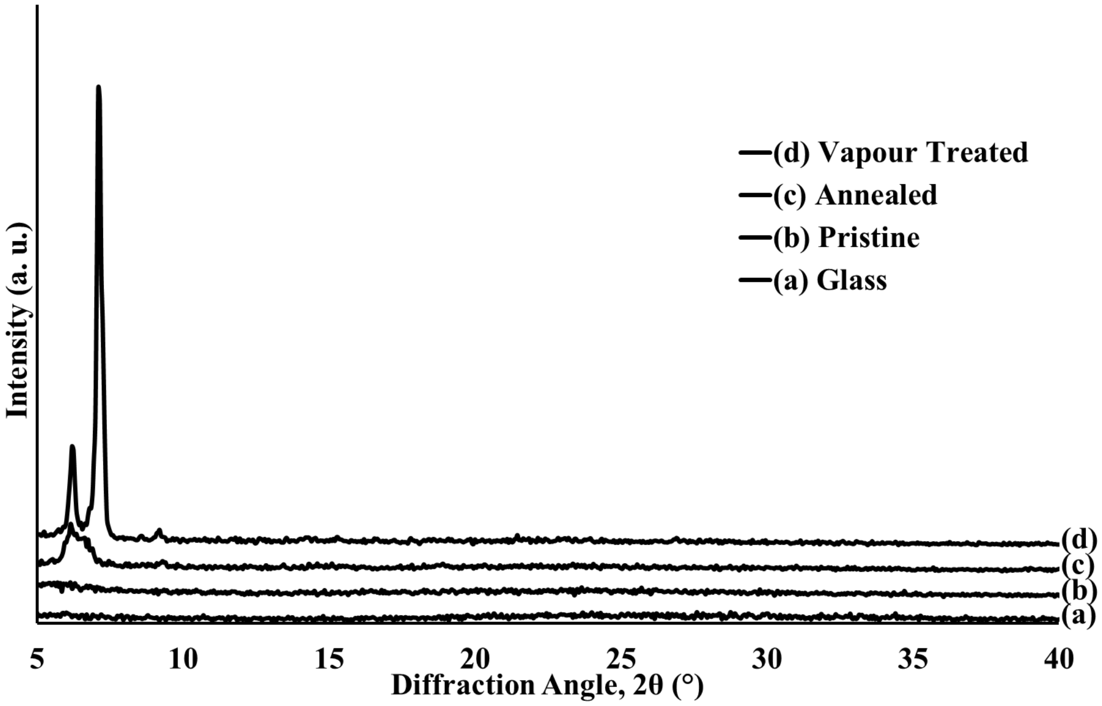

Figure 5.13 The XRD spectra of (a) glass substrate, (b) pristine, (c) annealed and (d) vapour treated VOPcPhO thin films.

In order to achieve a better assessment of the spectroscopic structure of the crystallisation behaviour in the VOPcPhO thin films, X-ray diffraction measurements were carried out. Figure 5.13 shows the XRD spectra of a plain glass, the pristine VOPcPhO thin film on a glass substrate, the annealed and vapour treated VOPcPhO thin films. The bottom purple spectrum, indicated by Figure 5.13(a), is the XRD spectrum of a plain glass, which was used as a reference. Based on these XRD spectra, it becomes obvious that the treated VOPcPhO thin films show distinctive differences in their crystallographic properties compared to the untreated pristine VOPcPhO thin film. Similar to the glass, the pristine VOPcPhO film does not show any diffraction peak, indicating that the spin-coated pristine VOPcPhO thin film produces a very disordered amorphous region and appears as phase-I. Such an amorphous region of VOPcPhO is expected to form in the organic semiconductor thin film, spin coated from a low boiling point solvent (in this case, chloroform). It is believed that there is a great tendency for VOPcPhO molecules to precipitate as a glassy solid (phase-I) rather than as the more stable crystalline form (phase-II) during the film formation, due to thermodynamically less stable dye aggregates that can be formed under fast drying (or spin coating) conditions (Law, 1985).

The annealed VOPcPhO thin films show a small and broad diffraction peak, with the maximum at a Bragg angle, $2\theta = 6.15°$, corresponding to the interstack spacing, d of 14.36Å. The existence of a tiny diffraction peak indicates that the annealed VOPcPhO thin film consists of a small percentage of crystallites within a glassy amorphous region. Based on the results from the unique near-IR absorbing properties, coupled with the XRD spectra, it can be anticipated that the annealed VOPcPhO thin film is phase-II VOPcPhO, similar to reported phase-II VOPc (Law, 1985). The energy released from the VOPcPhO thin film via the post thermal annealing is thought to be sufficient to induce the self-reassembling process. Thus, such molecular re-organisation has ensured a shorter stacking distance between the molecules, which in turn increase the crystallinity of the VOPcPhO thin film (Y. L. Pan, et al., 1998). However, the tiny diffraction peak is relatively broad, suggesting that the quality of the semi-crystalline structure in the annealed thin film is low and very disordered amorphous dominated region.

The XRD spectrum of the vapour treated VOPcPhO thin film shows two intense peaks at $2\theta = 6.2°$ and 7.1°. The corresponding interstack spacing, d are 14.24Å and 12.44Å, respectively. The sharp and intense diffraction peaks indicate that the thin film has a high crystallinity. From the XRD diffraction pattern of the two peaks, it appears that the vapour treated VOPcPhO thin film is associated with the coexistence of two different structure orientations in the film. It is attributed that the triclinic crystal structure (Yamashita, et al., 1993) which is responsible for the crystal orientation in the VOPcPhO film. Therefore, it indicates that the VOPcPhO thin film has been transformed from the amorphous structure to the crystalline structure by the vapour treatment. Unlike in the case of thermal annealing, the vapour treated thin film does not use energy from the heat to induce the crystallisation process, but rather is driven by the thermodynamic interactions between the solvent molecules and the VOPcPhO organic semiconductor molecules. Such interactions provide a medium for the solubilisation-crystallisation process of the VOPcPhO organic semiconductor molecules to take place. The results obtained from the XRD measurements support the findings from the optical absorption spectra of the VOPcPhO films. Thus, it is established that solvent vapour treatment is an effective process to induce crystallisation in the spin-coated films of low molecular weight organic semiconductors. Such crystallisation is very useful in an organic semiconductor, as it is associated with good electrical properties, such as conductivity and high charge mobility (Lanzi & Paganin, 2008; Y. S. Park & Kim, 2011).

Further investigations were conducted to obtain the average crystallite size of the vapour treated thin films. The average calculated crystallite size, τ for the lower peak at $2\theta = 6.2°$ is about 44.08nm, while for the higher peak at $2\theta = 7.1°$, τ is around 44.55nm. The average crystallite size of the higher peak is slightly, 1.07%, larger than the average crystallite size of the lower peak. This small difference in crystallite size, however, is negligible.

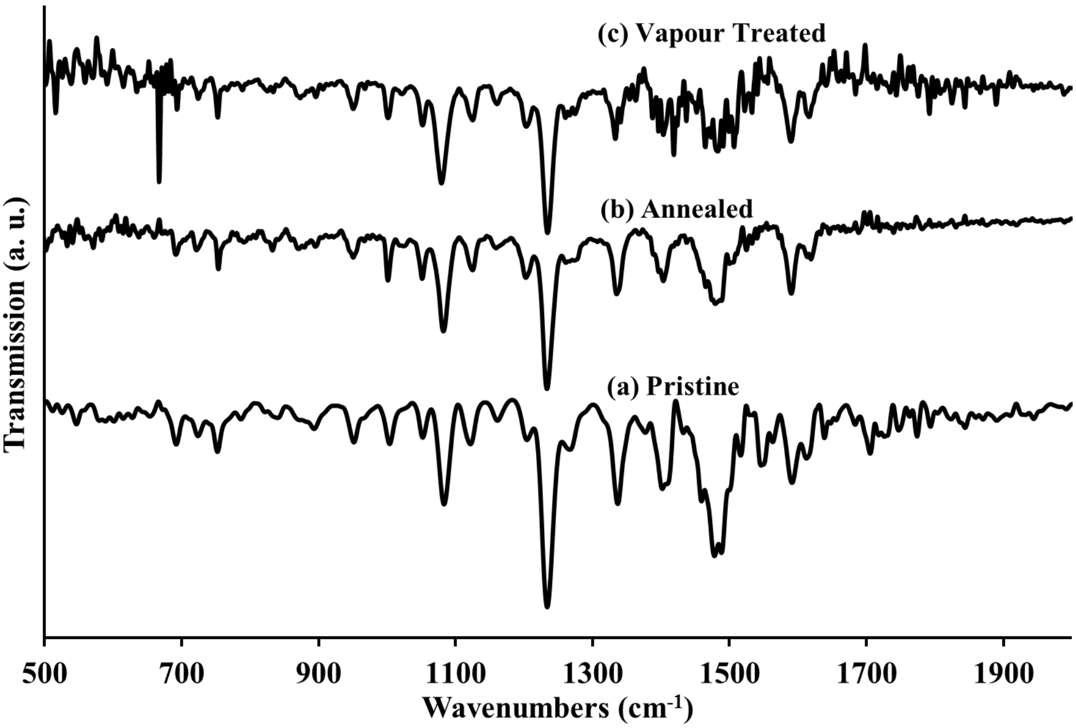

Figure 5.14 The Fourier Transform Infrared (FTIR) spectra of (a) pristine, (b) annealed and (c) vapour treated VOPcPhO thin films.

Figure 5.14 shows the FTIR results of the VOPcPhO thin films. Generally, the intensity and position of all the peaks are similar in the treated and untreated VOPcPhO thin films. The results indicate that the thermal as well as vapour treatments do not alter the chemical molecular structure of the VOPcPhO molecules. Therefore, the increase of crystallinity in the treated thin films is due to the spatial rearrangement of the VOPcPhO molecules.

In order to visualise the effects of the treatments on the surface morphology of the VOPcPhO thin films, FESEM images as show in Figure 5.15 are utilised. The FESEM image of the pristine VOPcPhO thin film, which is shown in Figure 5.15 (a), displayed a smooth, flat and homogenous surface. The particles located near the centre of the image are most probably due to the undissolved VOPcPhO powder in the chloroform solvent. No other particular structure can be seen in the image. As observed by the naked eye, and subsequently confirmed by the homogenous surface of the

FESEM image, this low molecular weight material of VOPcPhO has been well and evenly dispersed over the glass substrate via the spin coating technique.

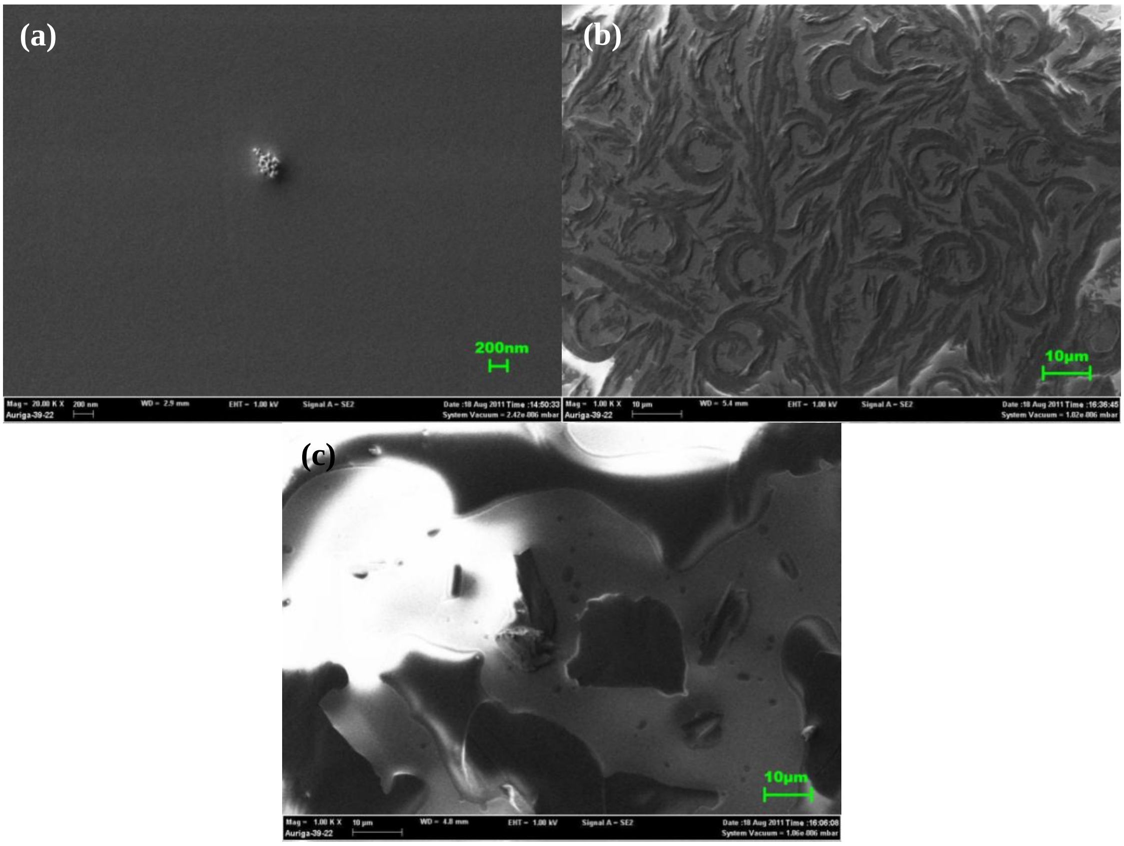

Figure 5.15 The FESEM images of (a) pristine, (b) annealed and (c) vapour treated VOPcPhO thin films.

Unlike the pristine sample, the treated thin films, however, revealed a completely different surface morphology. As can be seen in the FESEM image, which is indicated as Figure 5.15(b), the thermally annealed VOPcPhO thin film became porous, and thin flakes of a length up to one micron could be seen on the substrate surface. The distribution of the thin flakes displayed a very interesting pattern. The thin flakes formed like art work with some whirlpool patterns. With the energy acquired from the heat, the VOPcPhO molecules aggregated to form these thin flakes, as seen in the image. The energy added to the system seems likely to have overcome the surface free energy and thus allowed the free movement of the molecules to reorganise in a particular way, leading to the crystallisation process. The FESEM data confirmed that the thermal annealing led to phase separation (Teodosio Del Caño, et al., 2003). The change in morphology was correlated with the absorption properties. The aggregation created a porous thin film structure and caused the absorption of the thin film to be lower than that of the pristine sample.

The vapour treated VOPcPhO thin film aggregated into larger clusters, as can be seen in Figure 5.15(c). The thin film became very porous and the VOPcPhO molecules tended to assemble themselves into large rounded edged clusters following the solvent vapour process. The cluster size, measuring more than one tenth of a micron, might be responsible for the crystalline behaviour in the XRD spectrum of the vapour treated VOPcPhO thin films. The calculated average crystallite size was much smaller than the cluster size seen in the image. Therefore, it can be concluded that a large portion of the clusters are composed of amorphous structures. The aggregation of the molecules after undergoing the vapour treatment led to a very porous thin film, making the transmission of light relatively more efficient compared to the pristine and annealed thin films. Therefore, the absorption of the vapour treated thin films was the lowest. The absorption spectrum was in agreement with the FESEM results.

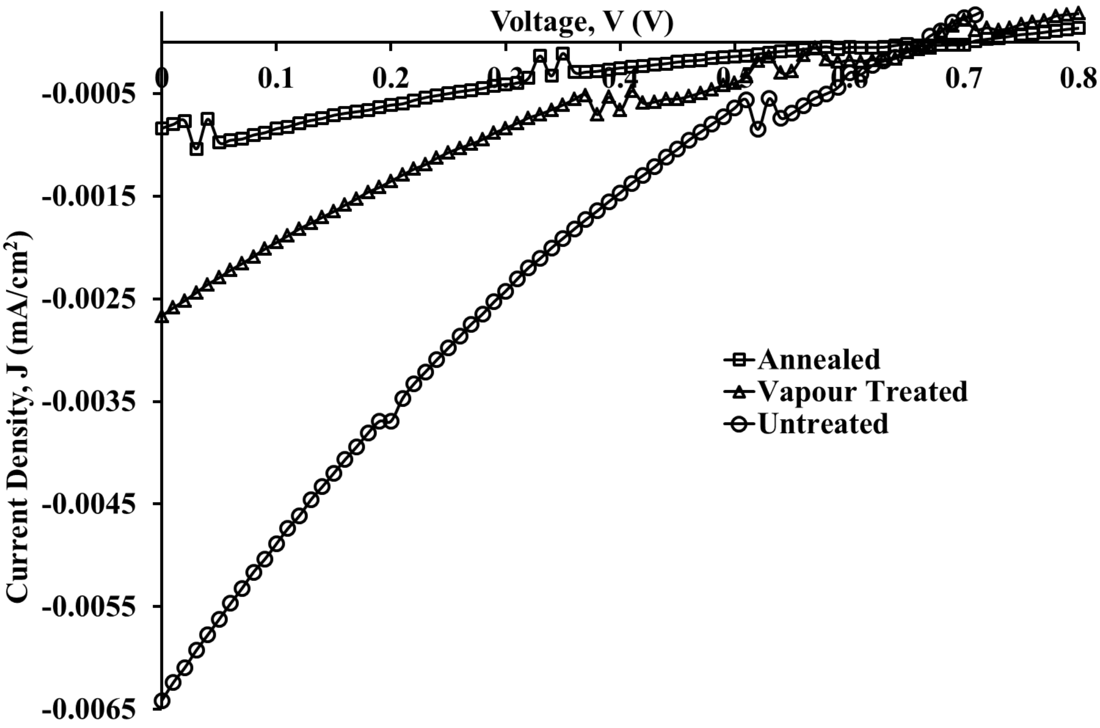

Figure 5.16 The J-V curves for the post thermal annealed, vapour treated and untreated OPVC.

Table 5.5 Photovoltaic parameters for the untreated and treated OPVC.

Device	J_{sc} (mA/cm^2)	V_{oc} (V)	FF	PCE ($\times 10^{-3}$%)	R_{sh} ($\times 10^4 \Omega cm^2$)	R_s ($\times 10^4 \Omega cm^2$)
Untreated	0.0064	0.66	0.18	0.75	6.17	13.16
Vapour Treated	0.0027	0.67	0.15	0.27	12.66	43.48
Post Thermal Annealed	0.0008	0.71	0.21	0.13	47.62	90.90

We expected the post thermal annealed and vapour treated OPVC will have better performance due to the better solar spectrum coverage and higher crystallinity of the treated VOPcPhO thin films compared to the pristine thin film. However, the J-V characteristics curves show that the performance of the treated OPVC dropped significantly compared to the untreated OPVC. The results are deviated from our expectations. From Figure 5.16 and Table 5.5, the V_{oc} and the FF of the devices do not deviate much and located at the range of 0.66V-0.71V and 0.15-0.21 respectively. However, the J_{sc} of the treated OPVC dropped to less than half of the value of the untreated OPVC. Consequently, the drastic reduction in J_{sc} gave a huge impact on the

PCE of the devices. The PCE of the untreated OPVC declined from 0.75×10^{-3}% to 0.27×10^{-3}% for the vapour treated OPVC and even further dropped to 0.13×10^{-3}% for the post thermal annealed OPVC. Please note that both the R_{sh} and R_s were increased by fold after the treatments. Perhaps they are able to give some clues to why the performance of the treated devices declined drastically after the treatments. R_{sh} arises from charge recombination at the donor/acceptor interface and surface current leakage while R_s is affected by the bulk resistance of the active layer and the contact resistance between the active layer and the electrode. The drastic increases in these parameters indicate that recombination rate of the charge carriers in the treated films are relatively high and the treated VOPcPhO layer probably do not form good contact with the ITO layer after treatments. The evidences are shown in the FESEM images in Figure 5.15 that very poor and uneven quality of films were produced after the treatments. The treated VOPcPhO thin films became too porous and large isolated clusters were formed throughout the films. Although the treated thin films displayed higher crystallinity in the XRD results but surface morphology of the thin films is also a key factor in determining the PCE of the OPVC. Hence the post thermal annealing and vapour treatments in the ambient are not efficient method to enhance the performance of bilayer VOPcPhO/PTCDA OPVC.

5.4 Multilayer VOPcPhO/PTCDA Organic Photovoltaic Cell

Attempts were done to fabricate multilayer VOPcPhO/PTCDA heterojunctions OPVC. In this work, four active layers were deposited onto the O_2 plasma treated ITO with PEDOT: PSS deposited on it. Therefore, the multilayer structure OPVC will consist of three VOPcPhO/PTCDA interfaces. The schematic structure of this multilayer structure OPVC is displayed in Figure 5.18. The performance of the multilayer structure OPVC was shown in Figure 5.17 and Table 5.6. The multilayer structure OPVC has a J_{sc} of 0.0377mA/cm^2 with a V_{oc} of 0.66 and FF of 0.22. The PCE of the multilayer structure OPVC enhanced to 5.40×10^{-3}% compared to 3.71×10^{-3}% of the bilayer structure OPVC. This 45.55% enhancement in PCE is largely due to the numbers of VOPcPhO/PTCDA interface exist in the device. However, it can be noticed that the increment in J_{sc} and PCE is not proportional to the number of interfaces of the device. As discussed in section 5.3, the VOPcPhO/PTCDA interface in the bilayer structure OPVC is the key place where the exciton dissociation took place. Since multilayer structure OPVC has three interfaces instead of one compared to bilayer structure OPVC, therefore it is expected that multilayer structure OPVC has a higher degree of exciton dissociation ability. Nevertheless, the thickness of the active layers in multilayer structure OPVC is two times compared to the bilayer structure OPVC thus the recombination probability is higher in multilayer structure OPVC. Anyway, the results are sufficient to further strengthen the suggestion in section 5.3 that the excitons can only dissociate at the VOPcPhO/PTCDA interface.

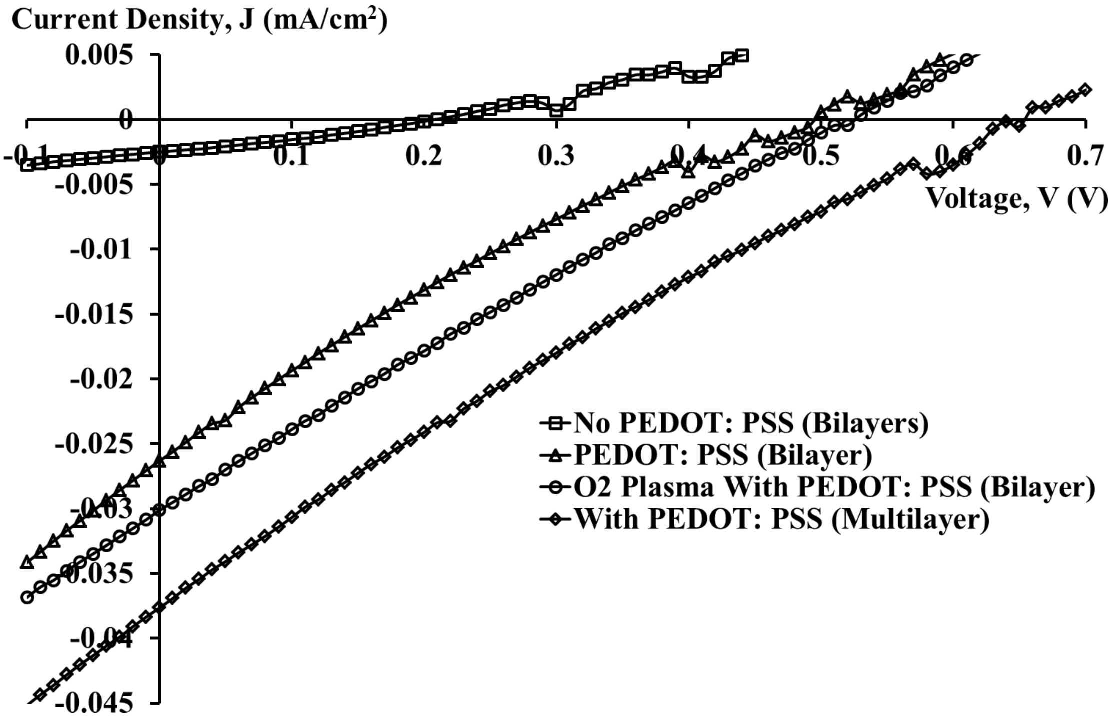

Figure 5.17 The J-V curves for the bilayer OPVC without PEDOT: PSS, bilayer OPVC with PEDOT: PSS, Bilayer OPVC treated by O_2 plasma and multilayer OPVC.

Table 5.6 Photovoltaic parameters for the OPVC without PEDOT: PSS, OPVC with PEDOT: PSS, OPVC treated by O_2 plasma and multilayer OPVC.

Device	J_{sc} (mA/cm^2)	V_{oc} (V)	FF	PCE ($\times 10^{-3}$%)	R_{sh} ($\times 10^4 \Omega cm^2$)	R_s ($\times 10^4 \Omega cm^2$)
Without PEDOT: PSS (Bilayer)	0.0025	0.21	0.31	0.16	10.87	5.65
With PEDOT: PSS (Bilayer)	0.0263	0.50	0.20	2.64	1.35	1.65
OPVC O_2 Plasma (Bilayer)	0.0301	0.53	0.23	3.71	1.55	2.04
Multilayer OPVC	0.0377	0.66	0.22	5.40	1.39	1.73

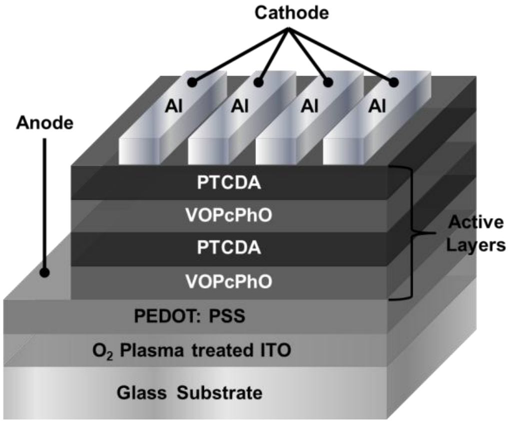

Figure 5.18 Schematic structure of a multilayer VOPcPhO/PTCDA heterojunction OPVC.

Chapter 6

Conclusions and Future Works

6.0 Conclusions

The characterisations of VOPcPhO and PTCDA thin films have been performed and the utilisation of these thin films to the bilayer heterojunction organic solar cell has shown improvement to some extent. VOPcPhO film has a solar spectrum coverage in the regions of UV (350nm to 500nm) and yellow to infrared (570nm to 900nm) while PTCDA film absorbs light in the region of blue to green (400nm to 600nm). Therefore, the absorption spectra of these two organic semiconductors are complementary to each other. Bilayer thin films based on these two organic semiconductors cover large portion of the solar spectrum from 350nm to 900nm corresponding to UV region to infrared region. Large coverage of solar spectrum making this bilayer thin films promising active layers to fabricate OPVC. The optical band gap, E_g of the VOPcPhO and PTCDA thin films determined from the UV-VIS spectra are found to be 1.67eV and 2.13eV respectively. Put simply, radiation with energy higher than 2.13eV corresponding to wavelength shorter than orange wavelength is sufficient to cause the electron excitation in the VOPcPhO, PTCDA or VOPcPhO/PTCDA bilayer thin films. Therefore, the practical application of this bilayer film into the heterojunction organic solar cell is high due to the relatively high probability of excitons creation under the solar radiation.

The results of this research studies have shown that the organic solar cells consist of either single layer VOPcPhO or PTCDA film do not show photovoltaic effect. Such behavior suggests that the internal electric field induced by the electrodes is not strong enough to cause the excitons to dissociate within the single layer based OPVCs. However, the photovoltaic effect was observed in the bilayer VOPcPhO/PTCDA OPVC as revealed in the fourth quadrant of the J-V curves. The simple ITO/VOPcPhO/PTCDA/Al structure OPVC has a V_{oc} of 0.21V, FF of 0.31 and PCE of 0.16×10^{-3}%. The existence of the VOPcPhO/PTCDA heterojunctions interface provides a sharp drop of potential which is thought to be able to separate the bounded state of electron hole pairs (excitons). Multilayer structure OPVC which consist of three heterojunctions interfaces further proved the hypothesis by showing 45% increment in the PCE.

Insertion of anode buffer layer (PEDOT: PSS) has proven to be able to significantly enhance the performance of the OPVC. The PCE of the OPVC included PEDOT: PSS buffer layer drastically increased 16 times to 2.64×10^{-3}% compared to the OPVC without PEDOT: PSS. The enhancements of the OPVC included PEDOT: PSS attributed to the better hole transport, improved surface smoothness of the ITO surface and the better matching work function of the ITO with the HOMO level of the active materials in the active layer. However, the FF decreased upon introducing PEDOT: PSS into the OPVC. It is thought that the OPVC behaved more ohmic in the fourth quadrant of the J-V curves due the drastic decreased of the R_{sh} and R_s values in the OPVC.

The oxygen plasma treatment on the ITO layer was utilised in order to further improve the efficiency of the OPVC. It was found that the PCE has increased about 40% for the device utilising O_2 plasma treated ITO. The increased of surface energy and work function of ITO are the main reasons of the enhancement of PCE in OPVC. Higher surface energy provides a better surface adhesiveness of PEDOT: PSS thin film and reduced the interfacial energy between the PEDOT: PSS and the active layer. Besides that, the increased in ITO work function makes available for a better matching of the HOMO level of the active layers. All these factors improved the hole transport of the OPVC and therefore increased the PCE of the OPVC.

The studies continue with the investigations of the effects of post thermal annealing and solvent vapor treatment on the OPVC. The treatments successfully transformed amorphous VOPcPhO thin film into the semi-crystalline structure (phase I → phase II). Two verifications have been obtained to prove the occurrence of such semi-crystalline structure; first was the unique feature in the infra-red region of the UV-

VIS absorption spectrum and second was the existence of XRD peaks. The light absorption is one of the criteria in determining the efficiency of OPVC. Even though the fulm of VOPcPhO has shown to be more ordered in the semi-crystalline structure (compared to amorphous), but this is not a secure in the increment of efficiency. Another factor of the film surface morphology and charge transport in the device also the prime importance factors in determining OPVC efficiency. In this research work, it was observed that the quality of the treated VOPcPhO film was very poor and uneven upon thermal and solvent treatments as shown in the FESEM images. Such poorer film morphology leads to higher resistivity features of R_{sh} and R_s. Hence this causes the rise in recombination rate of the charge carriers and therefore lowers the efficiency of the device containing the treated organic film.

It is worth to mention that all the post thermal and solvent treatments were performed under ambient condition. The above constraints of poorer surface morphology as well as higher resistivity may be avoided by performing the film treatment in an inert atmosphere such as utilization nitrogen gas flow in a glove box. Furthermore, all OPVC devices on this research work were fabricated in air and not encapsulated, which have been easily attacked by oxygen and water molecules. Thus, the degradation process has occurred causing the efficiency of the OPVC is very small. Hence as a conclusion, the post thermal annealing and vapour treatments in the ambient atmospheric condition are not efficient methods to enhance the performance of bilayer VOPcPhO/PTCDA OPVC.

6.1 Future Works

Although the employment of the bilayer heterojunction of VOPcPhO/PTCDA thin films to the OPVC was successful but more works need to carry out to improve the performance of the OPVC. Below are some suggestions that should be undertaken as future works:

1. The homebuilt thermal evaporator should be modified into at least two sources evaporator so that co-evaporation of two organic semiconductors can be done. Thermal evaporated bulk heterojunction OPVC then can be fabricated and comparison to the bilayer heterojunction OPVC can be made. Commonly, the bulk heterojunction OPVC has better performance compared to bilayer heterojunction OPVC due to their larger interface area and shorter path of exciton diffusion in the thin film.
2. The mobility of the charge carriers should be determined. These important electrical properties can reveal a lot of information about the behavior of the charge carriers in the OPVC. Electron and hole mobilities should be balanced in order to avoid traps of charge carriers near the interface.
3. The fabrication, treatments and characterisation of OPVC should be done in the glove box in order to prevent degradation of the device during these processes.
4. Encapsulation technology minimises the degradation of OPVC due to moisture, light, oxygen et cetera. Therefore, it should be applied on the fabricated devices to prolong the life span of the devices.

References

References

Adams, W. G., & Day, R. E. (1877). *The action of light on selenium*.

Ameri, T., Dennler, G., Lungenschmied, C., & Brabec, C. J. (2009). Organic tandem solar cells: A review. *Energy & Environmental Science, 2*(4), 347-363.

Bamsey, N. M., Yuen, A. P., Hor, A.-M., Klenkler, R., Preston, J. S., & Loutfy, R. O. (2011). Integration of an M-phthalocyanine layer into solution-processed organic photovoltaic cells for improved spectral coverage. *Solar Energy Materials and Solar Cells, 95*(7), 1970-1973.

Ben Chaabane, R., Ltaief, A., Dridi, C., Rahmouni, H., Bouazizi, A., & Ben Ouada, H. (2003). Study of organic thin film transistors based on nickel phthalocyanine: effect of annealing. *Thin Solid Films, 427*(1-2), 371-376.

Bergemann, K. J., & Forrest, S. R. (2011). Measurement of exciton diffusion lengths in optically thin organic films. *Applied Physics Letters, 99*(24), 243303-243303.

Berger, S., Heimer, K., Mack, H. G., & Ziegler, C. (2005). IR and SFM study of PTCDA thin films on different substrates. *Applied Surface Science, 252*(1), 81-84. doi: 10.1016/j.apsusc.2005.02.001

Bernède, J. C., Cattin, L., Morsli, M., & Berredjem, Y. (2008). Ultra-thin metal layer passivation of the transparent conductive anode in organic solar cells. *Solar Energy Materials and Solar Cells, 92*(11), 1508-1515.

Bricaud, Q., Cravino, A., Leriche, P., & Roncali, J. (2009). Poly(thiophenes) derivatized with oligo(oxyethylene) chains as donor materials for organic solar cells. *Solar Energy Materials and Solar Cells, 93*(9), 1624-1629.

Brovelli, F., Rivas, B. L., Bernède, J. C., del Valle, M. A., Díaz, F. R., & Berredjem, Y. (2007). Electrochemical and optical studies of 1,4-diaminoanthraquinone for solar cell applications. *Polymer Bulletin, 58*(3), 521-527.

Bruder, I., Karlsson, M., Eickemeyer, F., Hwang, J., Erk, P., Hagfeldt, A., . . . Pschirer, N. (2009). Efficient organic tandem cell combining a solid state dye-sensitized and a vacuum deposited bulk heterojunction solar cell. *Solar Energy Materials and Solar Cells, 93*(10), 1896-1899.

Chen, H.-Y., Hou, J., Zhang, S., Liang, Y., Yang, G., Yang, Y., . . . Li, G. (2009). Polymer solar cells with enhanced open-circuit voltage and efficiency. *Nat Photon, 3*(11), 649-653.

Cheyns, D., Rand, B. P., & Heremans, P. (2010). Organic tandem solar cells with complementary absorbing layers and a high open-circuit voltage. *Applied Physics Letters, 97*(3), 033301-033303.

Danziger, J., Dodelet, J. P., Lee, P., Nebesny, K. W., & Armstrong, N. R. (1991). Heterojunctions Formed from Phthalocyanine and Perylene Thin Films: Photoelect rochemical Characterization. *Chemstry of Materials, 3*(5), 821-829.

Del Caño, T., Antonio de Saja, J., & Aroca, R. F. (2003). Exciplex emission in mixed films of vanadylphthalocyanine and N,N'-bis(neopentyl)-3,4,9,10-perylenebis(dicarboximide). *Chemical Physics Letters, 377*(3-4), 347-353.

Del Caño, T., Parra, V., Rodríguez-Méndez, M. L., Aroca, R. F., & De Saja, J. A. (2005). Characterization of evaporated trivalent and tetravalent phthalocyanines thin films: different degree of organization. *Applied Surface Science, 246*(4), 327-333.

Derouiche, H., & Djara, V. (2007). Impact of the energy difference in LUMO and HOMO of the bulk heterojunctions components on the efficiency of organic solar cells. *Solar Energy Materials and Solar Cells, 91*(13), 1163-1167.

Erten, S., & Icli, S. (2008). Bilayer heterojunction solar cell based on naphthalene bis-benzimidazole. *Inorganica Chimica Acta, 361*(3), 595-600.

Frederik C, K. (2009). Fabrication and processing of polymer solar cells: A review of printing and coating techniques. *Solar Energy Materials and Solar Cells, 93*(4), 394-412.

Friedel, B., Keivanidis, P. E., Brenner, T. J. K., Abrusci, A., McNeill, C. R., Friend, R. H., & Greenham, N. C. (2009). Effects of Layer Thickness and Annealing of PEDOT:PSS Layers in Organic Photodetectors. *Macromolecules, 42*(17), 6741-6747. doi: 10.1021/ma901182u

Gabriel, M., St, amp, ouml, hr, M., & ller, R. (2002). Growth of 3,4,9,10-perylenetetracarboxylic-dianhydride (PTCDA) on Cu(110) studied by STM. *Applied Physics A: Materials Science & Processing, 74*(2), 303-305.

Glöckler, K., Seidel, C., Soukopp, A., Sokolowski, M., Umbach, E., Böhringer, M., . . . Schneider, W. D. (1998). Highly ordered structures and submolecular scanning tunnelling microscopy contrast of PTCDA and DM-PBDCI monolayers on Ag(111) and Ag(110). *Surface Science, 405*(1), 1-20.

Güllü, Ö., Çankaya, M., Biber, M., & Türüt, A. (2008). Fabrication and electrical properties of organic-on-inorganic Schottky devices. *Journal of Physics: Condensed Matter, 20*, 215210.

Gupta, D., Bag, M., & Narayan, K. S. (2008). Correlating reduced fill factor in polymer solar cells to contact effects. *Applied Physics Letters, 92*(9).

Hara, M., Satoh, A., Takami, N., & Ohsaki, T. (1995). Structural and Electrochemical Properties of Lithiated Polymerized Aromatics. Anodes for Lithium-Ion Cells. *The Journal of Physical Chemistry, 99*(44), 16338-16343. doi: 10.1021/j100044a021

Hashimoto, Y., & Hamagaki, M. (2006). Effect of oxygen plasma treatment of indium tin oxide for organic solar cell. *Electrical Engineering in Japan, 154*(4), 1-7. doi: 10.1002/eej.20313

Heggie, D. A., MacDonald, B. L., & Hill, I. G. (2006). Evidence of mobile charged impurities in organic heterojunction photovoltaic devices. *Journal of Applied Physics, 100*(10), 104505-104505-104504.

Heutz, S., & Jones, T. S. (2002). Structural and morphological modifications in double layer heterostructures containing H2Pc, perylene-3, 4, 9, 10-tetracarboxylic dianhydride and Alq3. *Journal of Applied Physics, 92*(6), 3039.

Ho, K.-C., & Tsou, Y.-H. (2001). Chemiresistor-type NO gas sensor based on nickel phthalocyanine thin films. *Sensors and Actuators B: Chemical, 77*(1-2), 253-259.

Hohnholz, D., Steinbrecher, S., & Hanack, M. (2000). Applications of phthalocyanines in organic light emitting devices. *Journal of Molecular Structure, 521*(1-3), 231-237.

Hoppe, H., & Sariciftci, N. S. (2004). Organic solar cells: An overview. *Journal of Materials Research, 19*(07), 1924-1945.

Hu, Z., Zhang, J., Hao, Z., & Zhao, Y. (2011). Influence of doped PEDOT:PSS on the performance of polymer solar cells. *Solar Energy Materials and Solar Cells, 95*(10), 2763-2767. doi: 10.1016/j.solmat.2011.04.040

Hudej, R., & Bratina, G. (2002). Evidence of bipolar charge transport in PTCDA. *Solid State Communications, 123*(3–4), 155-160. doi: 10.1016/s0038-1098(02)00204-1

Ichikawa, M., Kobayashi, K., Koyama, T., & Taniguchi, Y. (2007). Intense and efficient ultraviolet electroluminescence from organic light-emitting devices with fluorinated copper phthalocyanine as hole injection layer. *Thin Solid Films, 515*(7-8), 3932-3935.

Jain, V., Rajbongshi, B. K., Tej Mallajosyula, A., Bhattacharjya, G., Kumar Iyer, S. S., & Ramanathan, G. (2008). Photovoltaic effect in single-layer organic solar cell devices fabricated with two new imidazolin-5-one molecules. *Solar Energy Materials and Solar Cells, 92*(9), 1043-1046.

Kaiser, R., Friedrich, M., Schmitz-Hübsch, T., Sellam, F., Kampen, T. U., Leo, K., & Zahn, D. R. T. (1999). Ultra-thin PTCDA layers studied by optical spectroscopies. *Fresenius' Journal of Analytical Chemistry, 363*(2), 189-192. doi: 10.1007/s002160051169

Kaur, M., Gopal, A., Davis, R. M., & Heflin, J. R. (2009). Concentration gradient P3OT/PCBM photovoltaic devices fabricated by thermal interdiffusion of separately spin-cast organic layers. *Solar Energy Materials and Solar Cells, 93*(10), 1779-1784.

Kearns, D., & Calvin, M. (1958). Photovoltaic effect and photoconductivity in laminated organic systems. *Journal of Chemical Physics, 29*(4), 950-951.

Kekuda, D., Lin, H.-S., Chyi Wu, M., Huang, J.-S., Ho, K.-C., & Chu, C.-W. (2011). The effect of solvent induced crystallinity of polymer layer on poly(3-hexylthiophene)/C70 bilayer solar cells. *Solar Energy Materials and Solar Cells, 95*(2), 419-422.

Kim, J. Y., Lee, K., Coates, N. E., Moses, D., Nguyen, T.-Q., Dante, M., & Heeger, A. J. (2007). Efficient Tandem Polymer Solar Cells Fabricated by All-Solution Processing. *Science, 317*(5835), 222-225.

Kim, Y., Ballantyne, A. M., Nelson, J., & Bradley, D. D. C. (2009). Effects of thickness and thermal annealing of the PEDOT:PSS layer on the performance of polymer solar cells. *Organic Electronics, 10*(1), 205-209. doi: 10.1016/j.orgel.2008.10.003

Kim, Y., Monroe, M., Seol, J., Truong, N., Cho, S., Anderson, T., & Park, C. (2008). Optimization of organic bi-layer solar cell through systematic study of anode treatment and material thickness. *Korean Journal of Chemical Engineering, 25*(5), 1036-1039.

Kippelen, B., & Bredas, J.-L. (2009). Organic photovoltaics. *Energy & Environmental Science, 2*(3), 251-261.

Klofta, T., Linkous, C., & Armstrong, N. R. (1985). Photoelectrochemical studies of vanadyl phthalocyanine (VOPc) thin film electrodes. *Journal of Electroanalytical Chemistry and Interfacial Electrochemistry, 185*(1), 73-92.

Kolotovska, V., Friedrich, M., Zahn, D. R. T., & Salvan, G. (2006). Magnetic field influence on the molecular alignment of vanadyl phthalocyanine thin films. *Journal of Crystal Growth, 291*(1), 166-174.

Kwong, C. Y., Djurišiĉ, A. B., Chui, P. C., Lam, L. S. M., & Chan, W. K. (2003). Improvement of the efficiency of phthalocyanine organic Schottky solar cells with ITO electrode treatment. *Applied Physics A: Materials Science & Processing, 77*(3), 555-560.

Kymakis, E., Koudoumas, E., & Franghiadakis, I. (2006). Bi-layer photovoltaic devices with PPQ as the electron acceptor layer. *Solar Energy Materials and Solar Cells, 90*(12), 1705-1714.

Lane, P. A., Rostalski, J., Giebeler, C., Martin, S. J., Bradley, D. D. C., & Meissner, D. (2000). Electroabsorption studies of phthalocyanine/perylene solar cells. *Solar Energy Materials and Solar Cells, 63*(1), 3-13.

Lanzi, M., & Paganin, L. (2008). Study of the order-disorder transitions in methoxy-functionalized polyalkylthiophenes. *European Polymer Journal, 44*(12), 3987-3996.

Law, K. Y. (1985). An investigation of solvent-vapor-induced crystallization soluble vanadyl phthalocyanine dyes in polymer matrixes. *The Journal of Physical Chemistry, 89*(12), 2652-2657.

Law, K. Y. (1988). Effect of dye aggregation on the photogeneration efficiency of organic photoconductors. *The Journal of Physical Chemistry, 92*(14), 4226-4231.

Li, L., Tang, Q., Li, H., Hu, W., Yang, X., Shuai, Z., . . . Zhu, D. (2008). Organic thin-film transistors of phthalocyanines. *Pure and Applied Chemistry, 80*(11), 2231–2240.

Lian, K., Li, R., Wang, H., Zhang, J., & Gamota, D. (2010). Printed flexible memory devices using copper phthalocyanine. *Materials Science and Engineering: B, 167*(1), 12-16.

Liang, F., Shi, F., Fu, Y., Wang, L., Zhang, X., Xie, Z., & Su, Z. (2010). Donor-acceptor conjugates-functionalized zinc phthalocyanine: Towards broad absorption and application in organic solar cells. *Solar Energy Materials and Solar Cells, 94*(10), 1803-1808.

Liu, C. J., Peng, C. H., Ju, Y. H., & Hsieh, J. C. (1998). Titanyl phthalocyanine gas sensor for NO2 detection. *Sensors and Actuators B: Chemical, 52*(3), 264-269.

Liu, P., Li, Q., Huang, M., Pan, W., & Deng, W. (2006). High open circuit voltage organic photovoltaic cells based on oligothiophene derivatives. *Applied Physics Letters, 89*(21), 213501-213503.

Lunt, R. R., Giebink, N. C., Belak, A. A., Benziger, J. B., & Forrest, S. R. (2009). Exciton diffusion lengths of organic semiconductor thin films measured by spectrally resolved photoluminescence quenching. *Journal of Applied Physics, 105*(5), 053711-053717.

Majumdar, H. S., Bandyopadhyay, A., & Pal, A. J. (2003). Data-storage devices based on layer-by-layer self-assembled films of a phthalocyanine derivative. *Organic Electronics, 4*(1), 39-44.

Martin A, G. (2002). Photovoltaic principles. *Physica E: Low-dimensional Systems and Nanostructures, 14*(1-2), 11-17.

Maruyama, T., Hirasawa, A., Shindow, T., Akimoto, K., Kato, H., & Kakizaki, A. (2000). Energy-level alignment at NTCDA/metal and PTCDA/NTCDA interfaces studied by UPS. *Journal of Luminescence, 87-89*, 782-784.

Mathew, S., Sudarsanakumar, C., & Menon, C. S. (2010). Spectral, thermal and structural studies on aluminium phthalocyanine hydroxide thin films. *Optoelectronics and Advanced Materials - Rapid Communications, 4*(1), 63-69.

Mori, T., & Kato, K. (2007). Photovoltaic properties of organic thin-film solar cell using various exciton-diffusion blocking materials. *Journal of Photopolymer Science and Technology, 20*(1), 61-66.

Muhammad, F. F., Abdul Hapip, A. I., & Sulaiman, K. (2010). Study of optoelectronic energy bands and molecular energy levels of tris (8-hydroxyquinolinate) gallium and aluminum organometallic materials from their spectroscopic and electrochemical analysis. *Journal of Organometallic Chemistry, 695*(23), 2526-2531.

Nakano, H., Sakai, Y., Furuhashi, H., Yoshikawa, T., Maeda, A., Sawa, G., . . . Mizutani, T. (2001, 2001). *Effects of corona charging on nonlinear optical property and morphology of VOPc thin film prepared on polyimide substrate by molecular beam epitaxy.* Paper presented at the Electrical Insulation and Dielectric Phenomena, 2001 Annual Report. Conference on.

Nanai, N., Yudasaka, M., Ohki, Y., & Yoshimura, S. (1995). Structures of vanadyl phthalocyanine in bilayers of vanadyl phthalocyanine and perylenetetracarboxylic dianhydride. *Thin Solid Films, 265*(1-2), 1-2.

Nemykin, V. N., & Lukyanets, E. A. (2010). Synthesis of substituted phthalocyanines. *Archive for Organic Chemistry*, 136– 208.

Nénon, S., Kanehira, D., Yoshimoto, N., Fages, F., & Videlot-Ackermann, C. (2010). Shelf-life time test of p- and n-channel organic thin film transistors using copper phthalocyanines. *Thin Solid Films, 518*(19), 5593-5598.

Nomura, K., Oku, T., Suzuki, A., Kikuchi, K., & Kinoshita, G. The effects of exciton-diffusion blocking layers on pentacene/C60 bulk heterojunction solar cells. *Journal of Physics and Chemistry of Solids, 71*(3), 210-213.

Nomura, K., Oku, T., Suzuki, A., Kikuchi, K., & Kinoshita, G. (2010). The effects of exciton-diffusion blocking layers on pentacene/C60 bulk heterojunction solar cells. *Journal of Physics and Chemistry of Solids, 71*(3), 210-213.

Pan, Y.-l., Liao, X.-d., Wu, Y.-j., Chen, L.-b., You-yuan, Z., Shen, Y.-h., . . . Huang, D.-y. (1998a). Steady-state photovoltaic and electroreflective spectra in Al/vanadyl phthalocyanine (VOPc, in phase II)/indium-tin-oxide (ITO) sandwich cell. *Thin Solid Films, 324*(1-2), 209-213.

Pan, Y.-l., Liao, X.-d., Wu, Y.-j., Chen, L.-b., You-yuan, Z., Shen, Y.-h., . . . Huang, D.-y. (1998b). Steady-state photovoltaic and electroreflective spectra in Al/vanadyl phthalocyanine (VOPc, in phase II)/indium–tin–oxide (ITO) sandwich cell. *Thin Solid Films, 324*(1–2), 209-213. doi: 10.1016/s0040-6090(98)00357-5

Pan, Y. L., Wu, Y. J., Chen, L. B., Zhao, Y. Y., Shen, Y. H., Li, F. M., . . . Huang, D. H. (1998). Structure and spectroscopic characterization of polycrystalline vanadyl phthalocyanine (VOPc) films fabricated by vacuum deposition. *Applied Physics A: Materials Science & Processing, 66*(5), 569-573.

Park, S. H., Roy, A., Beaupre, S., Cho, S., Coates, N., Moon, J. S., . . . Heeger, A. J. (2009). Bulk heterojunction solar cells with internal quantum efficiency approaching 100%. *Nat Photon, 3*(5), 297-302.

Park, Y. S., & Kim, H.-K. (2011). Characteristics of sputtered Al-doped ZnO films for transparent electrodes of organic thin-film transistor. *Thin Solid Films, 519*(22), 8018-8022.

Pérez-Merchancano, S. T., Marques, G. E., & Bolivar-Marinez, L. E. (2008). Optical transitions in new trends organic materials. *Microelectronics Journal, 39*(3-4), 576-578.

Persson, N.-K., & Inganäs, O. (2006). Organic tandem solar cells--modelling and predictions. *Solar Energy Materials and Solar Cells, 90*(20), 3491-3507.

Petritsch, K., Dittmer, J. J., Marseglia, E. A., Friend, R. H., Lux, A., Rozenberg, G. G., . . . Holmes, A. B. (2000). Dye-based donor/acceptor solar cells. *Solar Energy Materials and Solar Cells, 61*(1), 63-72.

Qiao, Q., Beck, J., Lumpkin, R., Pretko, J., & McLeskey, J. J. T. (2006). A comparison of fluorine tin oxide and indium tin oxide as the transparent electrode for P3OT/TiO2 solar cells. *Solar Energy Materials and Solar Cells, 90*(7-8), 1034-1040.

Qiu, L., Zhai, J., Shen, Y., Guo, L., Ma, G., Liu, Y., . . . Qian, S. (2005). Preparation of a novel class of phthalocyanine containing cross-linked polymers and their thin films. *Thin Solid Films, 471*(1-2), 96-99.

Rejitha, B., & Menon, C. (2012). Post Deposition Annealing Effects on Optical, Electrical and Morphological Studies of ZnTTBPc Thin Films. *E-Journal of Chemistry, 9*(4), 1728-1736.

Saarenpää, H., Niemi, T., Tukiainen, A., Lemmetyinen, H., & Tkachenko, N. (2010). Aluminum doped zinc oxide films grown by atomic layer deposition for organic photovoltaic devices. *Solar Energy Materials and Solar Cells, 94*(8), 1379-1383.

Santos, L. F., & et al. (2008). Observation of persistent photoconductivity in vanadyl phthalocyanine. *Journal of Physics D: Applied Physics, 41*(12), 125107.

Sista, S., Park, M.-H., Hong, Z., Wu, Y., Hou, J., Kwan, W. L., . . . Yang, Y. (2010). Highly Efficient Tandem Polymer Photovoltaic Cells. *Advanced Materials, 22*(3), 380-383.

Smith, W. (1873). The action of light on selenium. *Telegraph Engineers, Journal of the Society of, 2*(4), 31-33.

Spanggaard, H., & Krebs, F. C. (2004). A brief history of the development of organic and polymeric photovoltaics. *Solar Energy Materials and Solar Cells, 83*(2-3), 125-146.

Takahashi, K., Kuraya, N., Yamaguchi, T., Komura, T., & Murata, K. (2000). Three-layer organic solar cell with high-power conversion efficiency of 3.5%. *Solar Energy Materials and Solar Cells, 61*(4), 403-416.

Takahashi, K., Tsuji, K., Imoto, K., Yamaguchi, T., Komura, T., & Murata, K. (2002). Enhanced photocurrent by Schottky-barrier solar cell composed of regioregular polythiophene with merocyanine dye. *Synthetic Metals, 130*(2), 177-183.

Tang, C. W. (1986). Two-layer organic photovoltaic cell. *Applied Physics Letters, 48*, 183-185.

Triyana, K., Yasuda, T., Fujita, K., & Tsutsui, T. (2005). Tandem-type organic solar cells by stacking different heterojunction materials. *Thin Solid Films, 477*(1-2), 198-202.

Wagner, T., Bannani, A., Bobisch, C., Karacuban, H., Stöhr, M., Gabriel, M., & Möller, R. (2004). Growth of 3,4,9,10-perylenetetracarboxylic-dianhydride crystallites on noble metal surfaces. *Organic Electronics, 5*(1-3), 35-43.

Wang, H., Song, D., Yang, J., Yu, B., Geng, Y., & Yan, D. (2007). High mobility vanadyl-phthalocyanine polycrystalline films for organic field-effect transistors. *Applied Physics Letters, 90*(25), 253510-253510-253513.

Xi, X., Meng, Q., Li, F., Ding, Y., Ji, J., Shi, Z., & Li, G. (2010). The characteristics of the small molecule organic solar cells with PEDOT:PSS/LiF double anode buffer layer system. *Solar Energy Materials and Solar Cells, 94*(3), 623-628. doi: 10.1016/j.solmat.2009.12.014

Yamashita, A., Maruno, T., & Hayashi, T. (1993). Absorption spectra of organic-molecular-beam-deposited vanadyl- and titanylphthalocyanine. *The Journal of Physical Chemistry, 97*(18), 4567-4569.

Yang, H. B., Song, Q. L., Gong, C., & Li, C. M. (2010). The degradation of indium tin oxide/pentacene/fullerene/tris-8-hydroxy-quinolinato aluminum/aluminum heterojunction organic solar cells: By oxygen or moisture? *Solar Energy Materials and Solar Cells, 94*(5), 846-849. doi: 10.1016/j.solmat.2010.01.006

Yang, J., & Nguyen, T.-Q. (2007). Effects of thin film processing on pentacene/C60 bilayer solar cell performance. *Organic Electronics, 8*(5), 566-574.

Yoo, I., Lee, M., Lee, C., Kim, D.-W., Moon, I. S., & Hwang, D.-H. (2005). The effect of a buffer layer on the photovoltaic properties of solar cells with P3OT:fullerene composites. *Synthetic Metals, 153*(1–3), 97-100. doi: 10.1016/j.synthmet.2005.07.182

You, Z. Z., & Dong, J. Y. (2007). Oxygen plasma treatment effects of indium-tin oxide in organic light-emitting devices. *Vacuum, 81*(7), 819-825. doi: 10.1016/j.vacuum.2006.09.004

Zhou, Y., Cheun, H., Choi, S., Fuentes-Hernandez, C., & Kippelen, B. (2011). Optimization of a polymer top electrode for inverted semitransparent organic solar cells. *Organic Electronics, 12*(5), 827-831.